Aus der Abteilung Molekulare Onkologie

(Prof. Dr. med. M. Dobbelstein)

der Medizinischen Fakultät der Universität Göttingen

im Göttinger Zentrum für Molekulare Biowissenschaften

Identification of microRNA 302

as an antagonist to p63 expression

INAUGURAL – DISSERTATION

zur Erlangung des Doktorgrades

der Medizinischen Fakultät

der Georg-August-Universität zu Göttingen

vorgelegt von

Andreas Scheel

aus Kassel

Göttingen 2010

Dekan: Prof. Dr. med. C. Frömmel

I. Berichterstatter: Prof. Dr. med. M. Dobbelstein

II. Berichterstatter/in:

III. Berichterstatter/in:

Tag der mündlichen Prüfung:

Table of Contents

Index of Abbreviations

α-	Anti-
AO	Antagonizing Oligonucleotide
ATP	Adenosintriphosphate
bp	Base Pairs
Brdm2	Mutant p63 allele without expression of α/β isoforms (Mills et al. 1999)
BS	Binding-site
BSA	Bovine Serum Albumin
c	Centi (10^{-2})
cDNA	Complementary DNA
ChIP	Chromatin Immunoprecipitation
CoA	Coenzyme A
C_t-Value	Threshold-cycle
Da	Dalton
DAPI	4,6-Diamino-2-phenylindole
DBD	DNA-binding Domain
Δx	Without x / Lacking x
DMEM	Dulbecco's Modified Eagle Medium
DMSO	Dimethyl Sulfoxide
DNA	Desoxyribonucleic Acid
dNTP	Desoxynucleosidtriphosphate
ds	Double-stranded
DTT	Dithiothreitol
EB	EB-Buffer
EDTA	Ethylenediaminetetraacetic Acid
eGFP	Enhanced Green Fluorescent Protein
EGTA	Ethylene Glycol Tetraacetic Acid
FCS	Foetal Calf Serum
HDAC	Histone Deacetylase
H_2O_{dd}	Double-distilled Water
IF	Immunofluorescence
GAPDH	Glycerinaldehyde 3-Phosphate Dehydrogenase
GTP	Guanosintriphosphate
h	Hour / Hours
K	Kilo(10^3)
L	Liter
LB	Luria Broth
LN_2	Liquid Nitrogen (-195,5°C)
LNA	Locked Nucleic Acid
µ	Micro (10^{-6})
m	Milli (10^{-3})
M	Molar
MeOH-RNA	2'-O-methylated Ribonucleic Acid
miR	MicroRNA Molecule
miRNA	MicroRNA
mRNA	Messenger-RNA
n	Nano (10^{-9})
N-	Amino-
NC	Nitrocellulosemembrane
nt	Nucleotides
OD_x	Optical Density at x Nanometers
p	Pico (10^{-12})
p63 -/-	p63 knock-out mouse (Yang et al. 1999)
PAGE	Polyacrylamide Gel Electrophoresis
PBS	Phosphate Buffered Saline
PCR	Polymerase Chain Reaction
PFA	Paraformaldehyde
PMSF	Phenylmethane-Sulphonylfluoride
PS	Phosphorothioate
QC	Quickchange
qRT-PCR	Quantitative real-time PCR
RISC	RNA-induced Silencing Complex
RLA	Relative Luciferase Activity
RLU	Relative Light Unit
RNA	Ribonucleic Acid
RNP	Ribonucleic Protein
ROI	Region-of-interest
rpm	Revolutions per Minute
RT	Room Temperature
SD	Standard Deviation
SDS	Sodium Dodecyl Sulfate
siRNA	Small Interfering RNA
ss	Single-stranded
TAD	Transactivation Domain
TAE	Tris-Acetate
TEMED	Tetramethyl-Ethylenediamine
Tris	Tris(hydroxymethyl)-Aminomethane
TSA	Trichostatin A
Tween-20	Polyoxyethylen(20)-Sorbitan-Monolaurat
v/v	Volume per Volume
U	Unit
UTR	Untranslated Region
WB	Western Blot
wt	Wild type / unmodified
w/v	Weight per Volume

Index of Figures

1 Introduction

1.1 The p53-family of transcription factors

1.1.1 Summary

Transcription factor p53 is a protein constitutively expressed in most cells of the human body. While quickly degraded by the ubiquitin-proteasome system under normal conditions, p53 protein is stabilized upon exposure to various extra- and intracellular stimuli and rapidly accumulates in the cells' nuclei. Depending on the nature, strength and duration of the stimulus, as well as the current state of the affected cell, p53 plays integral roles in the initiation of a spectrum of cellular responses ranging from growth arrest and repair to coordinated self-destruction of the cell, apoptosis (Figure 1.1). This power renders p53 one of the leading tumor suppressors. Disruption of p53 functioning in primary cells confers several characteristics of cancer cells at once, such as evasion of apoptosis and genomic instability; operational p53 is not tolerated by cancer cells (Hanahan and Weinberg 2000) .

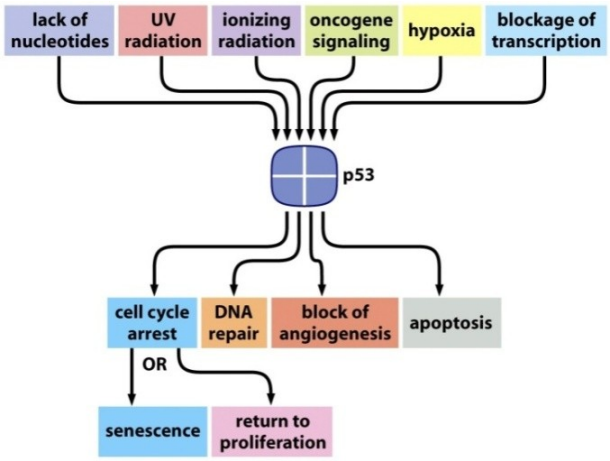

Figure 1.1: P53 activation and effects. P53 protein levels increase upon various stimuli and may cause a spectrum of responses spanning cell cycle arrest, DNA repair and apoptosis. The outcome depends on the type, strength and duration of the stimulus as well as on the cellular context (Adapted from Weinberg 2007, figure 9.8 p.316)

Consistently, p53 is the gene most frequently inactivated in tumors. Direct inactivation through mutation has been found in as many as 30-50% of all investigated tumors and in likely all other cases, p53 function is evaded by p53-antagonist MDM2 amplification, loss of p53 upstream-activator $p19^{ARF}$, or yet to be elucidated mechanisms (Vogelstein et al. 2000).

Two homologues of p53, termed p63 and p73 have been identified which share many structural and functional properties, yet have own expression patterns. While these genes may contribute to apoptosis, their main functions are distinct and are in contrast to p53 essential during development and in the maintenance of tissue stem cells. Relatively little is known about p63/p73 regulation. Especially the mechanisms underlying the temporal and spatial differences in expression have not been fully explained.

1.1.2 Target of viral proteins

The story of p53 started with a remarkable misinterpretation: p53 was first discovered in Simian virus 40 (SV40) infected mouse cells as a protein associated with SV40 Large T protein (Linzer and Levine 1979, Lane and Crawford 1979) and also in non-virus infected tumor cells. It could be demonstrated that transfection of primary fibroblasts with tumor-derived p53 cDNA facilitated malignant transformation in cooperation with known oncogenes (Eliyahu et al. 1984). These observations suggested p53 to be a cellular oncogene.

Only ten years later p53 was also cloned from primary, non-cancer cells and transfection of such cDNA inhibited rather than promoted malignant transformation (Finlay et al. 1989). The original tumor-derived cDNA turned out to harbour a point mutation causing substitution of one amino acid. This exchange was sufficient both to abolish the tumor suppressive properties and to make the resulting protein act dominant-negative on wild type cellular p53 (Hicks et al. 1991). It was subsequently revealed that p53 is not only frequently mutated in cancer cells but that it is also targeted by many viral proteins to hijack cell cycle control and to avoid apoptosis (reviewed by Levine 2009). Well-known examples besides SV40's Large T protein are the Adenoviridae which bind p53 through their E1b55k protein (Roth and Dobbelstein 2003) and the oncogenic types of human papillomaviruses which deregulate E6AP ubiquitin liagase via their E6 protein to increase p53 degradation (reviewed in Beaudenon and Huibregtse 2008). Viral proteins targeting p53 have been investigated intensively and are valuable research tools. However, no viral strategies to alter p63 or p73 functioning have been identified so far.

1.1.3 Functioning

P53 and its homologues act as tetramers (Figure 1.2a, Friedman PN et al. 1993, Davison et al. 1999). This explains how dominant-negative mutants exert their effect: If a wild type and a mutant allele are expressed at equal levels, 15 of the $2^4 = 16$ possible tetramers contain one or more mutant proteins reducing the level of functional complexes to 6.25% (Figure 1.2b).

It was indeed found that p53 mutations most frequently affect its DNA binding ability, while the region responsible for tetramerization is usually intact. Still, the p53 locus usually undergoes loss of heterozygosity in tumors, discarding the remaining wild type allele. It seems that even the remaining small amounts of functional p53 are disadvantageous for a cancer cells and are selected against.

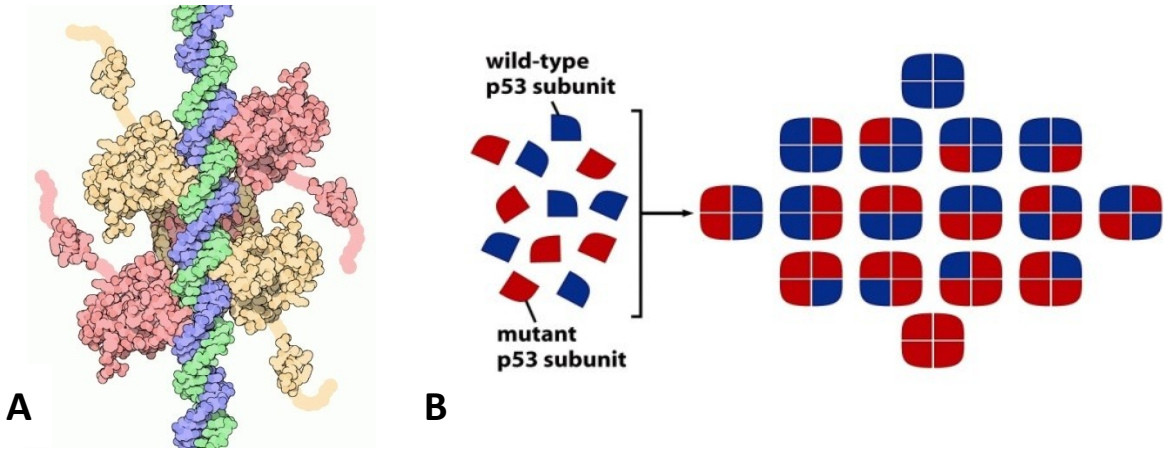

Figure 1.2: **P53 acts as a tetramer**. **A**: Illustration of tetrameric p53 bound to DNA. The free domains are the transactivation domains. (Illustration by D.S. Goodsell based on the crystal structure by Cho et al. 1994; taken from the protein database www.pdb.org by the Research Collaboratory for Structural Bioinformatics RCSB) **B**: Expression of mutant p53 from one allele reduces wild type tetramers to 1/16. (Diagram from Weinberg 2007, figure 9.7b, p.314)

P53 is an activator of transcription. The consensus sequence of p53-responsive genes is RRRCWWGYYY, R are purines, Y are pyrimidnes; W can be Adenine or Thymine. A p53-responsive element (RE) consists of two of these 10 base-pair (bp) sequences separated by a spacer of 0–21 bp (el-Deiry et al. 1992). Besides RE confirm to the consensus sequence, degenerated sequences may also be bound by p53.

P53-initiated apoptosis can be act both via the extrinsic and the intrinsic pathway. Activation of Bax, Noxa and Puma starts the intrinsic pathways while the extrinsic pathway can be influenced through regulation of Fas and induction of APAF1. MicroRNAs (miR) of the 34 family are directly induced by p53 and contribute to apoptosis (Hermeking 2007). Cell cycle arrest can be caused through induction of cycline-dependent kinases (CDK) inhibitors, p21 and p27 which bind and block cyclin-CDK complexes and cause arrest in G1-phase. Growth-arrest can also result from induction of miR-192 which regulates several transcripts involved in G1 and G2 checkpoints (Braun et al. 2008). P53 may induce XPC, -E and -G which are part of the global nucleotide-excision repair as well as translesion DNA-polymerases which circumvent damaged nucleotides and other proteins involved in DNA-repair.

Apart from its nuclear function, p53 has also been demonstrated to promote apoptosis through direct interaction with mitochondria and promotion of cytochrom-c release (Marchenko et al. 2000). In fact, p53 can induce apoptosis even in nuclei-free cytosolic extract (Ding et al. 1998) which highlights its abilities beyond regulation of transcription.

P63 can bind and transactivate many p53 regulated genes and can thus inflict cell cycle arrest and apoptosis (Yang et al. 1998). The isoform most potent in transactivation is TAp63γ which also most closely resembles p53. Besides common targets, p63 as well as p73 have also distinct targets which are not p53 responsive, such as cytokeratines involved in skin differentiation (e.g. K14) and developmental genes (e.g. Dlx3). ΔN isoforms may also activate certain genes even though they act repressive on most promoters. A direct interaction with mitochondria similar to p53 has not been described for p63.

1.1.4 Structure

The p53-family has a common structure composed of several distinct domains with specific functions: An amino-terminal transactivation domain (TAD, in p53 residues 1-43) is followed by a proline-rich domain (PRD, 61-94), the core is composed of a DNA-binding domain (DBD, 110-286) followed by an oligomerization domain (OD, 326-355) and regulatory elements towards the carboxyl terminus (residues 363-393) (Figure 1.3).

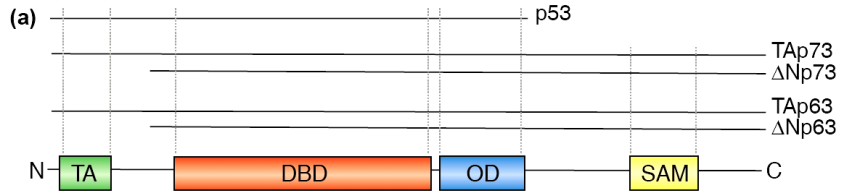

(b)

	TA	DBD	OD	SAM
p73 vs p63	37% (25%)	91% (86%)	74% (53%)	83% (53%)
p73 vs p53	30% (18%)	79% (62%)	33% (22%)	
p63 vs p53	26% (6%)	80% (58%)	31% (19%)	

(c)

	p63	p73	p53
DNA damage	+/–	++	+++
Cell cycle	+	++	+++
Apoptosis	+	++	+++
Senescence		+	+++
Development	Epidermal	Neural	
Knockout	Lethal	Severe	Late cancers

Figure 1.3: The p53 family. A: Protein domains in the different isoforms. ΔN isoforms lack the transactivation domain. **B:** Homology of the different family members. **C:** Comparison of involvement in different cellular processes and of knock-out phenotype. (Diagram from Melino et al. 2003, p.663)

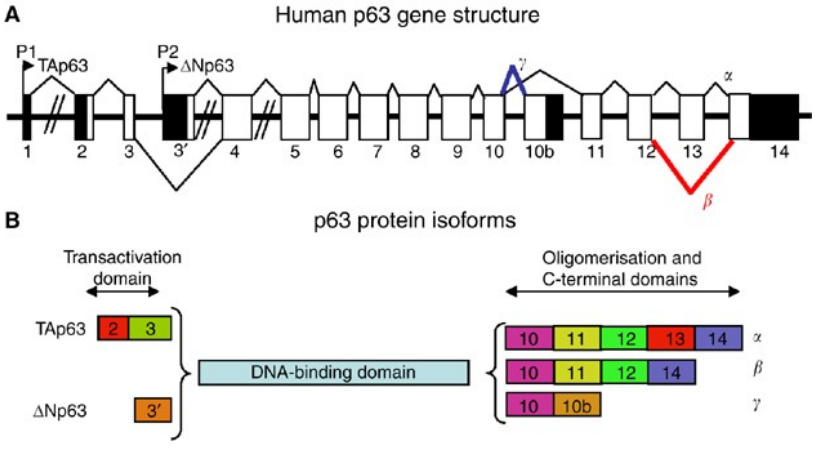

Figure 1.4: P63 isoforms. A: Gene structure, **B:** Proteins. Two N' terminal promoters give raise to isoforms containing (TA) or lacking (ΔN) the transactivation domain, C' terminal alternative splicing may skip exon 13 (β isoforms) or yield a different C' terminus (γ isoforms) (Diagram from Bourdon 2007, p.278)

Both p63 and p73 are subject to carboxyl-terminal alternative splicing and different promoters give rise to isoforms containing or lacking the TAD, termed TA- or ΔN- . In p63, α-isoforms contain 1-14 (TA) or 3'-14 (ΔN) while β-isoforms skip exon 13 and γ-isoforms end with an alternative exon 10' which is located between exons 10 and 11, though originally considered as exon 15. Thus, α- and β-isoforms share the same 3' UTR while the γ 3' UTR is distinct. Interestingly, only α-isoforms feature the sterile α-motif (SAM), a protein-protein interaction domain required for transactivation of certain genes (Figure 1.4, Yang et al. 1998, Radoja et al. 2007). Different isoforms have also been described for p53, yet the extend of the influence of such isoforms is controversial (reviewed in Murray-Zmijewski et al. 2006).

The DBD has a unique structure composed of two large loops held together by a coordinated zinc-ion that interact in the minor groove of the DNA and a loop-sheet-helix motif interacting with the major groove. The structure explains the destructive power of p53 point-mutations: One single improper amino acid side chain may render DNA-binding impossible. Particularly two arginines at positions 248 and 273 that directly interact with the DNA are most often subject of mutations (Cho et al. 1994).

The TAD, DBD and OD are the domains best conserved between p53/63/73 and between different species. P53 and p63/73 have around 60% similarity in their DBD including the most essential amino-acids responsible for DNA contact, while p63 and p73 even share approximately 80% (Figure 1.3 B, Deyoung and Ellisen 2007). Given their similar ODs, p63 and p73 may form heterotetramers, while they do not interact with wild type p53 on protein level. However, many DNA elements can be bound by more than one family member and synchronous expression likely causes competition (Davison et al. 1999, Yang et al. 1998). Phylogenetic analysis indicates that p63 is the oldest family member and might have given rise to p73 by gene duplication which in turn gave rise to p53 (Suh et al. 2006).

1.1.5 Core regulation

Regulation of p53 is as multi-sided as the functions it can exert. Usually strongly expressed in most cells, p53 is quickly bound by E3 ubiquitin ligase MDM2 via its TAD and is inactivated, ubiquitinated and degraded by the proteasome (Oliner et al. 1993). MDM2 is activated by p53 and a decrease of p53 subsequently also decreases MDM2 forming a feed-back loop. MDM2 is blocked by $p19^{ARF}$ which therefore indirectly elevates p53 levels (Zhang et al. 1998). ARF is itself blocked by p53, forming a second feed-back loop and can be directly

induced by E2F-1. E2F-1 in turn can be blocked by pRb linking the two pathways. Figure 1.5 summarizes this core regulation. On the level of a population of cells, p53-levels seem to be constant under normal conditions. However, if just a single cell is analyzed, an oscillation of p53 and MDM2 is revealed. Activation of p53 changes the frequency of these oscillations which enable p53 to execute its aforementioned functions (Lahav et al. 2004). Activation may occur via posttranslational modifications of p53: Signaling kinases such as Chk2 may phosphorylate p53's TAD, especially serine-15, and disrupt binding by MDM2. Similar effects may be caused by the small-molecule Nutlin-3a that fits into and clogs MDM2's hydrophobic binding-pocket (Vassilev et al. 2004). Many other posttranslational modifications have been described to altering p53 activation-status giving p53 the ability to differentially react to a broad range of cellular changes.

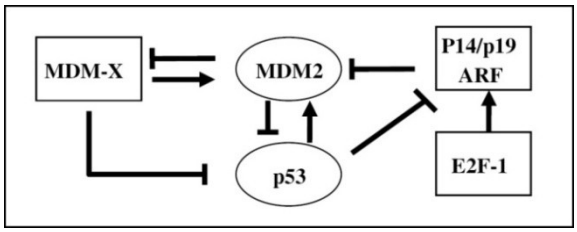

Figure 1.5: P53 core regulation. P53 is ubiquitinated by MDM2 causing its degradation. MDM2 is itself transcriptionally activated by p53 forming a feedback loop. $P19^{ARF}$ inhibits MDM2 by direct binding which increases proteolysis. $P19^{ARF}$ is itself blocked by p53 forming another regulatory loop (Figure adapted from Levine et al. 2006, p.1028)

E2F-1 can directly induce TAp73 which contributes to induction of apoptosis, while p53 can induce ΔNp73 by a p53RE in its promoter. Since ΔN73 expression counteracts p53, this constitutes another layer of regulation (Waltermann et al. 2003). However, these findings do not hold true for p63, for which neither a direct regulation by p53 nor E2F-1 has been found.

P63 is bound and ubiquitinated by ITCH, a HECT domain containing E3 ubiquitin ligase. The interaction partially resembles p53 degradation by MDM2, however, p63 is likely bound via a proline-rich-motif located in the C terminus rather than the TAD and also p63 has not been reported to induce ITCH. This interaction physiologically occurs in the skin and might be one of the mechanisms that downregulate ΔNp63α during keratinocyte differentiation (Rossi et al. 2006). ITCH has been reported to also downregulate p73 but not p53.

Despite p53's ability to directly induce a whole network of microRNAs (Hermeking 2007, Braun et al. 2008) no microRNAs upstream of the p53-family had been described at the start of this work.

1.2 The versatile roles of p63

1.2.1 Summary

Most proteins have families of homologues, yet p53 seemed to be an orphan for almost two decades. It was not until 1997 that its first homologue, p73, was discovered (Kaghad et al. 1997, Jost et al. 1997). By taking advantage of the strong conservation of the DBD (Figure 1.3), the third family member, p63, was identified a year later by PCR-screening of human and mouse genomic DNA (Yang et al. 1998), of urothelioma cDNA (Trink et al. 1998) and of skeletal muscle cDNA (Osada et al. 1998). Both p63 and p73 are expressed from two promoters yielding isoforms containing (TA-) or lacking (ΔN-) the N-terminal TAD. It was immediately recognized that the ΔN-isoforms could act in a dominant-negative fashion which occurs through two mechanisms: On the one hand, p53/63/73 can bind to the same sequence-elements which leads to gene-activation (TA) or repression (ΔN), though they each also have distinct target genes. On the other hand, given their strong homology, p63 and p73 form both homo- and heterotetramers and the balance of TA- and ΔN-isoforms is likely to determine the outcome of resulting tetramers (Lee HO et al. 2006, Davison et al. 1999). Direct interaction with p53 does not occur physiologically but apparently point mutations in p53's DBD leading to the mutant conformation also cause interaction with p63/73 which might partially explain the gain-of-function of p53 mutants. Surprisingly, the atypical interaction is mediated by the mutant p53's DBD rather than the OD (Gaiddon et al. 2001).

While p53 is ubiquitarily expressed in most humans tissues, p63 is expressed most strongly as ΔN-isoforms in stratified and transitional epithelia and in the prostate. Expression of TA-isoforms can be detected in germ-cells in both testes and the ovary, in the heart, kidneys, adrenal glands, thymus and in the nervous system.

First p63 knock-out mice where created in 1999 by deleting part of the DBD (Yang et al. 1999) and through insertional disruption leading to the mutant Brdm2 allele (Mills et al. 1999). While the $p63^{-/-}$ mouse by Yang et al. constitutes are true knock-out, it was recently revealed that the $p63^{Brdm2/Brdm2}$ mouse does express a functional p63γ-like protein in a physiological expression pattern and at normal concentrations (Wolff et al. 2009). Therefore, the Brdm2-mouse has to be considered a partial knock-out of α/β-isoforms.

Both model mice suffer from comparable, profound developmental defects which include the absence of hind-limbs, only rudimentarily developed fore-limbs, missing differentiation of the primitive ectoderm into epidermis together with the complete absence of skin-

appendage-structures such as hair-follicles, teeth and mammary-glands and also skeletal defects (Figure 1.6). While born alive, homozygous mice die shortly after birth due to dehydration and maternal neglect.

This phenotype is completely contrary to the $p53^{-/-}$ mouse which only occasionally exhibits little developmental defects but is strikingly susceptible to the formation of spontaneous tumors (Donehower et al. 1992, Sah et al. 1995). It was thus evident that p63 is more of a developmental gene than of a tumor suppressor. Later studies showed that $p63^{+/-}$ mice are developmentally sound but show a spectrum of spontaneous benign and malignant tumors (squamous cell hyperplasia and carcinoma, lung adenoma and histiocytic sarcoma) which differs from that of $p53^{+/-}$ mice (histiocytic sarcoma, osteosarcoma, thymic lymphoma and rhabdomamyosarcoma), indicating that while p63 does have tumor-suppressive properties, they are distinct of p53 (Flores et al. 2005).

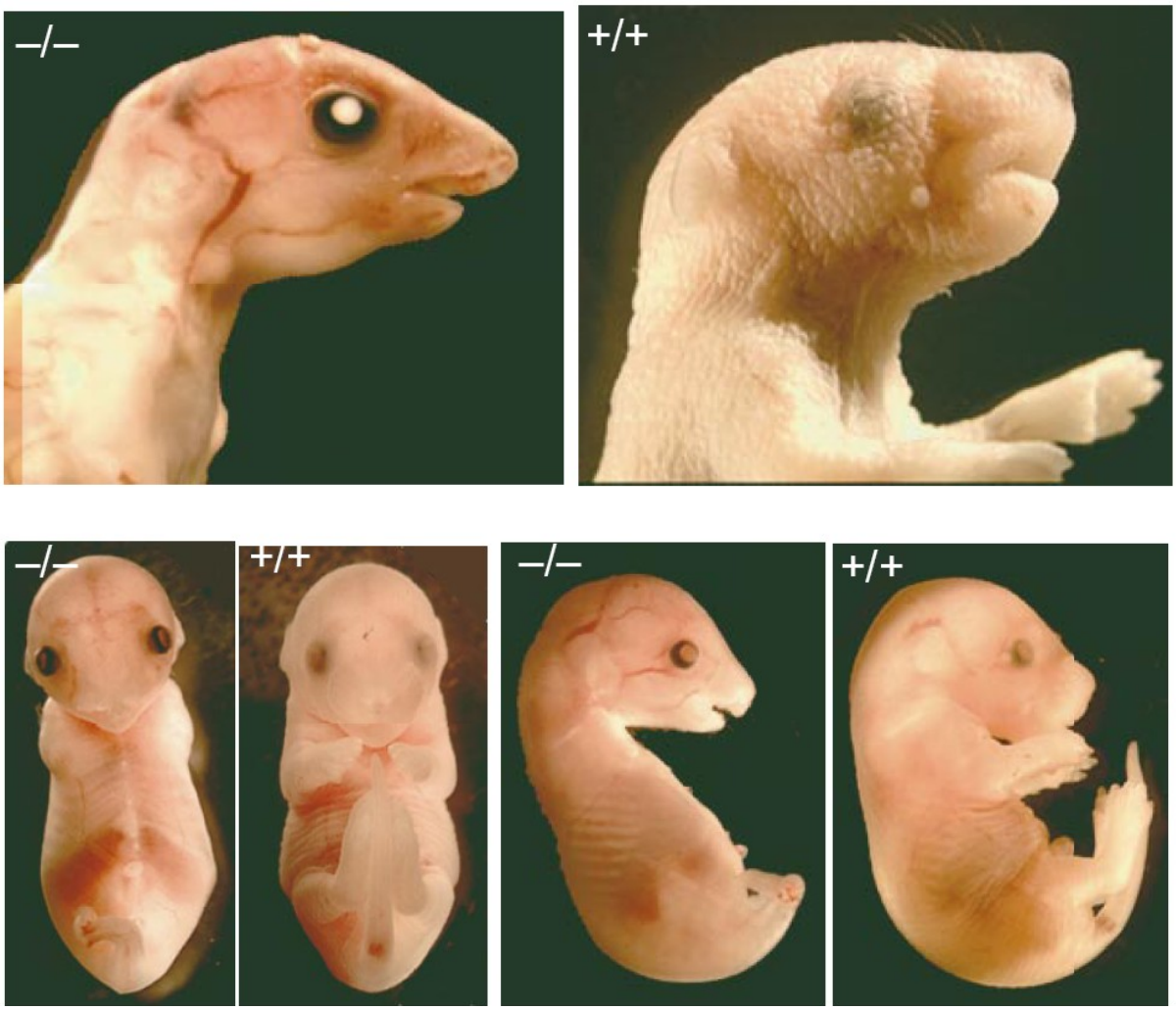

Figure 1.6: **Phenotype of $p63^{-/-}$ mice.** P63-deficient mice (-/-) show severe developmental defects compared to wild type (+/+) littermates. Differentiated epidermis and all skin appendage structures are missing, hind limbs are absent while fore limbs are just rudimentary. $P63^{-/-}$ mice are born alive but die shortly after birth from dehydration. (Photos from Yang et al. 1998, p.715)

1.2.2 Development and syndromes

Features of the $p63^{-/-}$ phenotype are reflected by six rare autosomal dominant human hereditary syndromes caused by p63 mutations: Ectrodactyly Ectodermal dysplasia Clefting (EEC), Split-Hand/Foot Malformations (SHFM) and the Acro-Dermato-Ungual-Lacrimal-Tooth (ADULT) Syndrome are caused by missense mutations within the DBD, while Ankyloblepharon Ectodermal dysplasia Clefting (AEC or Hay-Wells syndrome), Limb-Mammary Syndrome (LMS) and the Rapp-Hodgkin Syndrome are caused by mutations of the SAM-domain which is present only in the C terminus of α-isoforms. As indicated by the names of the syndromes, they constitute varying degrees abnormal development of the skin and its appendage structures and/or aberrant development of the extremities and of skeletal system (reviewed by Moll and Slade 2004).

Apparently, the SAM protein-protein interaction domain is essential for p63's functions during development. This is highlighted by both the similar phenotype of the full p63 knock-out mouse and the α/β partial knock-out as well as the similar symptoms of syndromes caused by mutations in the DBD and the SAM-domain. Indeed, it was demonstrated that p63α mutants from AEC patients have lost protein-protein interaction with ABBP1 which is required for alternative splicing of the fibroblast growth factor receptor 2 that is essential for differentiation of keratinocytes (Fomenkov et al. 2003). Also, transactivation of the homeobox gene Dlx3 by p63, another requirement for proper skin development, requires the presence of a functional SAM-domain (Radoja et al. 2007).

Besides p63 loss-of-function studies, forced expression has also been investigated. In certain contexts, p63 expression is sufficient to transdifferentiate epithelia and cause stratification, as demonstrated by the ectopical expression of p63 in the respiratory epithelium of the lung which causes transdifferentiation into a stratified phenotype (Koster et al. 2004).

1.2.3 Regulation of apoptosis; cancer

In-vitro reporter assays immediately confirmed that TAp63-isoforms may activate transcription of p53 target genes such as p21 and PUMA and may thus mediate cell cycle arrest and apoptosis in a similar fashion (Yang et al 1998). ΔN-isoforms, while also having distinct activation-properties on their own, may counteract transcriptional activation by TA-forms in a dominant-negative fashion which has also been described in-vivo during maturation of keratinocytes (Westfall et al. 2003).

Interestingly, TAp63α has only a little transactivation capacity compared to TAp63β and –γ due to the presence of a transactivation inhibitory domain (TID, Serber et al. 2002). The TID can be cleaved off by activated caspases causing TAp63α to contribute more efficiently to initiated apoptosis (Sayan et al. 2007). Of all isoforms, TAp63γ most closely resembles p53.

Besides the structural similarities p63 alterations occur only in a minority of tumors. The genomic region encompassing p63 is upregulated in early stages of certain carcinomas, especially in squamous cell carcinoma (SCC). The most abundant isoform in this context, ΔNp63α, was even termed 'amplified in squamous cell carcinoma' (AIS) by some authors (Hibi et al. 2000). P63 expression is frequently lost in more advanced SCCs and there seems to be a link to the epithelial-mesenchymal-transition (EMT), a cellular mechanism by which epithelial cells change their phenotype and acquire mesenchymal properties along with an increase in cell motility and invasiveness (reviewed in Scheel et al. 2007): On the one hand, it was demonstrated that EMT-inducing transcription factor Snail down-regulates ΔNp63α indirectly via repression of transcriptional enhancer C/EBP (Higashikawa et al. 2007) during tumor-progression, on the other hand, forced expression of TAp63α in the basal layer of the skin using a K14 promoter indirectly upregulates EMT-transcription factor Twist and causes skin hyperproliferation and an increase of carcinogen-induced skin tumors which also advance more rapidly (Koster et al. 2006). Given its frequent loss during progression of SCC, p63 expression is clinically correlated with the response to anti-cancer treatment with cis-platinum agents (Zangen et al. 2005).

P63 is expressed in the basal-layers of urothelium and of the prostate. In the later, p63 is a valuable diagnostic marker, as the expression is lost in most cases of prostate cancer and of its pre-invasive precursor, prostate intraepithelial lesion (Davis et al. 2002).

Investigation of $p63^{+/-}$ mice clearly shows an increased susceptibility to spontaneous tumor formation. This phenotype is aggravated in double-heterozygous $p53^{+/-}$, $p63^{+/-}$ mice and in $p73^{+/-}$, $p63^{+/-}$ mice. Interestingly, the later show a spectrum of tumors which features those tumors associated with deregulated p63-expression in humans (Flores et al. 2005). Evidence from the $p63^{Brdm2/Brdm2}$ mouse suggesting no higher susceptibility to spontaneous and induced tumors (Keyes et al. 2006) has to be seen under the recent finding, that such mice do express p63γ-like proteins which strongly resemble p53 (Wolff et al. 2009).

TAp63α appears to be the main mediator of apoptosis upon genotoxic stress in oocytes, where it is both the most abundant p63 isoform as well as the only p53 family member with nuclear localization. TAp63α expression can be observed in mice ovaries as the oocytes go into meiotic arrest. All primordial follicles show a strong nuclear expression of TAp63-protein which is again lost during maturation prior to ovulation (Suh et al. 2006). Expression of p63 and sensitivity to ionizing radiation are correlated and conversely, $p63^{-/-}$ oocytes lacking all p63 isoforms, as well as $TAp63^{-/-}$ oocytes specifically lacking TA isoforms, do not undergo apoptosis upon irradiation (Suh et al. 2006). This finding was confirmed in $p63^{Brdm2/Brdm2}$ mice which is consistent with the absence of TAp63γ in oocytes (Livera et al. 2008). In contrast to the differences in radiosensitivity, development of the oocytes and the ovary as a whole was normal in all three KO mice.

Interestingly, both Suh and Livera observe p63 phosphorylation upon irradiation of oocytes which occurs simultaneously with a pronounced increase in TAp63α transactivation activity. Suh et al. suggest that phosphorylation might counteract the TID at p63α's C terminus, though experimental dephosphorylation does not decrease the activity.

1.2.4 Stem cell maintenance and aging

Long-term studies of $p63^{Brdm2/+}$ mice revealed that the heterozygous loss of p63α/β isoforms is attended by reduced expectancy of life which is due to accelerated aging rather than increased tumor-formation (Keyes et al. 2005). Such mice have a median life span of 95 weeks while wild type littermates have a median expectancy of 121 weeks. Increased cellular senescence can be detected, i.e. cells which are considered to have permanently stopped cycling. They are characterized by increased activity of senescence-associated β-galactosidase and formation of nuclear bodies containing the promyelocytic leukemia protein as well as by higher protein levels of the tumor suppressors $p16^{Ink4a}$ and $p19^{ARF}$. Such cells have been described both as an endpoint of cultured cells and as an in-vivo finding associated with age. Senescence is considered an alternative cellular strategy to avoid tumor-formation at the cost of aging (Hayflick 1965, reviewed by Hoeijmakers 2009).

Accelerated aging has also been described in heterozygous $p53^{+/mt}$ mice, expressing an artificial mutant allele that is constitutively active (median life span 96 weeks vs. 118 of wild type littermates), as well as in pL53 mice which have about 20 copies of the temperature-sensitive Ala135Val mutant p53 allele. This allele is in mutant confirmation at 37.5°C and also causes greatly increased susceptibility for spontaneous tumors (Tyner et al. 2002).

However, 'super-p53' mice with 3 or 4 alleles of wild type p53 age at a normal rate while being more resistant to spontaneous tumors and to viral infections (García-Cao et al. 2002).

An isoform-specific knockout of TAp63 gives raise to normal developed mice which age much faster, the median life span of $TA^{-/-}$ mice is just 48 weeks compared to 102 weeks of wild type littermates. Investigation of the skin of $TA^{-/-}$ mice indicated that skin precursor cells located in dermal papillae and in the bulge region of hair follicles on the one hand proliferate at an increased rate but also undergo senescence more quickly while showing decreased genomic stability. Surprisingly, targeted-deletion of TAp63 only in cells expressing K14, a marker for the basal compartment of the skin, does not cause this phenotype (Su et al. 2009b). K14 is induced by ΔNp63 in what is considered the stem cell compartment of the skin by many authors. Finally, additional knockdown of $p19^{ARF}$, a tumor suppressor found upregulated in senescent cells, causes partial restoration of the defective development of $p63^{-/-}$ mouse (Su et al. 2009a).

Taken together, these findings suggest that a certain concentration of TAp63 and the balance of p63-isoforms are indispensable for the integrity of adult stem cells. This has been in particular investigated in the skin but might also hold true in other tissues. ΔN-isoforms on the other hand, seem to predominantly regulate the proliferating pool of keratinocytes in the basal layer of the skin and to guide terminal differentiation.

1.3 RNA-Interference and microRNAs

1.3.1 Biogenesis, composition and functioning

RNA (Figure 1.7) forms the core of the information flow in eukaryotic cells. Genetic information stored as DNA in the nucleus is mobilized, processed and regulated in the form of RNA and RNA is itself actively involved in the accomplishment of these tasks. During the 1970s and 1980s it became evident that RNA can spontaneously fold and give raise to tertiary structures capable of binding metal ions and other cofactors and of catalyzing chemical reactions. Such 'ribozymes' can also process RNA and the discovery of RNA-based ribonucleases and of self-splicing introns lead to the theorem of the 'RNA world' (Gilbert 1986). This

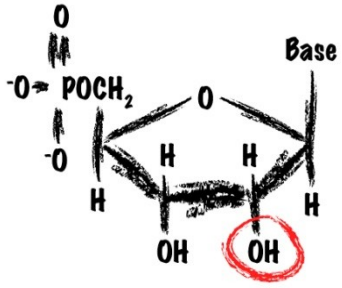

Figure 1.7: RNA nucleotide structure. RNA is distinguished from DNA by the hydroxyl group bound to the 2' carbon atom (highlighted red) which explains both the increased folding and interactions possibilities but also the decreased chemical stability. (Adapted from an illustration by Neilson and Sharp 2009, p. 569)

theorem suggests the origins of biological life to be RNA molecules forming hypercycles as described by Manfred Eigen, in which RNA serves as both the carrier of information and as the provider of catalytic activities. And indeed, ribozymes capable of RNA polymerization in a template dependent manner could experimentally created (Johnston et al. 2001).

Therefore it does not surprise that RNA is involved in essential cellular processes besides its role as messengerRNA (mRNA): RNA is a major component of the spliceosom machineries (reviewed in Wahl et al. 2009), as well as of ribosomes, contributes to mRNA processing and through transferRNA establishes the link between nucleic- and amino-acids. Another layer of regulation is formed by RNA-interference (RNAi), the regulation of transcription, mRNA stability and translation by small RNAs:

RNAi is caused by a ribonucleic protein complex termed RNA induced silencing complex (RISC) that binds to mRNAs and can cause various effects that influence translation and mRNA stability (Figure 1.8). Specificity of the RISC is mediated by 21-23bp long pieces of single-stranded RNA that interacts with mRNA by Watson-Crick base pairing (reviewed in Meister and Tuschl 2004). These can either be derived exogenously from small interfering RNAs (siRNAs) or can endogenously be created from RNA-coding genes which are transcribed as microRNAs (miRNA). During the 1990s evidence gathered about RNA capable of regulating other RNAs (Tuschl et al. 1995), cumulating in the observations that transfer of double-stranded RNA can downregulate genes in Caenorhabditis elegans (Fire et al. 1998) and in all other animalia, including human cell lines (Elbashir et al. 2001). In parallel, genes encoding RNAs causing RNAi were described in animalia, again first in C. elegans (Lee RC et al. 1993) and subsequently in all eukaryotes. While siRNA mediated RNAi is considered a defense mechanism against invasive nucleic acids such as transposons and transgenes as well as viral nucleic acids, miRNAs are a principle of gene regulation (reviewed in Carthew and Sontheimer 2009). Specific RNAi induced by artificially introduced RNA already has become an indispensable tool in the life sciences while the magnitude of its importance continuously raises (e.g. Moffat et al. 2006).

MiRNAs occur intergenic or in introns of other genes, alone or as clusters which give raise to polycistronic primary transcripts. Immediately after transcription each miRNA forms a self-duplex as they have a high internal complementary and is termed pri-miRNA. RNAse III enzyme Drosha cleaves these duplexes from the primary transcript with a characteristic 3'

overhang, the resulting hairpin-like structure is called pre-miRNA. Alternatively to Drosha-cleavage, splicing may also create pre-miRNAs. After export from the nucleus via Exportin 5, another RNAse III enzyme, Dicer, cleaves of the loop resulting in double-stranded RNA much like a siRNA. The strands are separated and preferentially one or both are associated with proteins of the Argonaute family to form the RISC (reviewed in Bartel 2004).

MiRNA binding is conferred mostly by the bases 2-8 of the miRNA, the so called 'seed'-sequence which has perfect complementarity with its target. The rest of the miRNA also contributes to the interaction both by classical Watson-Crick base pairing as well as by wobble pairs. This opens the possibility to investigate miRNA regulation by computational sequence analysis (Lewis et al. 2005, Griffiths-Jones et al. 2006) and indeed, sequence elements complementary to seed-sequences are found three times more frequently in the genome than could be explained by random distribution. These miRNA binding-sites are found in approximately 50% of all human protein coding genes, especially in transcription factors (Bartel 2004). Usually, several sites are found per gene, on average for four different miRNA indicating a functional redundancy (Friedman RC et al. 2009). Binding-sites are most frequently encountered in the 3' UTR of a mRNA though other locations are possible.

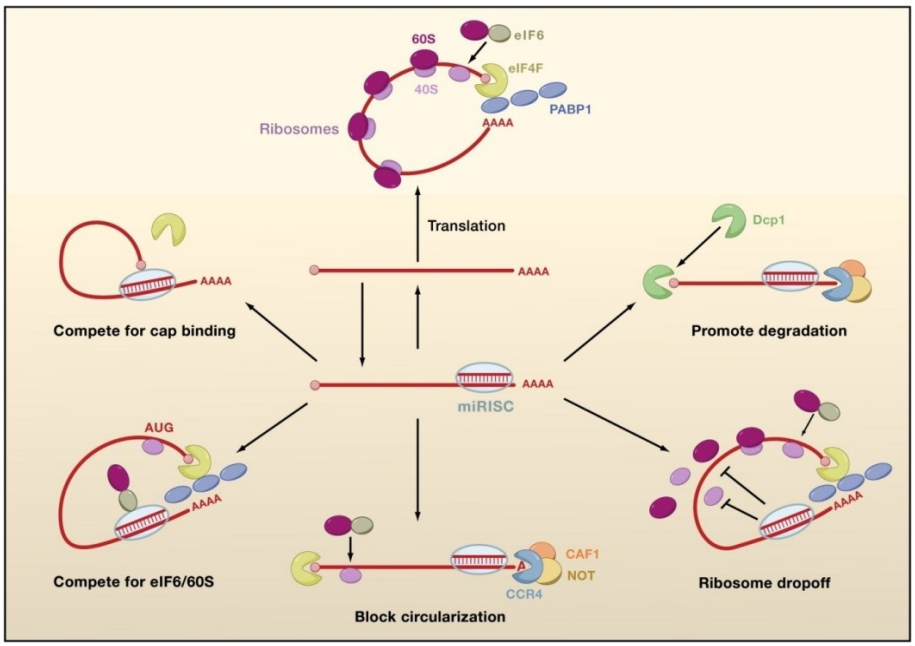

Figure 1.8: MicroRNA mediated effects. Guided by the specificity of miRNAs binding to their targets, the RISC complex mediates a spectrum of possible effects ranging from decreased translation to hydrolysis of the target mRNA. (Illustration adapted from Carthew and Sontheimer 2009, p.651)

MiRNAs are differentially expressed between cell types and during differentiation (Landgraf et al. 2007). Regulation by miRNAs has been proposed to contribute to differentiation by silencing genes involved in maintaining a more undifferentiated state (Bartel 2004). This fits with observed enrichment of miRNA binding-sites in transcription factors.

Currently, 751 miRNAs have been annotated in the human genome (miRBase, Griffiths-Jones et al. 2006), especially advances in deep-sequences techniques greatly increased the number of described miRNAs. Most miRNAs form families of homologous genes with related sequences adding another layer of redundancy.

1.3.2 Involvement in disease

Genetic alterations may affect any part of the human genome including non-coding RNA genes. Hence diseases caused by altered RNAs may result from deficits in any cellular mechanism which relies on RNA, ranging from splice defects both in cis and in trans to defective ribosome biogenesis (reviewed in Cooper et al. 2009).

Alterations concerning miRNAs have been predominantly described and investigated in cancer, though they also occur in other contexts such as degenerative and metabolic diseases. MicroRNAs in cancer frequently undergo changes of expression-levels including loss of tumor-suppressive miRNAs (e.g. Hermeking 2007, Braun et al. 2008) and overexpression of oncogenic miRNAs (e.g. Voorhoeve et al. 2006, le Sage et al. 2007). Changes of miRNA expression can affect different stages of cancer which is highlighted by miR-155, whose ectopical expression is sufficient to initiate leukemia in-vivo (Costinean et al. 2006) and by miR-10b and miR-373 which have been implicated in acquiring invasiveness during tumor progression (Ma et al. 2007, Huang et al. 2008). Most evidence is currently associative and only in some cases the precise mechanism of the respective miRNA has been satisfyingly explained (reviewed in Ventura and Jacks 2009).

The general loss of miRNAs by inactivation of central processing enzymes is oncogenic as is demonstrated by RNAi mediated knock-down of either Drosha, DGCR8 or Dicer (Kumar et al. 2007): Even though the RNAi strategy obviously only causes a reduction of miRNA maturation, several common tumor cell lines show a functional dedifferentiation indicated by increased proliferation in-vitro and tumorigenicity in-vivo as well as a faster progression of resulting tumors.

Changes in miRNA expression may be used as a 'finger-print' to identify clinical tumor samples in cases where other markers are insufficient (Ventura and Jacks 2009). A broad understanding of physiological and pathological miRNA functioning might translate into a myriad of therapeutic strategies should RNAi-based drugs overcome current difficulties in drug delivery (reviewed in Bonetta 2009).

1.4 Hypothesis

Given the impact of p63 on development and on stem cell maintenance (Yang et al. 1999, Keyes et al. 2005), together with its strong conservation among the vertebrates and the assumption that it is the 'oldest' member of the p53 family (Suh et al. 2006), we reasoned that microRNAs might be involved in establishing p63 expression patterns. MicroRNAs constitute an ancient regulatory principle found in all eukaryotes and contribute to differentiation by targeting transcription factors (Bartel 2004). To address this idea systematically, we chose to construct a high-throughput approach based the previously described 'miR-Vec' library of microRNA expression plasmids (Voorhoeve et al. 2006). Of the different possible experimental systems and read-outs, we selected quantitative immunofluorescence, as this technique allows the analysis of endogenous proteins. The two arising hypotheses are:

1.) P63 is regulated by microRNAs.
2.) Quantitative immunofluorescence in combination with the 'miR-Vec' library of microRNA expression plasmids (Voorhoeve et al. 2006) constitutes a suitable system to identify p63-regulating microRNAs .

To find arguments that support these hypotheses, this work describes the setting up, conduction and verification of a immunofluorescence based screen to identify p63-regulating microRNAs.

Since the experimentally setup of the experiments allowed to test the two hypotheses for p53 simultaneously just by adding another primary and secondary antibody during immunofluorescence staining, p53 regulation by microRNAs was addressed similarly.

2 Materials

2.1 Devices

Description	Name, Type	Manufacturer
Agitator, magnetic, heated	MR 3001	Heidolph, Schwabach, DE
Automation Workstation (Pipetting Robot)	BioMek 3000	Beckman Coulter Inc., Fullerton, CA, USA
Blotting-Chamber, semi-dry		Harnischmacher Labortechnik, Kassel, DE
Centrifuge, mini	GMC-060	LMS Co. & LTD, Tokyo, Japan
Centrifuge, tabletop, cooled	Centrifuge 5415 R	Eppendorf, Hamburg, DE
Centrifuge, tissue-culture, cooled	Megafuge 1.0 R	Heraeus /Thermo Electron, Waltham, MA, USA
Cryogenic Storage Unit	LS 4800	Tylor-Wharton, Theodore, AL, USA
+ Liquid Nitrogen Tank	XL 120	Tylor-Wharton, Theodore, AL, USA
Developing Machine	Optimax X-Ray Film Processor, 1170-1-000	Typon Medical, Burgdorf, Switzerland
Dispenser, semi-automatic, 96-well	MultiDrop Combi 836	Thermo Electron, Waltham, MA, USA
Electroporator	GenePulser 2	Biorad, Hercules Inc., CA, USA
Electrophoresis-System, SDS-PAGE	Minive complete	Amersham Biosciences, Piscataway, NJ, USA
Electrophoresis-Chambers, Agarose Gels	Mini 440; Midi 450	Harnischmacher Labortechnik, Kassel, DE
Fluorometer	Twinkle LB 970	Berthold Technologies, Bad Wildbad, DE
Freezer, -20°C	Liebherr "Premium" Product line	Liebherr Gruppe, Biberach an der Riss, DE
Freezer, -80°C	Hera freeze HFU 586 basic	Heraeus /Thermo Electron, Waltham, MA, USA
Fridge, 4°C	Liebherr "Premium" Product line	Liebherr Gruppe, Biberach an der Riss, DE
Genetic analyzer	ABI prism 310	Applied Biosystems, Carlsbad, CA, USA
Heating-Block, 96°C	HBT-1-131	Haep Labor Consult, Bovenden, DE
Hemocytometer	Neubauer improved	Brand GmbH, Wertheim, DE
Ice-Machine	B100	Ziegra, Ibernhagen, DE
Incubator, eucaryotic cultures, 37°C, 5% CO_2	Hera Cell 150	Heraeus /Thermo Electron, Waltham, MA, USA
Incubator, procaryotic cultures, 37°C	INB 400	Memmert, Schwabach, DE
Incubator, procaryotic cultures, 37°C, shaking	Minitron AI-70	Infors HT, Bottmingen, Switzerland
Laminar Flow Cabinet	Hera Safe HSPC12	Heraeus /Thermo Electron, Waltham, MA, USA
Luminometer	Centro LB 960	Berthold Technologies, Bad Wildbad, DE

Microscope, inverted, fluorescent	Axiovert 40 CFL	Carl Zeiss AG, Jena, DE
+ Mercury Arc Lamp	HBO 100	Osram GmbH, Munich, DE
+ Digital Photocamera	Powershot A620	Canon, Tokyo, Japan
Microcope, semi-automatic, fluorescent	Pathway HTS	Becton Dickinson, Franklin Lakes, NJ, USA
Microwave-Oven	MW 17705	Cinex GmbH, Ascheberg, DE
PCR-Machine	Thermocycler T personal	Biometra GmbH, Göttingen, DE
PCR-Machine, real-time	DNA Engine PTC 0200 + Chromo4TM	Biorad, Hercules Inc., CA, USA
pH-Meter	WTW-720	WTW, Weilheim, DE
+ pH-Electrode	WTW SenTix 21	WTW, Weilheim, DE
Pipets, adjustable, 0.1-2.5µL, 2-20µL, 20-200µL, 100-1000µL	"Research" 2100 product line	Eppendorf, Hamburg, DE
Pipet, 8-channel, adjustable 10-100µL	M100	BioHit, Helsiniki, Finland
Pipet, electric	Pipet Aid	Drummond Scientific, Broomall, PA, USA
Power Supply, Agarose-Gelelectrophoresis	PowerPac Basic	Biorad, Hercules Inc., CA, USA
Power Supply, SDS-PAGE	PowerPack P25T	Biometra GmbH, Göttingen, DE
Roller, for Falcon-Tubes	RM5 V-30 CAT	Labortechnik Fröbel, Lindau, DE
Scale, digital, De=0.1g	AccuLab LAC-6100.1	Sartorius, Göttingen, DE
Scale, digital, De=0.001g	LE62S	Sartorius, Göttingen, DE
Shaker	Promax 2020	Heidolph, Schwabach, DE
Shrink-Wrap-Machine	Vacupack Plus	Krups, Solingen, DE
Spectrophotometer	NanoDrop ND-1000	PeqLab, Erlangen, DE
Thermomixer	Thermomixer comfort	Eppendorf, Hamburg, DE
Timer, digital	WB388	Huger/ Oregon Scientific, Tualatin, OR, USA
UV-Transilluminator		Intas, Göttingen, DE
Vacuum-Pump	VacuSafe comfort	Integra Biosciences, Zürich, Switzerland
Vortex	Vortex-Genie 2 G-560E	Scientific Industries Inc., Bohemia, NY, USA
Water bath, 37°C	TW20	Julabo GmbH, Seelbach, DE

2.2 Software

Name, Version	**Producer (Commercial)**
Attovision 1.4	Becton Dickinson, Franklin Lakes, NJ, USA
BioMek System Software	Beckman Coulter Inc., Fullterton, CA, USA
MikroWin 2000	Mikrotek GmbH, Overath, Germany
MS Office 2007	Microsoft, Redmond, WA, USA
Vector NTI (10.3.0)	Invitrogen, Carlsbad, CA, USA

Name, Version	Source (Freeware / Public Licence)
BioEdit (7.0.9)	Tom Hall, http://www.mbio.ncsu.edu/BioEdit/BioEdit.html
Fluorescence Spectra Viewer	Invitrogen / Molecular Probes, Carlsbad, CA, USA, http://www.invitrogen.com/site/us/en/home/support/Research-Tools/Fluorescence-SpectraViewer.html
GENtle (1.8.7)	Magnus Manske, http://gentle.magnusmanske.de/
IDT OligoAnalyser	Integrated DNA Technologies, Coralville, IA, USA, http://eu.idtdna.com/analyzer/applications/oligoanalyzer/
NCBI Blast	National Center for Biotechnology Information, Bethesda, MD, USA, http://blast.ncbi.nlm.nih.gov
NEB Cutter	New England BioLabs, Ipswich, MA, USA, http://tools.neb.com/
R language for statistical computing (2.6.1)	R Foundation for Statistical Computing, Vienna, Austria, http://www.R-project.org
StrataGene QuickChange Design Tool	StrataGene / Agilent Technologies, Santa Clara, CA, USA, http://www.stratagene.com

2.3 Consumables

Describtion	Manufacturer
0.1 -10 µL Filtertips, RPT, steril	Starlab, Ahrensburg, DE
1.5 mL Safe-Lock Tubes	Eppendorf AG, Hamburg, DE
1000 µL Filtertips,Biosphere Filter Tips	Sarstedt AG, Nümbrecht DE
12-Well Plates, for cell culture	Greiner Bio-One GmbH, Frickenhausen DE
2 mL Safe-Lock Tubes	Eppendorf AG, Hamburg, DE
20 µL Filtertips,Biosphere Filter Tips	Sarstedt AG, Nümbrecht DE
200 µL Filtertips,Biosphere Filter Tips	Sarstedt AG, Nümbrecht DE
24-Well Plates, for cell culture	Greiner Bio-One GmbH, Frickenhausen DE
6-Well Plates, for cell culture	Greiner Bio-One GmbH, Frickenhausen DE
8 x 0.2 mL stripes for PCR	Bio-Rad GmbH, München, DE
96 well plate, black, for fluorometry	Greiner Bio-One GmbH, Frickenhausen DE
96-well plate, BD-Microtest, Optilux, black, clear bottom, sterile	Becton Dickinson, Franklin Lakes, NJ, USA
Adefodur Developing-Concentrate for developing machine	Omnilab , Bremen, DE
Adefodur Fixer-Concentrate for developing machine	Omnilab , Bremen, DE
Adhesive tape for labeling, autoclavable, blue	Heinemann Labortechnik, Duderstadt, DE
Adhesive tape for labeling, autoclavable, green	Heinemann Labortechnik, Duderstadt, DE
Adhesive tape for labeling, autoclavable, red	Heinemann Labortechnik, Duderstadt, DE
Aluminium Adhesive Seal for 96 well Platte	Heinemann Labortechnik, Duderstadt, DE
Cell-Scraper, 16 cm	Sarstedt AG, Nümbrecht DE
Cell-Scraper, 25 cm	Sarstedt AG, Nümbrecht DE
4-ChamberSlides, LabTek, glass; for IF	Nunc GmbH & Co. KG, Wiesbaden
Chromatography-Paper, 3MM, pure cellulose,	Whatman GmbH, Dassel, DE

460x570 mm	
Comb 1.5 mm, 10 lanes, for PAGE	Harnischmacher Labortechnik, Kassel, DE
Coverglasses, 24x55 mm, Farbr. Menzel	Harnischmacher Labortechnik, Kassel, DE
Eppendorf Combitips plus Standard, 0.1 mL	Eppendorf AG, Hamburg, DE
Eppendorf Combitips plus, Biopur, 10 mL	Eppendorf AG, Hamburg, DE
Falcon-Tube 15mL, 120x17 mm	Greiner Bio-One GmbH, Frickenhausen DE
Falcon-Tube 50mL, 114x28 mm	Greiner Bio-One GmbH, Frickenhausen DE
Gene Pulser Cuvette 0.1 cm gap for eletroporation	Bio-Rad GmbH, München, DE
Glasplates, 100x105x2 mm, for PAGE	Harnischmacher Labortechnik, Kassel, DE
Kryoboxes, laminated cardboard	Heinemann Labortechnik, Duderstadt, DE
Kryoboxes, PP, 9x9	Heinemann Labortechnik, Duderstadt, DE
Kryotubes CryoLine (1.8 mL)	Nunc GmbH & Co. KG, Wiesbaden
Microseal B Seal for PCR-plates	Bio-Rad GmbH, München, DE
Microtiter-Plates, PS, steril, U-shaped	Heinemann Labortechnik, Duderstadt, DE
Multiplate 96-Well unskirted PCR plates, white	Bio-Rad GmbH, München, DE
Nitrocellulose-Membran, Protan BA83 (30 cm x 3 m)	Omnilab , Bremen, DE
Pasteurpipettes, 150 mm, short	Heinemann Labortechnik, Duderstadt, DE
Pasteurpipettes, 230 mm, long	Heinemann Labortechnik, Duderstadt, DE
Petri-Dish , 92x16 cm,	Sarstedt AG, Nümbrecht DE
Pipette-Tips 0.1-2.5 µL, long	MBP / Heinemann Labortechnik, Duderstadt, DE
Pipette-Tips 0.1-2.5 µL, short	PSMI / Heinemann Labortechnik, Duderstadt, DE
Pipette-Tips 100-1000 µL	PSB / Heinemann Labortechnik, Duderstadt, DE
Pipette-Tips 20-200 µL	Greiner Bio-One GmbH, Frickenhausen DE
Safe Lock Tubes , Eppendorf, PCR clean, RNAse frei	Eppendorf AG, Hamburg, DE
Serological Pipettes 10 mL, sterile	Sarstedt AG, Nümbrecht DE
Serological Pipettes 25 mL, sterile	Sarstedt AG, Nümbrecht DE
Serological Pipettes 5 mL, sterile	Sarstedt AG, Nümbrecht DE
Sponge, Dacron, 9 x 10.5 cm, 6 mm (1/4") thick	GE Healthcare, Fairfield, CT, USA
Tissue culture dish, 100 x20 mm	Greiner Bio-One GmbH, Frickenhausen DE
Tissue culture dish, 145 x 20 mm	Greiner Bio-One GmbH, Frickenhausen DE
Tissue culture dish, 60 x 15 mm	Greiner Bio-One GmbH, Frickenhausen DE
X-Ray Films, Fuji, RX blue, 13x18 cm	Ernst Christiansen GmbH, Planegg, DE
X-Ray Films, Fuji, RX blue, 18 x 24 cm	Ernst Christiansen GmbH, Planegg, DE

2.4 Chemicals

Chemicals were purchased from Carl Roth GmbH & Co. KG, (Karlsruhe, Germany), Sigma-Aldrich GmbH (München, Germany) or Merck KGaA (Darmstadt, Germany) in 'pro analysi' grade unless stated otherwise.

2.5 Kits

Description	Manufacturer
10X Taq Buffer +KCl +15 mM MgCl2	Fermentas Inc., Burlington, ON, Canada
BCA Protein Assay Kit	Pierce / Thermo Fisher Scientific, Waltham, MA, USA
BigDye Terminator v3.1 Cycle Sequencing Kit	Applied Biosystems, Foster City, CA, USA
dNTP mix	Fermentas Inc., Burlington, ON, Canada
E.Z.N.A. Plasmid-Miniprepkit I	Peqlab Biotechnologie GmbH, Erlangen
E.Z.N.A. Plasmid-Miniprepkit II	Peqlab Biotechnologie GmbH, Erlangen
FuGene 6 Transfection-Reagent	Roche Diagnostics GmbH, Mannheim, De
HiPerFect Transfection-Reagent	Qiagen, Venlo, The Netherlands
iQ SYBR Green Supermix	Biorad, Hercules Inc., CA, USA
iScript cDNA Synthesis Kit	Biorad, Hercules Inc., CA, USA
Lipofectamine 2000 Transfection-Reagent	Invitrogen, Carlsbad, CA, USA
MinElute Gel Extraction Kit	Qiagen, Venlo, The Netherlands
mirVana miRNA Isolation Kit	Ambion, Austin, USA
Montáge Plasmid Miniprep 96 HTS Kit	Milipore, Billerica, MA, USA
PreMiR miRNA Precursor Molecules	Ambion, Austin, USA
QiaQuick PCR Purification Kit	Qiagen, Venlo, The Netherlands
Quant-iT dsDNA HS Fluorescent DNA Detection Kit	Invitrogen, Carlsbad, CA, USA
SuperSignal West Dura Extended Duration Substrate (Stable Peroxide Buffer and Luminol/Enhancer Solution)	Perbio Science GmbH, Bonn, De
SuperSignal West Femto Extended Duration Substrate (Stable Peroxide Buffer and Luminol/Enhancer Solution)	Perbio Science GmbH, Bonn, De
TaqMan MicroRNA Assays	Applied Biosystems, Foster City, CA, USA

2.6 Antibodies

Primary

Target-Protein	Name, ID	Type	Manufacturer
p63, all isoforms	4A4, sc-8431	Mouse, monoclonal	Santa Cruz Biotechnology, Santa Cruz, CA, USA
p53	FL-393, sc-6243	Rabbit, polyclonal	Santa Cruz Biotechnology, Santa Cruz, CA, USA
β-Actin	ab6276-100	Mouse, monoclonal	Abcam, Cambridge, UK
GFP	632375	Mouse, monoclonal	Clontech, Mountain View, CA, USA
p21	WAF1 Ab-1, OP64	Mouse, monoclonal	Calbiochem / Merck Ltd., Beeston, UK
phospho-Histone H2A.X (Ser139)	JBW301, 05-636	Mouse, monoclonal	Upstate / Milipore, Billerica, MA, USA
ITCH	ITCH, 611198	Mouse, monoclonal	BD Biosciences, Franklin Lakes, NJ, USA

Secondary

Type	Details	Manufacturer
α-Mouse HRP	Peroxidase-conjugated affiniPure F(ab')2 Fragment, donkey antimouse IgG (H+L)	Jackson ImmunoResearch, West Grove, USA
α-Rabbit HRP	Peroxidase-conjugated affiniPure F(ab')2 Fragment, donkey antirabbit IgG (H+L)	Jackson ImmunoResearch, West Grove, USA
α-Mouse AlexaFluor-546	Fluorophore-conjugated monoclonal antibodies, peak fluorescence 546nm	Invitrogen / Molecular Probes, Carlsbad, CA, USA
α-Rabbit AlexaFluor-647	Fluorophore-conjugated monoclonal antibodies, peak fluorescence 647nm	Invitrogen / Molecular Probes, Carlsbad, CA, USA

2.7 Oligonucleotides

Name	Direction	Sequence
Mutagenesis Primer:		
BS1_Mutagenesis	for	TGGGGGGCATTGAGTATTGTTTAAAATGTCGACTTGTTTTGGATGG
BS1_Mutagenesis	rev	CCATCCAAAACAAGTCGACATTTTAAACAATACTCAATGCCCCCCA
BS1_Mutagenesis_Verification	for	GCTTGCAGAACTGTAGCTG
BS1_Mutagenesis_Verification	rev	CATCATCGTCACTCACATGTAG
BS2_Mutagenesis	for	GTTGTACTTAAATGGTAATAAGTCGACTGTAAACTTCTGCAACAAG
BS2_Mutagenesis	rev	CTTGTTGCAGAAGTTTACAGTCGACTTATTACCATTTAAGTACAAC
BS2_Mutagenesis_Verification	for	GGGATAGTGGGATTTCCAGAAC
BS2_Mutagenesis_Verification	rev	GACATAGCTCGGAAGTCCTAG
Real-Time PCR Primer:		
hsa_p63_qRT-PCR	for	AGAGAGAGGGACTTGAGTTCTG
hsa_p63_qRT-PCR	rev	TGGTCCATGCTGTTCAGGAGC
hsa_GAPDH_qRT-PCR	for	GAAGGTCGGAGTCAACGGATTTG
hsa_GAPDH_qRT-PCR	rev	CAGAGATGATGACCCTTTTGGCTC
Antisense Oligos:		
anti-miR-302		[mA][mC][mU][mA][mA]A*A*C*A*T*G*G*A*A*G*C[mA][mC][mU][mU][mA]
reversed control α-miR-302		[mA][mU][mU][mC][mA]C*G*A*A*G*G*T*A*C*A*A[mA][mA][mU][mC][mA]
anti-miR-485		[mG][mA][mA][mU][mU]C*A*T*C*A*C*G*G*C*C*A*G[mC][mC][mU][mC][mU]
reversed control α-miR-485		[mU][mC][mU][mC][mC]G*A*C*C*G*G*C*A*C*T*A*C[mU][mU][mA][mA][mG]

All sequence are in 5'-3' orientation. N (A,T,G,C) DNA-bases, [mN] 2'-O-Methylated RNA-bases and * phosphorothioate-links. For / Rev: Direction, Forward or reverse.

2.8 Enzymes

Name	Manufacturer
Taq DNA-Polymerase	Fermentas Inc., Burlington, ON, Canada
Pfu Turbo DNA-Polymerase	Stratagene, La Jolla, USA
Restriction Enzymes	Fermentas Inc., Burlington, ON, Canada
T4 DNA-Ligase	Fermentas Inc., Burlington, ON, Canada
RNAse A	Qiagen, Venlo, The Netherlands
Calf Intestine Phosphatase	Roche Diagnostics GmbH, Mannheim, De

2.9 Vectors

2.9.1 Vector maps

pGL3control (Firefly luciferase reporter plasmid, SV40 promoter)

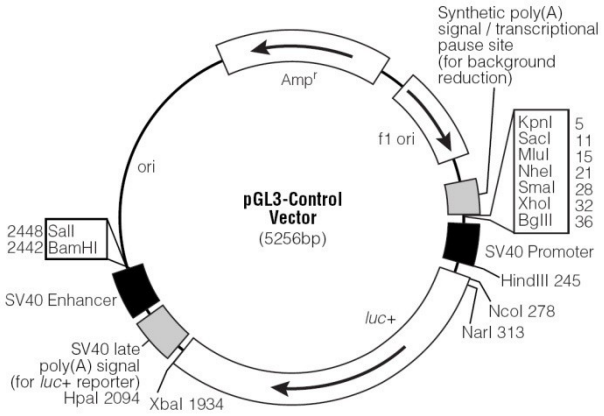

pMIR-report (Firefly luciferase reporter plasmid, CMV promoter)

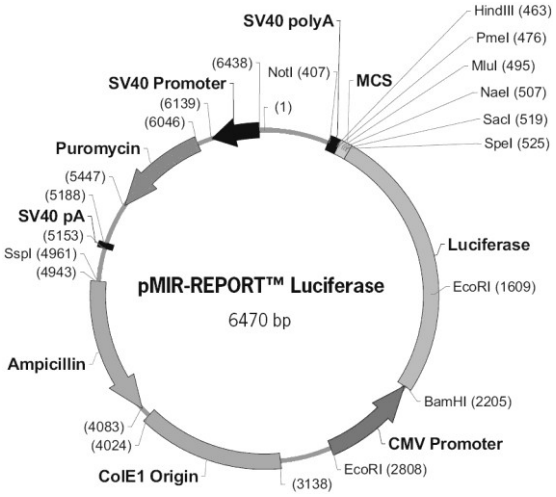

pRL-TK (Renilla luciferase expression plasmid)

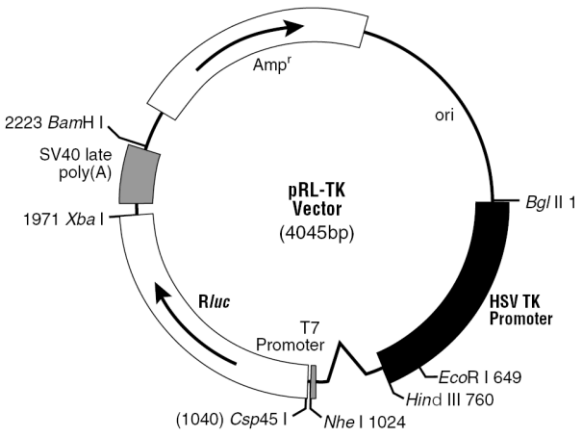

Both pGL3control and pRL-TK are products of Promega Corporation, Madison, WI, USA, pMIR-report is a product by Ambion, Austin, TX, USA. The vector maps are adapted from the respective manuals.

pcDNA3 (Universal expression vector, CMV promoter)

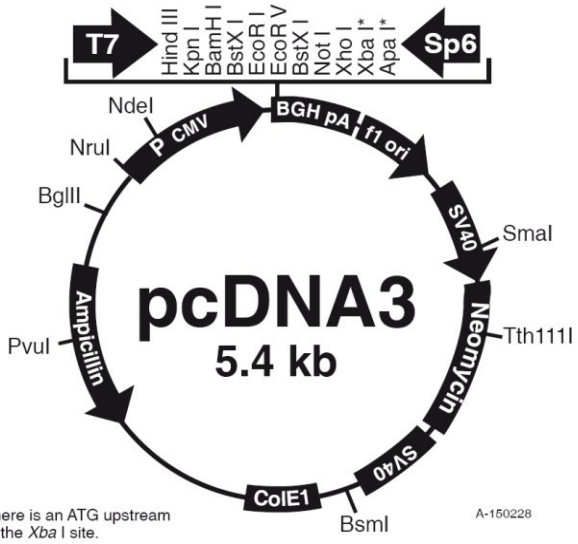

PcDNA3 is a product by Invitrogen Corporation, Carlsbad, CA, USA. The vector map is adapted from the manual.

2.9.2 Constructs

pcDNA3-p63α-3'UTR

A PCR fragment comprising the entire 5' UTR and coding sequence of TAp63α was amplified from human testes and cloned into the multiple cloning site of pcDNA3. The 2.8 kBp long p63α 3' UTR from an IMAGE clone (IMAGp998D2012268Q3) was cloned behind the fragment to obtain the native full length cDNA. The sequence was verified by DNA-sequencing forward and backward using primers binding either the T7 or Sp6 phage promoters.

pGL3control-p63α-3'UTR

The p63α 3' UTR from IMAGE clone (IMAGp998D2012268Q3) was cloned behind the luciferase gene using the XbaI restriction site. The sequence was verified by DNA-sequencing forward and backward using primers binding either the SV40 promoter or the SV40 late poly(A) signal.

pMIR-report-p53-3'UTR

The 1.1 kBp long 3' UTR of p53 was amplified from genomic DNA extracted from U2OS cells and cloned behind the luciferase gene of pMIR-report. The construct was verified by DNA sequencing forward and backward using primers binding the end of the luciferase gene and the end of the p53 UTR.

pSUPER-shp63

PSUPER is an expression plasmid for shRNAs. Be inserting a custom sequence, any protein may be targeted (Brummelkamp et al. 2002). A pSUPER construct directed against p63 (pSUPER-shp63) was a gift from Caterina Missero (Telethon Institute, Naples, Italy). The hybridizing sequence 5'-CAG CCA TGC CCA GTA TGT A-3' is part of p63 exon 6 which is contained in all known isoforms. After amplification of the plasmid in DH10B bacteria, the identity of the plasmid and the sequence of the insert was confirmed by DNA-sequencing forward and backward using primers binding either the T7 or T3 phage promoters.

pSUPER-shp53

This plasmid was a gift from Casimir Bamberger (ETH Zürich, Switzerland). The hybridizing sequence is 5'-GAC UCC AGU GGU AAU CUA C-3' and is contained in all p53 isoforms. After amplification of the plasmid in DH10B bacteria, the identity of the plasmid and the sequence of the insert was confirmed by DNA-sequencing forward and backward using primers binding either the T7 or T3 phage promoters. The pSUPER plasmid was created by TR Brummelkamp (Brummelkamp et al. 2002).

pRK5myc-ITCH

pRK5myc-ITCH C830A

These two plasmids were gifts from Tony Pawson (Karolinska Institute, Stockholm, Sweden). The C830A mutant has an inactivated HECT domain devoid of ubiquitination activity (Winberg et al. 2000). Expression of ITCH from both plasmids was verified by immunofluorescence with an antibody binding outside the HECT domain.

2.10 Bacteria

A strain of apathogenic, electro-competent Escherichia coli was used in all procedures requiring bacteria: ElectroMAX DH10B Cells by Invitrogen GmbH, Karlsruhe.

2.11 Eukaryontic cell lines

'5637'

'5637' is a bladder carcinoma cell line derived from a primary state 2 tumor in a 68-year old man (Fogh 1978). They are epithelial-like cells which grow remarkably adherent and are

known to produce a range of cytokines (SCF, IL-1, IL-6, G-CSF, GM-CSF etc.). Like all urothelia, 5637 constitutively express p63, mostly ΔNp63α (Lee HO et al. 2006). Cells were obtained from DSMZ, Braunschweig, Germany.

Remarkable mutations: TP53 (R280T), pRB1 (Y325*)

Growth medium: RPMI 1640, 10% FCS, Glutamine 2mM; Antibiotics: Penicillin (50 units/mL), Streptomycin (50 µg/mL), Tetracycline (2 µg/mL)

NCI-H1299

A cell line derived from a lymphnode-metastasis of non-small cell lung carcinoma (adenocarcinoma) of a 43-year old male. This cell line has a partial p53-deletion and is devoid of p53-expression ($p53^{-/-}$). Adherently growing cells with a remarkably high transfection-efficiency. Cells were a kind gift by Arnold Levine (formerly Princeton University, now Rockefeller University, NY, USA).

Growth medium: DMEM, 25mM HEPES, 10% FCS, Glutamine 2mM; Antibiotics: Penicillin (50 units/mL), Streptomycin (50 µg/mL), Tetracycline (2 µg/mL), Ciprofloxacin (10 µg/mL).

U2OS

An osteosarcoma cell line derived from primary sarcoma of the tibia of a 15-year old girl in 1964. Adherently growing cells devoid of telomerase-overexpression and with numerous chromosomal aberrations. The remarkable qualities of this cell line is their wild type, functionally active TP53 and their high plasmid-transfection efficiency. Cells were obtained from ATCC, Manassas, VA, USA (ATCC-Number: HTB-96).

Growth medium: DMEM, 25mM HEPES, 10% FCS, Glutamine 2mM; Antibiotics: Penicillin (50 units/mL), Streptomycin (50 µg/mL), Tetracycline (2 µg/mL), Ciprofloxacin (10 µg/mL).

GH

A human testicular germ cell tumor cell line. Adherently growing cells expressing wild type p53 and low amounts of p63, mostly TAp63γ. Treatment with Trichostatin A (100-500nM) quickly causes an increase in p63-expression; on immunoblots, mostly TAp63α is detectable. These cells were a kind gift by Roswitha Löwer (Paul Ehrlich Institute, Germany).

Growth Medium: DMEM, 25mM HEPES, 10% FCS, Glutamine 2mM; Antibiotics: Penicillin (50 units/mL), Streptomycin (50 µg/mL)

3 Methods

3.1 Buffers & self-made reagents

10x Blot Transfer Buffer (BTB)

Tris	48mM
Glycine	39mM
SDS	10 % (w/v)

1x BTB

10x BTB	10%
Methanol	20%

DNA Loading Buffer 6x

Saccharose	40 % (w/v)
Glycerol	10 % (w/v)
Bromphenol blue	0.25 % (w/v)

Elution Buffer

Tris pH 8.5	10mM

Laemmli Buffer 6x

Tris-HCl pH 6.8	0.35 M
Glycerol	30 % (v/v)
SDS	10 % (w/v)
DTT	9.3 % (w/v)
Bromphenol blue	0.012 % (w/v)

LB-Agar

Bacto-Agar	7.5 g
LB-Medium	ad 500 mL

LB-Medium

Trypton	1 % (w/v)
Yeast extract	0.5 % (w/v)
NaCl	0.5 % (w/v)

Luciferase Buffer, Firefly

Glycylglycine	25mM
K_2HPO_4	15mM
EGTA	4mM
pH 8.0	

Luciferase Buffer, Renilla

NaCl	1.1 M
Na_2EDTA	2.2mM
K_2HPO_4	0.22 M
pH 5.1	

Luciferase Working Solution, Firefly

$MgSO_4$	15mM
ATP	4mM
DTT	1.25mM
CoA	0.1mM
Luciferin	80µM
in Luciferase Buffer, Firefly	

Luciferase Working Solution, Renilla

BSA	0.5mg/mL
NaN_3	1.5mM
Coelenterazine	1.5µM
in Luciferase Buffer, Renila	

Phosphate Buffered Saline (PBS)

	Final Concentration	**10x**
NaCl	137 mM	1.35M
KCl	2.5 mM	25mM
Na_2HPO_4	8 mM	80mM
KH_2PO_4	1.47 mM	14.7mM
pH 7.4		

PBS++

PBS	1x
$CaCl_2$	0.9mM
$MgCl_2$	0.5mM

PBS-T

PBS	1x
Tween-20	0.1 (v/v)

Blocking Solution (for PAGE)

PBS-T	1x
Milk powder	5 % (w/v)

Ponceau S Solution

Ponceau S	0.5 % (w/v)
Acetic acid	1% (v/v)

RIPA-Buffer

Tris-HCl pH 7.5	20 mM
EDTA	10 mM
NaCl	150 mM
Deoxycholic Acid	1 % (w/v)
SDS	0.1 % (w/v)
Triton-X 100	1 % (v/v)
Iodoacetamid	10 mM
PMSF	1 mM
Trasylol	5 % (v/v) (equals 100,000 KIE)

SDS Running Buffer (for PAGE)

Tris-Base	25 mM
Glycin	192 mM
SDS	0.1 % (w/v)

Tris-Acetate (TAE)

	Final Concentration	**50x**
Tris-Base	40mM	2M
EDTA	2mM	0.1M
Acetic Acid	40mM	1M

3.2 Plasmid preparation

3.2.1 Bacteria transformation

Recombinant plasmids were amplified in-vivo using the apathogenic Escherichia coli strain DH10B. Commercial electrocompetent 'Electromax DH10B' were electroporated with the respective plasmid and plated on agar-plates. Selection of positive transformed bacteria was achieved by antibiotics contained in the agar which can only be sustained by transformed bacteria producing a resistence-factor that is expressed from the plasmid. In most cases, ampicillin was used as a selection-drug and β-lactamase as the appropriate resistence-factor.

3.2.2 Plasmid purification and quantification

Colonies of transformed bacteria were used to inoculate liquid cultures of LB-medium with the respective antibiotic. After 12-16h of incubation in a 37°C shaking incubator, plasmids were purified using E.Z.N.A. Plasmid-Miniprepkits (Peqlab). These kits provide a quick and convenient way of plasmid purification by combining alkaline lysis of the bacteria and spin-column purification. RNAse-A treatment ensured DNA-puritiy. Quantification and quality verificatiion was performed by photospectroscopy using a NanoDrop spectrometer (Peqlab).

3.2.3 Glyercol stocks

Small quantities of the liquid bacteria-cultures can be stored for extended periodes at -80°C if the are mixed with 80% glycerol in a ratio of 5:1 (e.g. 250 µL culture + 50 µL glyercol 80%) and frozen rapidly. This has the advantage of sparing the transformation step if the plasmid has to be prepared again, as tiny fragments of the frozen culture can be used to inoculate a new liquid culture.

3.3 Eukaryotic cell culturing

3.3.1 Culturing of adherent eukaryotic cells

Several cell lines derived from human tumors were cultivated in tissue-culture dishes. These dishes have a modified surface that allows attachment of adherently growing cells, the lid lies loosely to allow ventilation. Cells were incubated at 37°C, 5% CO_2, atmospheric oxygen and saturated humidity. Cultures were checked for visible contaminations every day as can be detected by a clouding of the medium or visible objects in phase-contrast microscopy; tests for mycoplasm-contamination were performed twice per year. Experiments were usually performed in well-plates.

3.3.2 Media

Reagents:

RPMI Medium 1640	Gibco/ Invitrogen, Carlsbad, CA, USA
Dulbecco's Modified Eagle Medium, 25 mM HEPES (DMEM)	Gibco/ Invitrogen, Carlsbad, CA, USA
Fetal Calf Serum (FCS)	Gibco/ Invitrogen, Carlsbad, CA, USA
L-Glutamin	Gibco/ Invitrogen, Carlsbad, CA, USA
Penicillin-Streptomycin solution	Gibco/ Invitrogen, Carlsbad, CA, USA
Tetracycline	Sigma Aldrich, St. Louis, MO, USA
Ciprofloxacin (Ciprobay)	Bayer AG, Leverkusen, De
Trypsin	Gibco/ Invitrogen, Carlsbad, CA, USA
PBS	See section 3.1

'5637' cells were grown in 'RPMI + S +A': RPMI 1640, 10% FCS, Glutamine 2mM; Antibiotics: Penicillin (50 units/mL), Streptomycin (50 µg/mL), Tetracycline (2 µg/mL).
Plasmid transfections were performed in 'RPMI +S –A': RPMI 1640, 10% FCS, Glutamine 2mM; No antibiotics. Transfections mixes were prepared in 'RPMI –' : Pure RPMI 1640.

NCI-H1299 and **U2OS cells** were grown in 'DMEM +S +A': DMEM, 25mM HEPES, 10% FCS, Glutamine 2mM; Antibiotics: Penicillin (50 units/mL), Streptomycin (50 µg/mL), Tetracycline (2 µg/mL), Ciprofloxacin (10 µg/mL). **GH cells** were grown in a similar medium without tetracycline and without ciprofloxacin. Plasmid-transfections were performed in 'DMEM +S –A': DMEM 1640, 10% FCS, Glutamine 2mM; No antibiotics. Transfections mixes were prepared in 'DMEM –' : Pure DMEM.

3.3.3 Splitting and counting

Cells were splitted every 3 – 4 days in a ratio of 1:4 – 1:8 to keep them at a reasonable confluency of 20 – 70%. If required, medium was changed in between. Splitting of all described adherent cell lines was performed by aspirating the old medium, carefully washing the cells with PBS (37°C), adding a thin layer of trypsin serin proteinase (37°C) to hydrolyze extracellular proteins responsible for cell-attachment and incubation until all cells were detached. For 100 x 20 mm dish, about 3 mL trypsin are required and detachment occurred within 3 – 10 minutes, depending on activity of the trypsin and specific cell-type; while H1299 and GH cells detach easily, 5637 cells required longer incubation. Afterwards, cells were resuspended in fresh medium (37°C) and diluted as desired.

Cells in suspension were counted for experiments using a Neubauer improved hemocytometer. 10 µL cell-suspension were put in the cytometer, 4 x 1 mm^2 were counted using phase-contrast microscopy and the average was calculated to lessen variance.

3.3.4 Freezing and thawing

For long-term storage, cells were frozen in aliquots containing 2 – 5 * 10^6 cells in 1 mL cryomedium, i.e. 7:2:1 Medium (DMEM / RPMI 1640, depending on cell-line) : FCS : DMSO. After trypsinization, centrifugation and resuspension in cryomedium which had been precooled to 4°C, cells were immediately frozen at -80°C. 24 – 48 h later, they were transferred to the cryogenic storage unit which maintains a temperature of -196°C with liquid nitrogen.

Thawing was conducted carefully to avoid toxicity by the DMSO: The respective aliquot was rapidly thawed and as soon as possible dissolved in ~ 20 mL of appropriate medium, preheated to 37°C. After gentle mixing the cells were centrifuged (10 min, 800 rpm in the tissue-culture centrifuge), the supernatant was aspirated and the cells resuspended in 12 mL medium and transferred into a tissue-culture dish. Medium was changed again after 24 h to removed last traces of DMSO.

3.4 Transfer of nucleic acids

3.4.1 Plasmid transfection

Transfections with plasmids were usually conducted in 12-well plates using 4 µL Lipofectamine2000 and 1.2 µg total plasmid. Cells were seeded 24 h prior to transfection at a density of 80 000 cells/well in 1 mL appropriate medium with antibiotics. The plasmid and lipofectamine were diluted separately in 100 µL DMEM – (or RPMI –), incubated at room-temperature for 5 minutes and combined. The combined transfection-mixes were gently mixed and incubated for another 15 minutes at room-temperature. During the incubation, medium was removed from the cells to be transfected and replaced with 800 µL antibiotics-free medium, DMEM +S –A or RPMI +S –A (37°C). The ready transfection-mixes were then added dropwise to the wells. To ensure equal distribution, the well-plates were put on a rocking-platfrom inside the cell-culture incubator for 15 minutes. Cells were transfected for 4 h before the medium was replaced with DMEM +S +A (or RPMI +S +A).

The enhanced green fluorescent protein (eGFP) was often used as a transfection control. In fluorescence-microscopy, expression of eGFP was detectable starting 12 h after transfection. It should be noted that the total amount of plasmid was never changed. In case that less plasmid was to be transfected, the missing amount was filled up with the empty vector containing no insert. This is important as the ratio of transfection-agent to plasmid influences the formation of plasmid-containing micelles.

For the 24-well format, 600 ng plasmid were used with 2 µL Lipofectamine2000 and approximately 40 000 cells/well in 500 µL medium were seeded 24h prior to transfection.

3.4.2 Antisense-Oligonucleotid transfection

To antagonize microRNAs 302a-d simultaneously, the following hybrid-oligo was used:

5'- [mA][mC][mU][mA][mA]A*A*C*A*T*G*G*A*A*G*C[mA][mC][mU][mU][mA] -3'

[mN] indicate 2'-O-MeOH-RNA bases, N DNA bases and * phosphorothioat-bonds. This sequence has a perfect complementarity to miR-302b and single nucleotide mismatch to miR-302a,c,d (Figure 4.16). A similar hybrid-oligo with reversed sequence served as negative control. For experiments, GH cells were seeded 30h prior to transfection in 12-well plates, 70 000 cells/well. Transfections were performed using 8µL HiPerFect and a final antisense-oligo concentration of 200nM. TAp63α was induced 16h after transfection using 150nM Trichostatin A and cells were harvested 16-36h later.

The antagonization of microRNA-485 was done using an oligo construct with the sequence:
5'-[mG][mA][mA][mU][mU][dC]*A*T*C*A*C*G*G*C*C*A*G[mC][mC][mU][mC][mU]
A likewise constructed oligonucleotide with reversed sequence was used as negative control. Since the same GH cells were used to investigate miR-302 and miR-485, similar transfection conditions were chosen.

3.4.3 SiRNA transfection

Endogenous p63 was antagonized by using a siRNA with the sequence 5'-AAC CAU GAG CUG AGC CGU GAA-3' and its reverse complement. For GH cells, transfection was performed by incubation of 70,000 cells/well in 12-well-plates for 40h with 100 nM siRNA combined with 2 µL Lipofectamine2000. GH cells were seeded 30h prior to transfection.

3.4.4 Pre-miR transfections

5637 cells were 'reverse transfected' in 6-well plates using 5µL Lipofectamine™2000 and the respective Pre-miRs™ (Ambion) at 5nM final concentration by seeding 300 000 cells/well and immediately adding the transfection-mix. Fresh medium was added after 24h and the cells were harvested 48h after transfection.

3.5 Protein-Detection with immunoblots

Proteinsblots with antibody staining of specific proteins (Immunoblots) were achieved by lysing the cells to be analyzed in a denaturing buffer, separation of the proteins by denaturing gel electrophoresis, blotting of the separated proteins on a nitrocellulose membrane, binding of the desired protein by peroxidase-coupled antibodies and subsequent chemoluminescence detection:

Cell lysis

Adherently growing cells were either scraped into the growth medium or detached by incubation with trypsin. The floating cells were transferred into ice-cold eppendorf cups and centrifuged 5min at 1200 rpm in a tabletop centrifuged cooled to 4°C. The growth medium was decanted and the cells lysed on ice in RIPA buffer, usually using 100µL for one well of a 12-well plate. 20µL 6x Laemmli buffer was added and the mixture was vigorously shaken to

ensure complete lysis. To denature the proteins, samples were incubated 5min at 96°C and either stored at -20°C or immediately used for gel electrophoresis.

Gel electrophoresis

To separate proteins, gel electrophoresis with sodium dodecyl sulfate (SDS) containing polyacrylamide gels (SDS-PAGE) was used. SDS is an anionic detergent that binds all proteins and causes them to be negatively charged. The charge is proportional to the length of the peptide chain of each protein, so the electrophoretic mobility mostly depends on protein size. A reducing thiol in the lysis buffer (dithiothreitol, DTT) removes disulfide bonds. By applying direct current, the denatured proteins move through a polyacrylamide gel.

This gel is composed of two different layers: Proteins first pass through a stacking layer which focuses the loaded proteins into a thin band, a larger resolving layer than separates the proteins. While the stacking layer was equal in all experiments, the acrylamide concentration of the resolving gel can be varied: Low concentrations result in bigger pores in the gel which are more suitable for separation of large proteins, high concentrations are more convenient for separating small proteins. Composition of different gels:

Stacking gel, 5% acrylamide

	5ml, 1 Gels	**8ml, 2 gels**
H_2O	3.4 mL	5.5 mL
30% acrylamide	0.83 mL	1.3 mL
1M Tris pH 6.8	0.63ml	1 mL
10% SDS in H_2O	50 µL	80 µL
10% APS in H_2O	50 µL	80 µL
TEMED	5µL	8 µL

Resolving gel, 25ml for two gels (15ml are sufficient for one gel):

Acrylamide concentration:	**8%**	**10%**	**12%**
H_2O	11.5 mL	9.9 mL	8.2 mL
30% acrylamide	6.7 mL	8.3 mL	10 mL
1.5M Tris pH 8.8	6.3	6.3	6.3
10% SDS in H_2O	250 µL	250 µL	250 µL
10% APS in H_2O	250 µL	250 µL	250 µL
TEMED	15 µL	10 µL	10 µL

The gels were cast with 1.5mm thickness. Prior to electrophoresis, cell lysates were incubated for 5min at 96°C, shaken vigorously at 4°C for 15min and centrifuged 5min at 13 000 rpm. Usually, 20 – 30µL lysate were loaded per lane. A dyed loading standard was included in all experiments to judge protein sizes and separation. Gels were run at 120V.

Blotting

Separated proteins were blotted onto nitrocellulose membrans with the semidry technique. Here, the gel lays on the membrane and three layers of whatman paper on either side of the stack are soaked with BTB buffer. The stack is placed in a semidry blotting chamber which applys an even direct current to the whole surface of the stack, causing proteins to move onto the membrane. Usually, each gel was blotted at a constant 16V for 90min. Equal transfer of the proteins was checked by Ponceau S staining, a reversible, general protein dye.

Immunostaining

To detect specific proteins, the membrans were stained with antibodies. After blocking the membrane for 30min in blocking solution containing 5% milk powder to inhibit unspecific binding, the membrane was incubated over night at 4°C with the primary antibody. The concentration depends on the respective antibody, on average 1:1000.

The membrans were washed 2x for 10min with PBS-T, put 1x 10min in blocking solution and incubate with with the secondary, peroxidase-coupled antibody for 1-2h at room temperature. The concentration of the secondary antibody depends on the expected strength of the signal, usually 1:10 000 was used, for BetaActin, 1:40 000 is sufficient. After washing the membrane again 3x for 10min with PBS-T, chemo-luminescence kits (Immobilon Western Chemiluminescent HRP substrate for most purposes, Super Signal West Femto for low-concentration proteins) were used to detect the bound antibodies. The signal was captured with x-ray films and the films developed with an Optimax X-Ray Film Processor.

3.6 Polymerase-Chain-Reaction

3.6.1 Standard PCR

Standard PCRs were used during cloning, site-directed mutagenesis and to establish primers for real-time PCR. A standard reaction is composed of the following volumina; for multiple reaction, a master mix can be prepared:

	Per reaction
10x Taq buffer KCl+	5 µL
20mM dNTP mix	0.5 µL
Primer rev 10µM	4.5 µL
Primer for 10µM	4.5 µL
TaqDNA-Polymerase	0.25 µL
25 mM $MgCl_2$	6 µL
Template	~ 1 µL
H_2O_{dd}	add to 50 µL

A standard program encompasses the following steps:

Temperature	Time	Step	Cycles
95°C	1-2 min	DNA melting	1
95°C	30 sec	DNA melting	30-40
60°C	30 sec	Primer annealing	
72°C	0.5-2 min	Extension	
45-95°C		Melting curve	1

The annealing temperature depends on the respective primers, the extension time correlates with the expected product (1min/500bp) and the cycle-number with the template concentration and primer specificity.

PCR products can be visualized by agarose gel electrophoresis: 10-20µL PCR product are mixed with DNA loading dye (2-4µL to yield 1x concentration) and loaded onto a 1% or 2% agarose/TAE gel, depending on the size of the product. After running the gel 30-60min at 120V, the gel can be stained with ethidiumbromide and the DNA visualized by UV illumination.

3.6.2 Quantification of mRNAs: Real-time PCR

Real-time PCR is the current standard technique to quantify expression of a manageable number of genes. The procedure encompasses the following steps: Total RNA is extracted from cells and is transcribed into cDNA using a reverse transcriptase kit. The cDNA is used as a template in a PCR which also contains an intercalating DNA dye, SYBR Green. The fluorescence signal increases proportionally with the amount of double-stranded DNA and allows quantification of a gene of interest relative to another gene or to different experimental conditions.

RNA extraction

RNA extraction was achieved by phenol-chloroform extraction: The cells of interest were lysed in Trizol (Invitrogen), a phenol / guanidinium thiocyanate mixture directly in their well-plate or dish, e.g. 1ml Trizol per well on a 6-well plate. The lysate was mixed with 200µL chloroform, vortexed vigorously and incubated for 5min at room temperature. Centrifugation for 15min at 12 000 rpm at 4°C caused separation of a lower organic phase and an upper aqueous phase, in which the RNA is dissolved. DNA and proteins precipitate in a visible interphase. The aqueous phase was carefully decanted without disturbing the interphase and the RNA was precipitated by the addition of 500µL isopropanol, 10min incubation at room temperature and centrifugation for 10min at 12 000 rpm at 4°C. The resulting pellet was washed with ethanol 100% and ethanol 70% to increase purity, air dried and finally resuspended in 20-50µL nuclease-free water (Ambion).

RNA concentration and purity was determined by photospectroscopy. The ratio of absorbance at 260nm to 280nm is indicative for DNA contaminations: A ratio of ~ 2.0 is considered contamination free RNA, pure DNA has a ratio of ~ 1.8. Contaminations with proteins will also cause lower ratios. The 260/230nm ratio is another indicator and should be 2.0 – 2.2 for pure nucleic acids. Carbohydrates and phenol have absorbance peaks near 230nm, Trizol has two peaks at 230nm and 270nm.

Sodium acetate precipitation

The purity of RNA as well as of any other nucleic acid such as PCR products, can be increased by sodium acetate precipitation: Per 30µl of nucleic acid sample, 1 µl EDTA 125mM, 1 µl sodium acetate 3M and 50µl ethanol 100% are added, the mixture is vortexed and incubated for 5 min at room temperature. Centrifugation for 15min at 14000 rpm without cooling separates a pellet which is washed with 70µl ethanol 70% and centrifuged for 10min at 14000 rpm. The supernatant is decanted and the pellet is air dried for 15 min and resuspended in an appropriate volume of nuclease free water.

Reverse transcription

Reverse transcription was done with the iScript™cDNA Synthesis Kit (Biorad). It relies on a modified Moloney murine leukemia virus-derived reverse transcriptase and contains all necessary ingredients for the reaction in addition to an RNAse inhibitor. Random hexamer primer as well as oligo dT-primer which bind the 3' end of mRNA are used to transcribe all mRNAs into cDNAs. The following volumina are necessary for one reaction and were prepared as master-mixes without RNA for multiple samples:

	Per sample:
5x iSript Reaction mix	4 µL
iSript Reverse Transcriptase	1 µL
RNA	~ 1 µg total RNA
H_2O_{dd}	add to 20 µL

The ready reaction mix was incubated 5min at 25°C, 30min at 42°C and 5 min at 85°C. Resulting cDNA was immediately used for real-time PCR or stored at -20°C.

Real-time PCR and quantification

Real-time PCR was carried out with iQ^{TM} SYBR Green Supermix (Biorad), a ready-to-use PCR mix which already contains hot-start Taq polymerase. A master mix was prepared, per sample the following volumina are required:

	Final concentration	**Per reaction**
2x iQ supermix	1x	12.5 µL
H_2O_{dd}		10 µL
Primer forward 10µM	300 nM	0.75 µL
Primer reverse 10µM	300 nM	0.75 µL
cDNA		1 µL
Total volume		25 µL

A usual program is listed below, the annealing temperature depends on the respective primers:

Temperature	Time	Step	Cycles
95°C	3 min	DNA melting, iTaq DNA Polymerase Activation	1
95°C	15 sec	DNA melting	45
60°C	30 sec	Primer annealing	
72°C	45 sec	Extension	
45-95°C		Melting curve	1

During optimal reaction conditions, the DNA product increases exponentially. If the SYBR green derived fluorescence signal is plotted against the cycle number on a logarithmic scale, this exponential phase is visible as a straight line. A threshold cycle (C_t-value) is define, at which the fluorescence signal emerges from the background. The $\Delta\Delta C_t$ method allows relative quantification by comparing the C_t values of a gene of interest (gene) to a reference gene (ref). The relative expression is $2^{-(\mathrm{Ct(gene)}-\mathrm{Ct(ref)})}$ or $2^{-\Delta\mathrm{Ct}}$. The relative expression of a sample B can be normlized to a sample A by calculating $\frac{2^{\mathrm{Ct(ref\ B)}-\mathrm{Ct(gene\ B)}}}{2^{\mathrm{Ct(ref\ A)}-\mathrm{Ct(gene\ A)}}}$ which is $2^{\mathrm{Ct(ref\ A)}+\mathrm{Ct(ref\ B)}-\mathrm{Ct(gene\ A)}-\mathrm{Ct(gene\ B)}}$ or $2^{-\Delta\Delta\mathrm{Ct}}$. GAPDH, a standard reference gene, was used for normalization in all experiments.

3.6.3 Quantification of microRNAs: TaqMan assays

To quantify microRNAs, a slightly different approach compared to quantification of the longer mRNAs was chosen: Adjusted conditions are required to extract small RNA (< 200nt) from cell lysates. Give the tiny size of microRNAs, so called hairpin-primers are used which extend a specific microRNA and facilitate detection. Finally, instead of an intercalating DNA dye, fluorescently labeled probes are used, whose signal is activated upon incorporated into a new PCR-product ('TaqMan' probes by Applied Biosystems).

MiRNA extraction

MiRNAs were extracted using mirVana microRNA extraction kits (Ambion) which combine phenol-chloroform extraction with spin-column purification to separate RNAs < 200nt. The kit was used according the manufacturer's instructions and miRNAs where resuspended in nuclease-free water.

MiRNA reverse transcription

Given the tiny size of miRNAs, specialized primers are necessary which form a hairpin structured duplex. A overhang is complementary to a specific miRNA. Such primers cause the product of the PCR to be much longer than the original miRNA, facilitating detection. In this project, commercial primers by Applied Biosystems were used for the respective miRNAs and for RNU6B, a miRNA-sized non-coding RNA was used for normalization.

TaqMan assays and quantification

TaqMan probes (Applied Biosystems) are an alternative approach to real-time PCR: Instead of using an intercalating DNA dye, a DNA probe complementary to a specific product is used which is labeled with both a fluorophore and a quencher that extincts the emitted signal. Upon incorporation, the probe is hydrolyzed by the exonuclease-activity of Taq DNA-polymerase which releases the fluorophore. For relative quantification, the $\Delta\Delta C_t$ method as described in section 3.6.2 was used.

3.6.4 Site-directed mutagenesis

Site-directed mutagenesis is a specialized PCR method to deliberately change the nucleotide sequence of an expression plasmid. To achieve this, a long primer (~30 – 50nt) is designed which contains the changed sequence in its center. It is also possible to delete larger sequences by using a primer that bridges the ends. A reversed and complementary primer of the same sequence is added and the whole plasmid is amplified by PCR with an adequately long extension time. The product is purified and transformed into bacteria. The resulting colonies are checked for positive clones either by direct sequencing, or by PCR amplifying the region of interest and digestion of the resulting product with restriction enzymes that either cut or do not cut in positive clones.

MiR-302 binding sites within the human p63α-3'UTR were predicted with TargetScan (Lewis et al. 2005) and site-directed mutagenesis was performed using Pfu Ultra™ DNA-polymerase (Stratagene) and the following primers:

ΔBinding Site 1: (50bp deletion)

Forward 5'-TGGGGGGCATTGAGTATTGTTTAAAATGTCGACTTGTTTTGGATGG-3'

Reverse 5'-CCATCCAAAACAAGTACATTTTAAACAATGCACTCAATGCCCCCCA-3'

ΔBinding Site 2: (Insertion of 2bp)

Forward 5'-GTTGTACTTAAATGGTAATAAGTCGACTGTAAACTTCTGCAACAAG-3'

Reverse 5'-CTTGTTGCAGAAGTTTACAGTCGACTTATTACCATTTAAGTACAAC-3'

The design of the primers was facilitated by the StrataGene QuickChange Design tool are verified with the IDT OligoAnalyzer (see section 2.2) to make sure that the quite long primer do not form undesired hairpins, homo- or heterodimers. Figure 4.10 shows the p63 3' UTR sequence before and after mutagenesis.

Each mutagenesis PCR was prepared with:

	Final concentration	**Per reaction**
Pfu Buffer 10x	1x	5 µL
dNTP-mix, 20mM each	2mM	0.5 µL
Primer forward 10µM	500 nM	2.5 µL
Primer reverse 10µM	500 nM	2.5 µL
dsDNA (Plasmid)	1.5 ng/µL	75ng
Pfu Ultra (2.5U/µL)		1µL
H_2O_{dd}		add to 50µL
Total volume		50 µL

And performed with the program:

Temperature	Time	Step	Cycles
95°C	3 min	DNA melting	1
95°C	30 sec	DNA melting	20
55°C	1 min	Primer annealing	
68°C	18 min	Extension	
45-95°C		Melting curve	1

The annealing temperature depends on the respective primers.

Extension time is calculated by the formula 2min/kBp + 2min:

2min * (5.2kBp[pGL3control]+2.8kBp[p63 3'UTR]) + 2min = 2min * 8 + 2min = 18min.

In both cases, a new Sal1 restriction-site is created upon successful mutagenesis. Results were verified by restriction-digest with Sal1 (Fermentas) and by subsequent DNA-sequencing.

3.6.5 Dye-terminator sequencing

DNA sequences were determined with the dye-terminator method and capillary gel electrophoresis. This method consists of two steps: First, a PCR is performed with the unknown sequence as template. This can be either a PCR amplicon from a previous reaction, or a plasmid. Only one primer is used and the dNTP nucleotides are mixed with fluorophore-conjugated ddNTP nucleotides (BigDye Terminator v3.1 by Applied Biosystems). These nucleotides lack a 3' hydroxyl group which results in termination of a growing amplicon upon incorporation. Each base (A, T, C, G) is labeled with a different fluorophore. Since the incorporation occurs at random, products differing by one base will be created. Second, the products are resolved and detected by electrophoresis; in this work, by an automated capillary electrophoresis system (ABI prism 310) which determines the sequence by the order of the different fluorophores passing through an acrylamide filled capillary.

3.7 Dual-Luciferase-Assay

3.7.1 Principle

Luciferase-assays are a convenient method to quantify the impact of various sequence-elements on both transcription and translation. The sequence under investigation is cloned into a luciferase expression plasmid, either up- or downstream of the luciferase-gene and the plasmid is transfected into eukaryotic cells. After an appropriate incubation-time, the cells are lysed and the activity of the luciferase-protein is quantified using a luminometer. To normalize differences in transfection-efficiency, a second luciferase requiring a different substrate is cotransfected, hence the designation dual-luciferase assay (DLA).

In this work, the p63 3' UTR was cloned into a firefly luciferase expression-plasmid (pGL3control) and normalized against cotransfected renilla luciferase (pRL-TK, both plasmids by Promega Inc.). Activities were quantified on 96-well plates with a injector-coupled luminometer (Centro LB 960 by Berthold Technologies) using self-made substrates (cf. section 3.1, adapted from Dyer et al. 2000). For each well, firefly luciferase substrate is injected first and the luminescence is quantified before the substrate for renilla-luciferase is injected via a separate injector. The second substrate both provides the renilla luciferase with the colenterazine required for luminescence and quenches the firefly-luciferase with sodium azide (NaN_3), a potent enzyme inhibitor that leaves renilla-luciferase unaffected.

3.7.2 Coexpressions assays

To investigate possible direct microRNA-interactions, the pGL3control-p63-3'-UTR plasmid (cf. section 2.9) was cotransfected with miR-Vec plasmids. Renilla-luciferase was cotransfected for normalization. In an usual set-up, H1299 cells were seeded in 12-well plates 24 h prior to transfection, at a density of 80,000 cells/well in 1 mL DMEM +S +A. Transfections were performed by combining 4 µL Lipofectamine2000 and 1.2 µg total plasmid, i.e. 200 ng firefly-luciferase containing the 3' UTR, 50ng renilla-luciferase for transfection-control and either 950 ng control vector (hTR = miR-Vec control) or 800 ng miR-Vec plasmid coding for a microRNA and 150 ng control vector. The transfection-mix was prepared in DMEM – and the transfection carried out in DMEM +S –A. Fresh medium was added 4 h after transfection and DLA was performed 24 h after transfection. Similarly, the constructs containing UTR-sequences with mutated miR-302 binding sites were tested.

3.7.3 Assaying endogenous microRNA-activity

Firefly-luciferase constructs containing the wild type p63 3' UTR or mutated sequences lacking one or two putative miR-302 binding sites were expressed in GH cells which have high levels of endogenous miR-302 and for comparison in U2OS cells which lack miR-302 expression. Renilla-luciferase was coexpressed for normalization. Both GH and U2OS cells were seed in 24-well plates 24h prior to transfection at a density of 30 000 cells/well in 500 µL DMEM +S +A. Transfections were performed by combining 2 µL Lipofectamine2000 and 0.6 µg total plasmid, i.e. 50 ng firefly-luciferase containing the respective insert, 50ng renilla-luciferase and 500ng empty vector (hTR = miR-Vec control). Fresh medium was added 4 h later and DLA was performed 48 h after transfection.

3.8 MiR-Vec MicroRNA library screen

3.8.1 Plasmid preparation

The miR-Vec plasmids were prepared using Montáge Plasmid Miniprep 96 HTS kits (Milipore) on a BioMek 2000 laboratory automation workstation. Using the 96-well format, the kit combines alkaline lysis of liquid bacterial-cultures with mechanical plasmid separation. Plasmid concentrations were quantified using the Quant-iT dsDNA HS assay (Invitrogen) in combination with a BioMek 3000 workstation and a Twinkle LB 970 fluorometer. This fluorescence-assay can measure double-stranded DNA in concentrations from 0.01 ng/µL to

100 ng/µL so the prepared plasmids were diluted 1:50 since they yielded 200 – 900 ng/µL. After quantification, plasmids were diluted in elution buffer to 100 ng/µL stocks and to 35 ng/µL for use in the screen.

3.8.2 Transient transfection

5637 cells were seeded 10h prior to transfection on Falcon Optilux 96-well plates at a density of 7000 cells/well in a total volume of 150µL RPMI +S –A. To ensure equal seeding, 50µL medium were added to the wells before 100µL medium containing the 7000 cells were gently transferred by the BioMek 3000 Laboratory Automation Workstation. Transient transfections were performed with the BioMek using 0.6 µL FuGene 6 combined with 0.3 µg total plasmid/well, i.e. 270 ng miR-Vec plasmid and 30 ng eGFP expression plasmid for transfection control. The transfection-mixes were prepared with the BioMek at 1.3x concentration in 50µL RPMI –, i.e. 0.79µL FuGene + 0.39 µg plasmids. Transfection-mixes were incubated 20 minutes at room-temperature to allow formation of plasmid-FuGene micelles. The ready mixes were diluted to 65µL and 50µL were added to the cells, yielding the desired final concentrations. The extra 15µL were necessary since it is nearly impossible to accurately pipet all liquid from a well using an automatic device. After 24h of transfection the medium was changed; another 24h later, the cells were fixed with 4 % (v/v) formaldehyde.

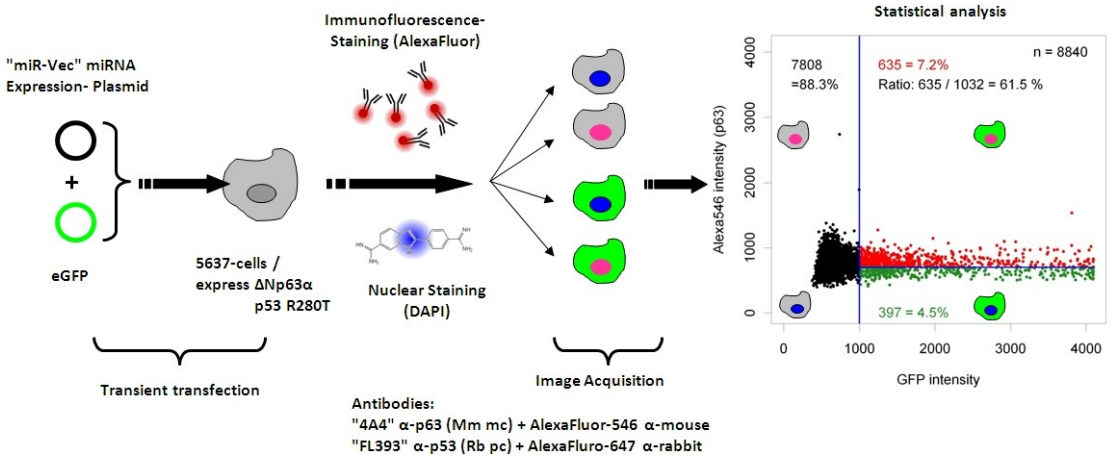

Figure 3.1: **Workflow of the miR-Vec screen.** '5637' cells are transiently transfected with the miR-Vec plasmids and an eGFP expression plasmid. After 48h of incubation, cells are fixed and immunofluorescence-stained for p63 and p53. Digital photomicroscopy is performed semi-automatically. The obtained images are processed and the data statistically analyzed.

3.8.3 Quantitative immunofluorescence

Immunofluorescence-staining for p63 was performed using the 4A4 anti-p63 mouse monoclonal antibody and the AlexaFluor-546 anti-mouse antibody both at 1:500 dilution in PBS containing 10 % (v/v) FCS. Simultaneously, p53 was stained using FL393 rabbit polyclonal antibodies at 1:400 and the AlexaFluor-647 anti-rabbit antibody at 1:500. Nuclei were visualized by DAPI-staining. All steps of the staining protocol are listed below; the washing steps were facilitated by a MultiDrop semi-automatic liquid-dispenser. The BioMek was not suited for the washing step since it is not fast enough for this issue.

Step	Reagent	Volume	Duration	Frequency
Washing	PBS++	100 µL	A few seconds	2x
Fixation	4 % (v/v) Paraformaldehyde	100 µL	20 min, room temperature (RT)	1x
Washing	PBS++	100 µL	A few seconds	2x
Permeabilization	0,2%TritonX-100	100 µL	25 min RT	1x
Washing	PBS++	100 µL	A few seconds	4x
Blocking	Blocking Solution	100 µL	10 min RT	1x
Incubation with primary antibodies	Blockingsolution + antibodies	70 µL	1 h RT	1x
Washing I	PBS++	100 µL	A few seconds	2x
Washing II	PBS++	100 µL	5 min	1x
Incubation with secondary antibodies	Blockingsolution + antibodies	70 µL	30 min RT in the dark	1x
Washing I	PBS++	100 µL	A few seconds	2x
Washing II	PBS++	100 µL	5 min	1x
DAPI-staining	DAPI-solution	75 µL	5 min	1x
Washing	PBS++	100 µL	A few seconds	2x
Add 80 µL PBS++ and store at room temperature				

Digital photomicrography was performed with a Pathway HT Cell Imaging System at 100x magnification (Figure 3.2) using AttoVision image acquisition software. The employed optical filters (Table 3.1) allowed capturing of distinct fluorescent signals without perceptible spectral overlap (Figure 4.1). The system is based on a Hamamatsu Orca 12-bit greyscale digital camera which allows distinguishment of 2^{12} intensity values for each fluorescence channel, thus 0 – 4095. Image-processing, i.e. recognition of regions-of-interests (ROIs) and their quantification was also performed with Attovision.

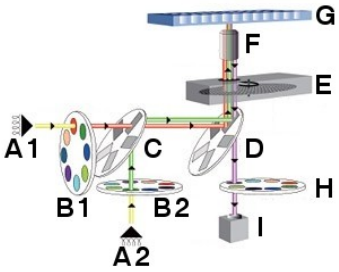

Figure 3.2: **Optical pathways of the Pathway HT cell imaging system.** The system features two mercury arc lamps (**A1,2**) with separate excitation filters (**B1,2**). The two sources can be used independently (**C** is a mirror for A2 or open for A1) or in combination (**C** is a dichroic filter). Different epifluorescence dichroic mirrors (**D**) can be employed though here the same was used for all channels. A pin-hole spinning disk (**E**) allows confocal microscopy and a multitude of objectives (**F**) are possible. The optical 96-well plate (**G**) is viewed from below. Images are captured by a CCD-camera **(I)** after passing the emission filter (**H**) (Illustration adapted from the BD Pathway HT user manual).

Dye	Excitation Source & Filter	Excitation Dichroic	Epifluorescence Dichroic Mirror	Emission Filter
DAPI	A1 380/10	Open	84000	435LP
eGFP	A1 470/40	Open	84000	515LP
Alexa546	A2 548/20	Mirror	84000	FURA/TRITC
Alexa647	A2 635/20	Mirror	84000	84101

Table 3.1: Optical components used for the four fluorescence-channels. Using the same epifluorescence dichroic mirror in all channels ensures perfectly congruent images.

3.8.4 Statistical analysis

Statistical data analysis was carried out using a collection of scripts for 'R' statistical computing language (R Development Core Team 2007) that were written for this work. R is an open-source software, the employed version 2.6.1 was distributed under the GNU General Public License Version 2. The custom scripts for this work directly use the ROI-files created by Attovision: The data of each experiment were imported into R, converted into a compact table and stored as a text file. This file could subsequently be analyzed as described in section 4.1.5.

Data-conversion was achieved mainly by using R functions *grep()* for pattern matching and *scan()* for reading of data at a specific position within a file. The data for each well were located within the Attovision-file and contracted into one *dataframe*. Scatterplots were drawn using the R function *plot()* and threshold-based analysis (Figures 4.03 A , 4.05 A) was based upon the function *split()* which divides R objects according to a numerical or logical value. Boxplot analysis (Chambers et al. 1983) was based on the function *boxplot()*, the results were sorted using *order()* which was applied to all data of a given experiment using *tapply()* (Figures 4.03 B, 4.05 B). Final results were stored as graphical files and as CSV-tables by the scripts.

4 Results

4.1 Immunofluorescence-based screening identifies novel antagonists of p63 expression

4.1.1 Summary

To set up a comprehensive evaluation of how expression of individual microRNAs (miRNAs) affects the cellular levels of p63 and p53 a high content cell screening approach was employed based on plasmid transfection and subsequent immunofluorescence analysis. A previously published collection of 350 individual expression plasmids for most of the commonly expressed human miRNAs (Voorhoeve et al. 2006, Huang et al. 2008) was transiently expressed in '5637' cells on 96-well plates with each well containing one specific miRNA expression plasmid together with an enhanced Green Fluorescent Protein (eGFP) expression plasmid. Immunofluorescence-microscopy allowed the identification of transfected cells by their GFP-fluorescence and the quantification of the cellular levels of proteins of interest to evaluate a possible influence of the respective miRNA. An overview of the workflow is depicted in figure 3.1 . The screen was performed two independent times and the obtained data were combined and analyzed together.

4.1.2 Cellular system

'5637', a cell line derived from the primary stage 2 bladder carcinoma in a 68 year old man (Fogh 1978) was chosen as model system for its constitutive expression of p63 and for its transfectability. Urothelium strongly expresses p63 with ΔNp63α being the most abundant isoform, a characteristic still apparent in this tumour cell line (Lee HO et al. 2006). P53 is mutated in 5637 cells (R280T) and accumulated to high amounts. R280T disrupts the DNA-binding domain causing loss of p53-functioning. Another possible cell line, EPC hTERT, primary, immortalized yet not transformed keratinocytes, turned out not to be suited for the screen because of their low transfection efficiency. The use of endogenous p63 as opposed to exogenous p63 from a cotransfected expression vector was favoured since this approach allows the identification of miRNAs influencing p63 both directly and indirectly via factors involved in p63 expression and/or protein-stability. Also, trial experiments ahead of the screen indicated a greater variance of experimental setups using exogenous p63 compared to endogenous. P53 is accumulated to unusual high cellular concentrations in 5637 cells yet is still confined to the nucleus. On the one hand mutant p53 has the disadvantage of having

lost much of its physiological regulatory network and being more stable on protein level which renders the detection of a concentration change more challenging. On the other hand the high protein concentration facilitates reliable quantification by immunofluorescence and the loss of regulatory mechanisms decreases the biological variance.

4.1.3 Transient transfections

The transfection conditions were optimized for both 5637 cells and for the 96-well plate format. 0.6 µL FuGene 6 combined with 0.3 µg plasmid yielded the highest efficiency in this context with transfection-rates up to 33%. An expression plasmid for eGFP was cotransfection in an eGFP:miR-Vec ratio of 1:9 (30ng eGFP + 270ng miR-Vec) to identify successfully transfected cells. Plasmids were prepared with the aid of BioMek 2000 and 3000 workstations. Fluorometric DNA quantification with a 96-well plate reader was used, a sensitive and convenient technique for large scale approaches. Transfections in the 96-well format was performed using a BioMek 3000 workstation. Positive and negative controls as well as an unstained control were included in all well plates.

4.1.4 Immunofluorescence analysis

After 48h of incubation cells were fixed and immunostained for both p63 and p53. The nuclei were counterstained with the nucleic acid dye DAPI. Digital photomicroscopy was performed with a Pathway HT cell imaging system. The Pathway HT uses two mercury arc-lamps with separate excitation filters. The same epifluorescence dichromatic mirror was used for all four color-channels to ensure congruent images (Figure 3.2). The employed optical components are listed in table 3.1. Secondary antibodies conjugated to fluorophores with distinct excitation and emission spectra in combination with specific optical filters allowed capturing of the four channels with no perceptible spectral overlap (Figure 4.01).

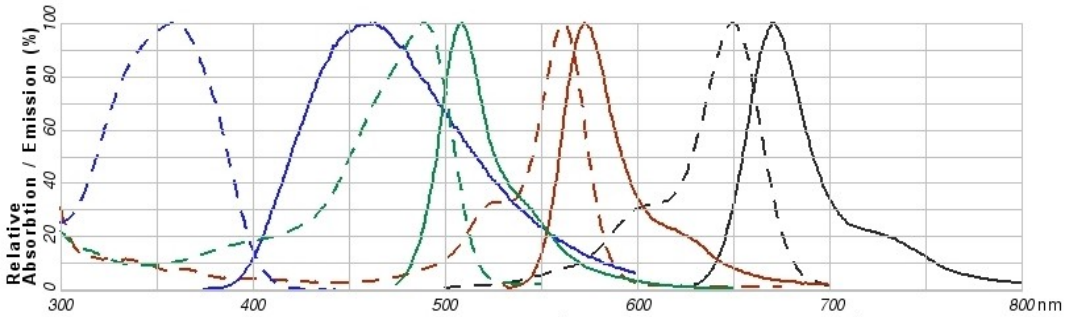

Figure 4.01: **Spectra** of the four employed fluorescent dyes. **Dotted lines**: Excitation, **Solid lines**: Emission. **Blue**: DAPI, **Green**: eGFP, **Red**: AlexaFluor-546 (p63), **Black**: AlexaFluor-647 (p53). Image created with 'Fluorescence Spectra Viewer' (Invitrogen) cf. section 2.2 .

Image analysis was carried out with Attovision image acquisition and processing software. The Pathway HT features a 12bit greyscale digital camera which allows measurement of 2^{12} different intensity values ranging from 0 (black) to 4095 (white).

For each transfection, between 1000 and 2000 individual cells were first identified based on DAPI-staining. The obtained Regions-of-Interest (ROIs, i.e. the nuclei) were applied to the other fluorescence channels and GFP-fluorescence, p63-derived light red fluorescence (~546nm) and p53-derivated bright red (~647nm) were quantified for each ROI (Figure 4.02).

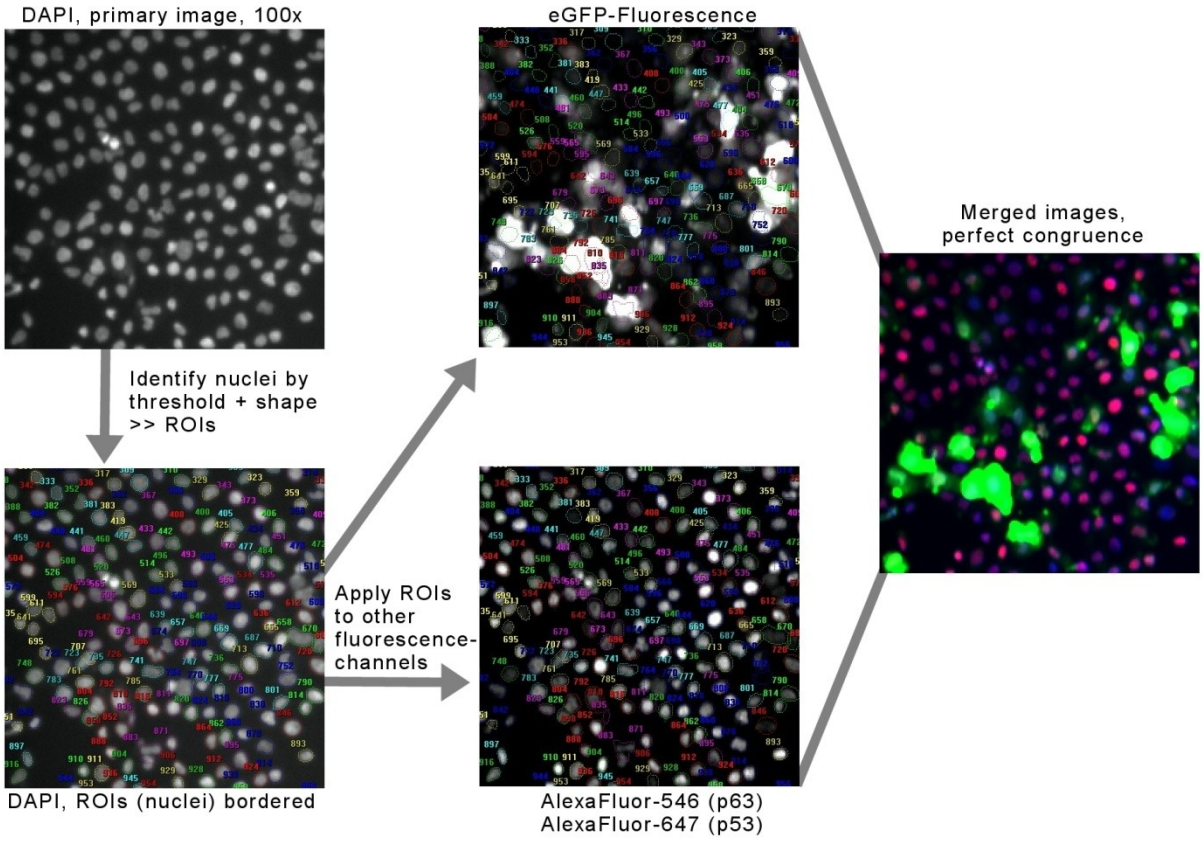

Figure 4.02: Example of primary data from the miR-Vec screen and image analysis. Nuclei are recognized in the DAPI-channel using combined threshold and shape filtering. The obtained ROIs are applied to the other fluorescence-channels (GFP, AlexaFluor-546 stained p63 and Alexa-647 stained p53). Use of the same epifluorescence dichroic mirror in all channels yields congruent images.

This allowed an evaluation of how the three fluorescence intensities were distributed among the cell population for each of the miRNA expression plasmids. The GFP-fluorescence was used to identify efficiently transfected cells. Deviations in either p63 or p53 levels among these cells was indicative of a regulatory effect by the miRNA species transfected in the respective well. An explanatory overview of this approach is provided in figure 4.02 . Control experiments omitting the GFP expression plasmids or the red fluorescent antibody resulted in the expected absence of signals (Figure 4.03 A). The system was further validated by control transfections, consisting in shRNA expression constructs (Brummelkamp et al. 2002)

to target p63 (pSUPER-shp63: Positive control for p63-decrease / negative control for p53-decrase) and p53 (pSUPER-shp53: Negative control for p63-decrease / positive control for p53-decrease) (Figures 4.03 A, 4.04). Additionally, the known p63-targeting ubiquitin ligase ITCH (Rossi et al. 2006) was overexpressed and compared to its inactive mutant ITCH C830A (Figure 4.04, Winberg et al. 2000).

4.1.5 Statistical analysis

Analysis of obtained intensity values was performed with a self-made set of scripts for 'R' statistical computing language (R Development Core Team 2007) to directly process data-files created by Attovision. The ROI data of the two independent runs of the screen were combined and analyzed together. By using a threshold, GFP positive (intensity >= 1000) nuclei were gated to exclude untransfected cells (Figure 4.03 A). To obtain a comprehensive representation of the intensity distributions for each miRNA, the p63/p53-derived fluorescence values were displayed as boxplots (Chambers et al. 1983) and ordered accordingly to the median intensity for each miRNA (Figures 4.03 B, 4.05 B. Boxplots, corresponding 'five numbers' and z-values are listed in the appendix, section 8).

A trimmed mean fluorescence intensity for each miRNA was calculated using the values contained within the boxes and their whiskers, thus excluding strongly deviating intensities. Assuming that in most wells intensity differences are caused by random factors and that only very few miRNAs have a specific effect, the intensities on each plate should be normally distributed. Thus, statistical significances were evaluated by transforming the obtained trimmed mean values into z-scores (a.k.a. standard score), $z = \frac{x-\mu}{\sigma}$, where μ is the expected value $\mu = \frac{1}{n} \cdot \sum_{i=1}^{n} x_i$ and σ the standard deviation $\sigma = \sqrt{\frac{1}{n} \cdot \sum_{i=1}^{n} (x_i - \mu)^2}$ of the fluorescence of the 88 miRNA-containing wells of the respective plate.

For p63, the employed positive controls (ITCH, pSUPER-shp63) were reliably identified as highly significant while negative controls (pSUPER-shp53, control expression vector 'hTR') yielded insignificant results. Interestingly, transfection of the inactive ITCH C830A caused increased p63 levels in most experiments which was not expected.

Only two miR-Vec constructs reached z-scores <= -2z and are considered 'hits': One is the miRNA 302 cluster on plate 1, the other is an uncharacterized miRNA candidate on plate 2 named 'X49' by Voorhoeve et al. 2006 (Figure 4.04, appendix section 8.1).

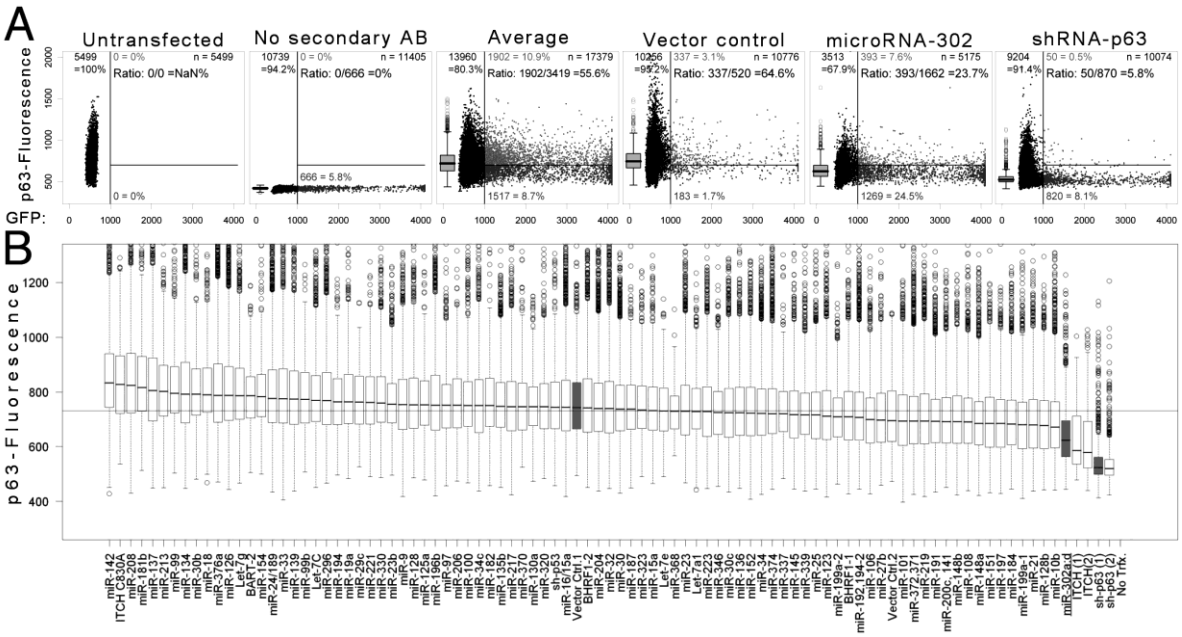

Figure 4.03: Statistical analysis to identify p63-regulating microRNAs, plate 1 of 4. Combined data of two experiments. **(A)** Analysis of immunofluorescence in single wells. In each scatter plot, GFP-fluorescence is displayed along the x-axis; the p63-derived immunofluorescence signal is shown on the y-axis. Each dot represents an individual cell. Untransfected cells have no GFP signal (first diagram), whereas omission of the fluorescent antibody abolished the red fluorescent signal (second diagram). Thresholds were set to define GFP-positive and thus successfully transfected cells (vertical line in all diagrams) and p63-positive cells (horizontal line). In each case, the ratio of p63 and GFP double-positive cells (light grey) to all GFP-positive cells (light and dark grey) is indicated as a percentage. Boxplots to summarize p63-fluorescence of the GFP-positive cells are displayed in grey at the left of the two-dimensional diagrams. The diagram 'Average' was obtained by the combination of 95 randomly selected cells from each miR-Vec transfected well. 'Vector control' indicates that the miRNA expression plasmid was used without a miRNA encoding insert. An expression plasmid for a shRNA to p63 was used as a positive control. **(B)** Quantitative evaluation of p63-derived fluorescence upon transfection of miRNAs, visualized by boxplots using the same principles as explained in (A). A complete list of all screen-data can be found in the appendix, section 8.

Figure 4.04: P63 z-scores of Plate 1. Combined data of two experiments. Besides the positive controls (red) only miRNA-302 is highly significant (x<= -2z). The negative controls (green) are insignificant (-z <= x <= z) except for ITCH C830A which seems to cause an significant (x >= z) upregulation of p63 protein levels.

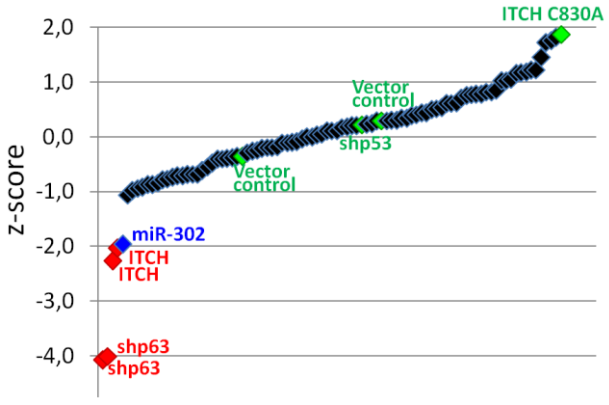

MiR-302 was further investigated; X49, which is located on Chromosome 1p51, might become of interest once it is fully annotated by successful cloning or by deep sequencing techniques.

In the case of p53, the data were not as reliable as the p63 data as quantification of the Alexa-647 antibody was disturbed by strong background fluorescence. Additionally, the mutant p53 protein seems to have a long half-life as transfection of the pSUPER-shp53 positive control did not yield a very strong knockdown. Given the little discrimination between the positive controls and samples, it is likely that the impact of random effects such as differences in immunofluorescence-staining is much larger than in the p63 data.

Still, one miRNA stuck out of the crowd: MiR-485 forms a cluster together with miR-668 and this cluster is contained twice in the miR-Vec library on two different plates. On plate 4, miR485~668 yielded the strongest downregulation of p53, right next to the positive controls (Figures 4.05, 4.06) and on plate 2, it achieved the second strongest effect. Since miR-485 was the only miRNA with a possible effect to have predicted binding sites with the p53 3' UTR (determined by TargetScan, Lewis et al. 2005), this miRNA was further investigated together with other candidates and turned out to be the only miRNA to cause reproducible effects in verification experiments.

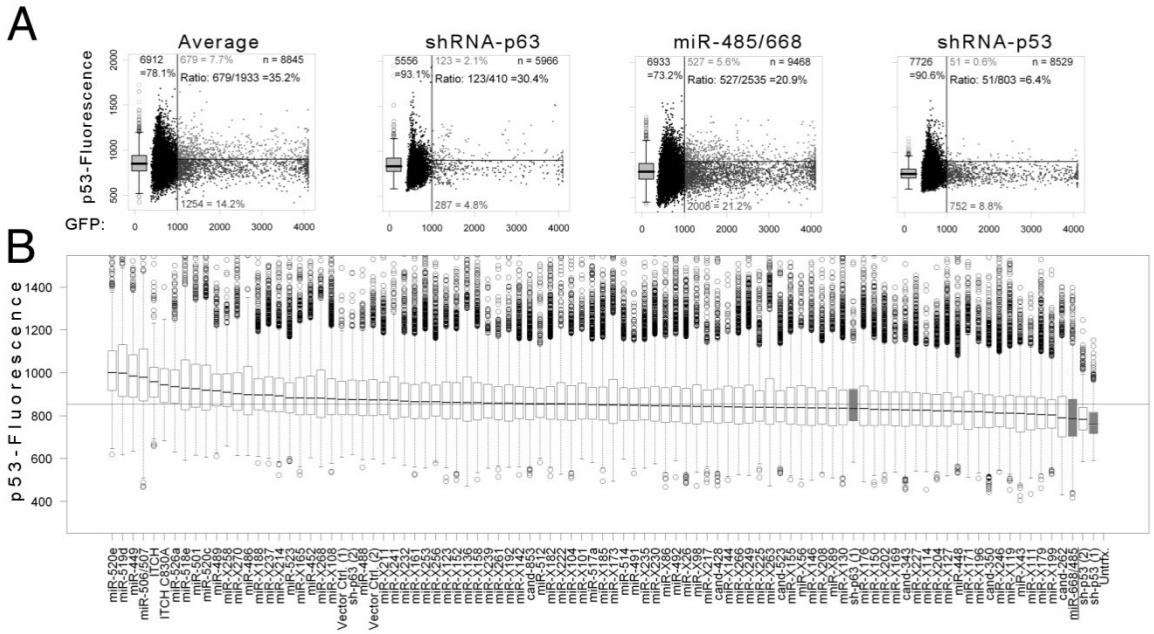

Figure 4.05: Statistical analysis to identify p53-regulating miRNAs. Plate 4 of 4, combined data of two experiments. Analysis similar to figure 4.03. Here, shRNA-p63 serves as negative and shRNA-p53 as positive control. **(A)** Analysis of single wells **(B)** Quantitative evaluation of p53-derived fluorescence by boxplots. Controls are highlighted by solid grey boxes.

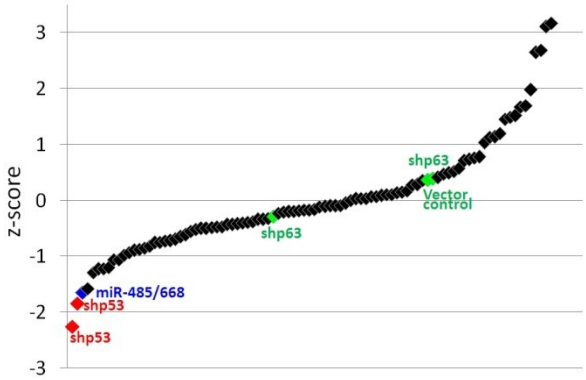

Figure 4.06: P53 z-scores of Plate 1. Combined data of two experiments. While the negative controls (green) are compatible, only one of the two positive controls on this plate is highly significant. MiR-485~668 shows the strongest decrease of p53, yet is only significant, not highly significant, along with several other miRNAs.

4.2 Characterization of the miR-302 p63 interaction

4.2.1 MiR-302 is capable of reducing p63 protein and mRNA levels

To verify interesting candidate-regulators from the screen, a plasmid expressing a full-length p63 isoform cloned from testicular tissue (cf. Section 2.9.2, pcDNA3-p63α-3'UTR) was cotransfected with the respective miR-Vec plasmid and the cells were analyzed by immuno-blotting. Again, eGFP was cotransfected to ensure equal transfection efficiency and rule out strong unspecific effects. As cellular system, H1299 cells were used for their superior transfection efficiency and lack of both endogenous p63 and p53. In this approach, p63 could again be downregulated by pSUPER-shp63. Besides candidates from the screen, related miRNAs were also tested.

As shown in figure 4.07 A, miR-302 strongly reduced the levels of the overexpressed p63 but not the amount of cotransfected eGFP. It can be concluded that miR-302 can downregulate the levels of p63 in an experimental setting that considerably differs from the initial screen. The employed cell species, the source of p63 (expression plasmid vs. endogenous gene product) and the read-out (immunoblot vs. immunofluorescence) were all different and yet both approaches revealed strong reduction of p63 levels by miR-302. In contrast, many other miRNA species were not found to affect the amounts of p63 on immunoblot level, even if they had a similar seed sequence for mRNA targeting. It should be noted, however, that the overexpression of the sequence-related miR-372 and -373 led to p63 reduction in some experiments but with considerable variability. In contrast, the p63-suppressive effect of miR-302 was constantly observed.

The miR-302 expression plasmid contains the sequences miR-302a, b, c, d and miR-367. The 302 miRNAs are all highly homologous to each other, in particular at their seed sequence at the 5' side that is thought to determine most of the target specificity (Figure 4.16). It was therefore tested, if a single miRNA of this cluster could still downregulate p63 levels. 5637 cells (carrying endogenous ΔNp63α) were transfected with synthetic miRNA 302b ('premiR' by Ambion Inc.). Again, immunoblot analysis revealed strong reduction of p63 levels (Figure. 4.07 B). Interestingly, analysis by quantitative real-time PCR revealed that miR-302b was also capable of reducing p63 mRNA levels (Figure 4.07 C), suggesting that it suppresses gene expression through mRNA degradation. In addition, miR-302 might still act as an inhibitor of p63 translation.

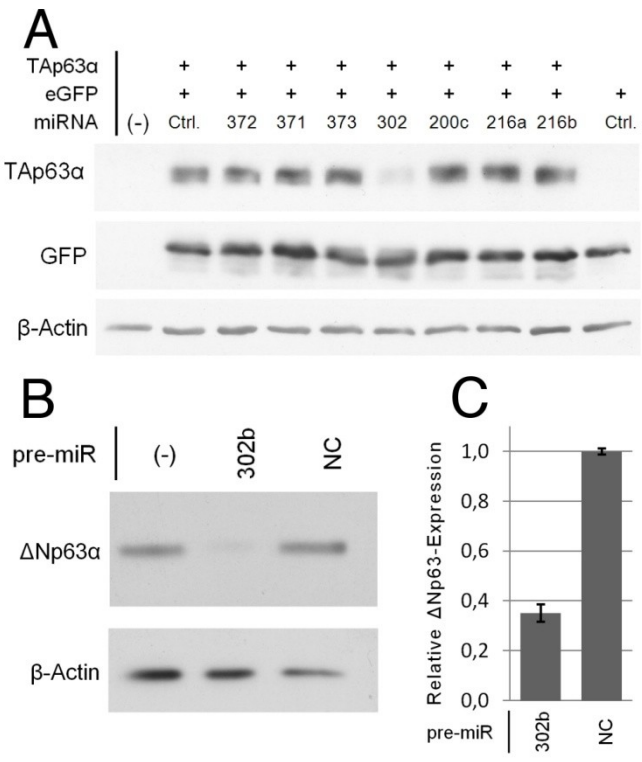

Figure 4.07: Reduced p63 protein and mRNA levels upon miR302 expression
(A) Levels of p63 upon co-transfection of expression plasmids for p63 and various miRNAs. Coexpression of miR-Vec plasmids and full-length TAp63α (including its 3'UTR) was achieved by co-transfecting 800ng miR-Vec plasmid for the indicated miRNA species, 200ng TAp63α and 200ng eGFP expression plasmid. 48h after transfection, the p63 was detected by immunoblot analysis. β-actin staining served as a loading control, GFP-staining as a transfection control. MiR-302 and -216 are candidate-regulators while miR-372 and -373 have a sequence related to the miR-302 family and share the same seed-sequence. MiR-200c is unrelated and was included for comparison. **(B)** Levels of endogenous p63 in 5637 cells were detected by immunoblot analysis upon transfection of 5nM synthetic miR-302b or control RNA (NC). **(C)** Levels of endogenous p63 mRNA were detected by quantitative RT-PCR upon treatment of 5637 cells as in B.

4.2.2 MiR-302 targets two sites within the 3' untranslated region of p63 alpha

To investigate the mechanism underlying the p63-repression by miR-302, dual-luciferase assays were performed with a plasmid (pGL3control) containing the 2.8 kBp long 3' UTR of p63α (cf. Section 2.9.2). The UTR is cloned at the 3'-end of firefly luciferase causing the transcript to be subject to the same regulatory mechanisms that apply to p63-isoforms bearing this UTR. To normalize-out variations in transfection efficiency and concentrations, a second plasmid was cotransfected which expresses renilla luciferase. The activities of the

two enzymes were measured within the same sample by using specific substrates with the renilla-substrate containing an enzyme-inhibitor (sodium azide, NaN_3) that blocks firefly-luciferase activity. The Firefly/Renilla ratio ('Relative Luciferase Activity') is indicative of a possible regulation of the firefly-UTR construct.

Cotransfection of the two luciferase-plasmids with the miR-302 encoding plasmid showed a ~50% reduction of the relative luciferase activity compared to cotransfection with a control plasmid ('hTR') and to other miRNAs. The difference was already statistically significant 12h after transfection and persisted in a 60h time-course (Figure 4.08). Again, the related miRNAs 372 and 373 showed some regulatory activity but not consistently. It might be that additional factors are involved in the action of these miRNAs.

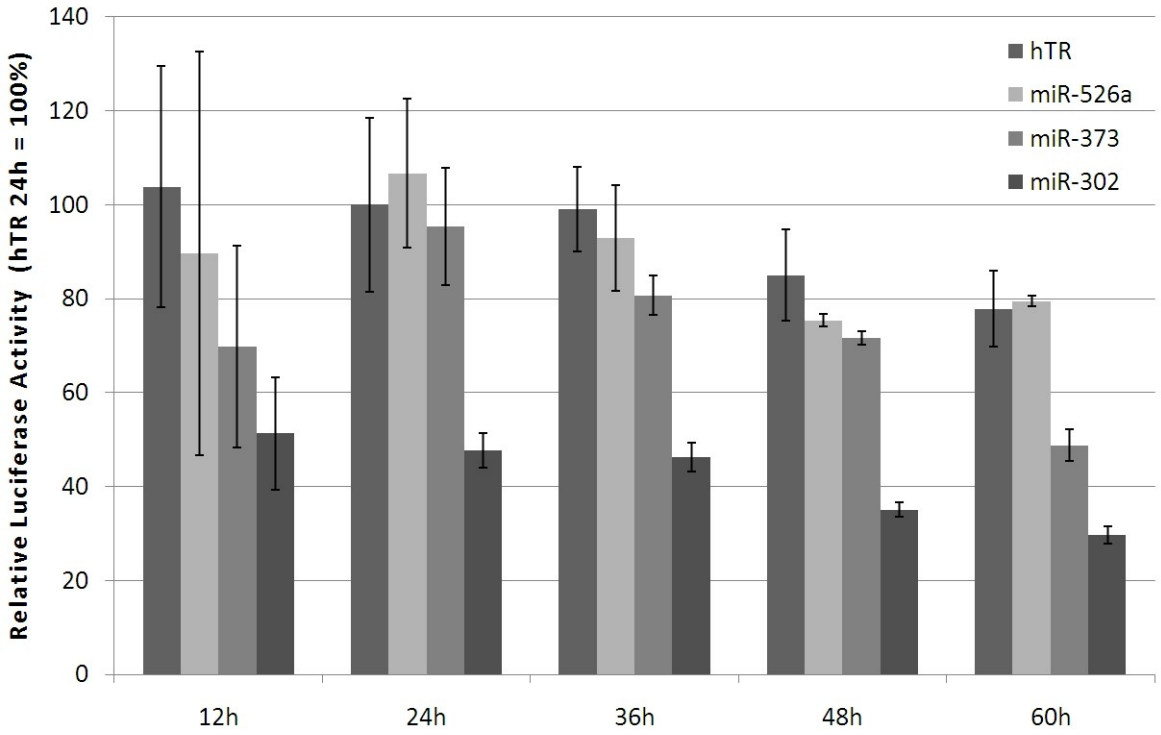

Figure 4.08: Luciferase Assay time course. H1299 cells were transfected with 50ng renilla-luciferase, 200ng firefly-luciferase fused to the p63α 3' UTR, 150ng hTR and 800ng of the indicated miR-Vec plasmid. Dual luciferase assays performed after the indicated duration of transfection. Samples as biological triplicates, columns and error bars represent the mean and standard deviation of firefly/renilla-luciferase ratios.

The ratio of transfected miR-302 and firefly-luciferase plasmid did not affect the strength of the repression which was consistently around 50% (Figure 4.09). This might indicate the presence of some regulatory mechanism limiting the effect of miR-302, on the other hand, SV40- and CMV-promoter containing plasmids cause supra-physiological expression that charges many cellular machineries to capacity.

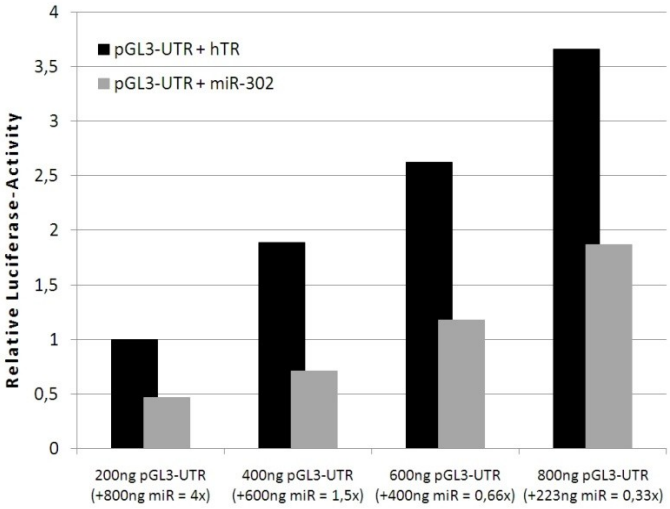

Figure 4.09: Cotransfection of different ratios of luciferase-UTR and miR-302 or 'hTR' control plasmid (4x to 0.33x) alters the overall activity of luciferase, while the impact of miR-302 is consistent. H1299 cells transfected with 50ng renilla-luciferase, the indicated amount of firefly-luciferase (pGL3control-UTR) and either the indicate amount of miR-302 expression-plasmid or enough 'hTR' plasmid to achieve 1200ng total plasmid. Dual luciferase assays performed 24h after transfection.

Given the apparent direct interaction of miR-302 and the p63α 3' UTR, two sequence elements with complementarity to miR-302 could be identified in the UTR using the TargetScan algorithm (Figures 4.10, 4.11 A; Lewis et al. 2005). To verify that these physical binding sites are also biologically relevant, site-directed mutagenesis was performed, individually and in combination, with the luciferase-plasmid carrying the p63α 3' UTR. Binding site 1 (BS1) was removed by a 50bp deletion while binding site 2 (BS2) was disrupted through insertion of two nucleotides into the base-pairs complementary to the seed-region of miR-302. Both mutations were designed to cause the creation of a palindrome (GTCGAC) which is recognized by restriction-enzyme Sal-1, facilitating the selection of positive clones. Positive clones were additionally verified by capillary electrophoresis-sequencing using the dye-terminator method. Cotransfection of the three obtained mutant plasmids with the miR-302 expression plasmid and subsequent luciferase assays revealed that both putative target sites indeed contribute to the suppressive effect of miR-302 (Figure 4.11 B), suggesting a plausible mechanism of how miR-302 can directly downregulate the expression of p63.

Interestingly, the binding sites were found to be conserved in several species including H. Sapiens, rat, mouse and dog (miRBase, Griffith-Jones et al. 2006). In the human genome, no polymorphisms are annotated in these binding elements ('dbSNP' build 130, The National Center for Biotechnology, Bethesda, USA; http://www.ncbi.nlm.nih.gov/SNP/).

Given the importance of the p63α 3' UTR sequence elements which are complementary to the miR-302 seed sequence, as well as the finding that transfection of synthetic miR-302b alone is sufficient for p63α downregulation, it seems that miR-302 are responsible for the effect, not miR-367 which is part of the same cluster and is contained in the miR-Vec plasmid. Still, it cannot be ruled out that miR-367 contributes to the suppression.

p63α 3' UTR, BS1 5'..aaatgt^ aatttaaatg**AAAGAAAATTGAGTT**
GCACTTAttgaccatttttaattt ^acttgt..

ΔBS1 5'..aaatgtCGacttgt..

p63α 3' UTR, BS2 5'..caaagttttgtt**GTACTTAAATGG**
TAATAAGCACTgtaaacttctgcaa..

ΔBS2 5'..caaagttttgtt**gtacttaaatgg**
taataagTcG**act**gtaaacttctgcaa..

Figure 4.10: Details of site-directed mutagenesis. In ΔBS1, 50bp containing BS1 were deleted while ΔBS2 was created by inserting two nucleotides into the region complementary to miR-302's seed-sequence. Binding-sites highlighted bold, inserted nucleotides red. Both mutations include the formation of a Sal-1 restriction site (GTCGA).

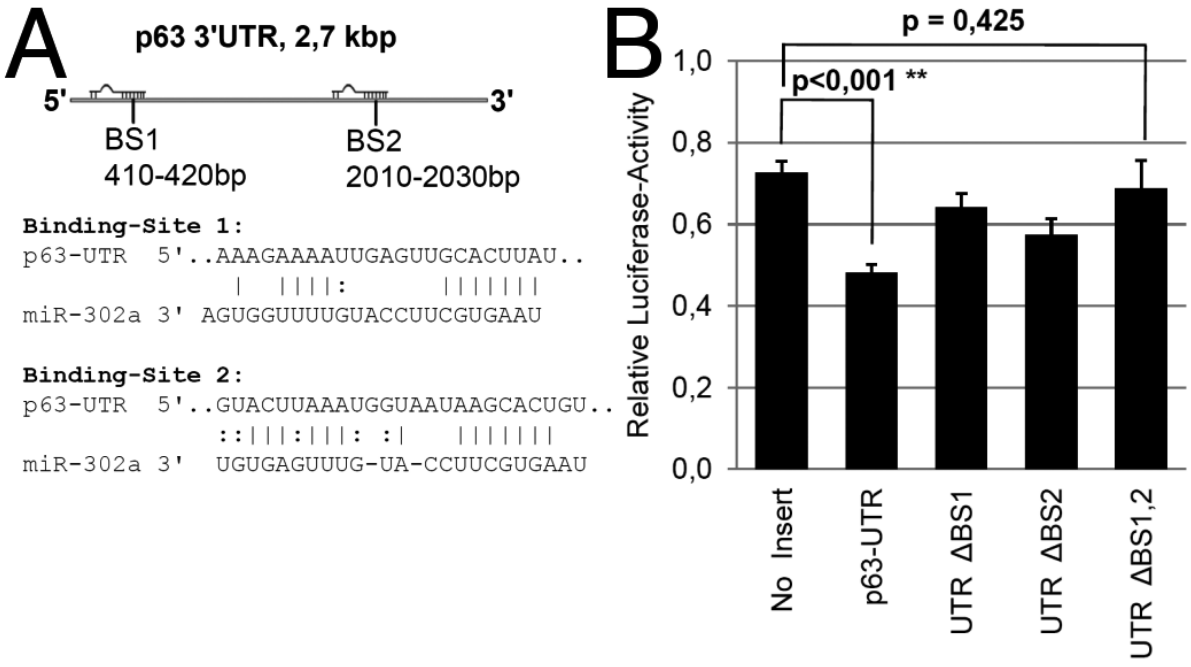

Figure 4.11: MiR-302 target sites within the 3' UTR of p63 mRNA. (A) Candidate binding sites for miR-302a in the 3' UTR of the p63α mRNA as identified by TargetScan (Lewis et al.2005). Binding site 1 (BS1) was found to be conserved among several species (human, rat, mouse, dog). No known single-nucleotide-polymorphisms are described for BS1 and BS2. **(B)** Impact of miR-302 on the expression of a luciferase reporter that contains the p63 3' UTR with or without the putative miR-302 binding sites. H1299 cells transfected with 200ng firefly-luciferase expression plasmid containing the indicated UTR insert, 50ng renilla-luciferase expression plasmid for transfection-control and either 950ng empty vector (miR-Vec control) or 800ng miR-Vec miR-302 and 150ng control vector. Dual-luciferase-assays performed 24h after transfection. In each case, after normalization with renilla luciferase, the ratio of luciferase activities in the presence vs. absence of miR-302 was calculated. Samples as biological triplicates, columns and error bars represent the mean and standard deviation these ratios. Student's T tests were performed to calculate the significance levels by that the indicated values are distinct.

4.3 MiR-302 in testicular cancer contributes to p63 suppression

4.3.1 Endogenous miR-302 is sufficient to antagonize p63.

Mir-302 is one of the most cell specific miRNAs identified so far (Landgraf et al. 2007). It is mostly expressed in embryonic tissues, e. g. stem cells (Barroso-delJesus et al. 2008, Landgraf et al. 2007) and also in germ cells (Tang et al. 2007). It is therefore conceivable that miR-302 might negatively regulate the expression of full-length p63 in these contexts. To examine this, cells expressing miR-302 and p63 at detectable levels were identified. MiRNA-expressions were investigated with quantitative real-time PCR using commercial TaqMan-kits (Ambion) for miR-302b and for RNU6B which served as house-keeping gene. Testicular cancer cells, e. g. GH cells, were found to contain high levels of miR-302 (Figure 4.12). The concentration was over two orders of magnitude higher in comparison to a collection of RNA isolated from various adult human tissues (Figure 4.13).

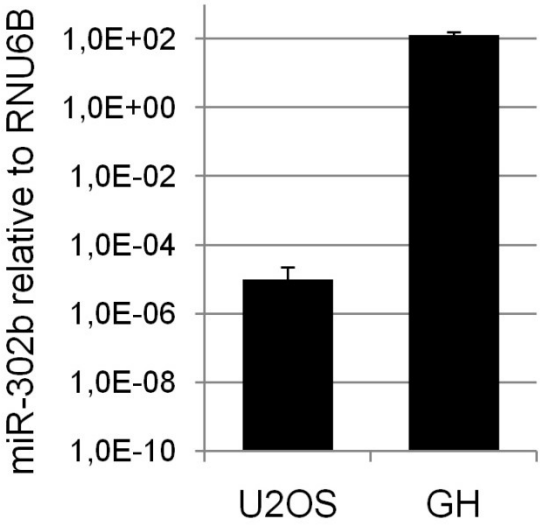

Figure 4.12: MiR-302b expression relative to RNU6B. GH testicular cancer cells vs. U2OS osteosarcoma cells, expression-levels were determined with TaqMan assays. The columns represent the average of independent biological triplicates and the error-bars indicate the standard-deviation.

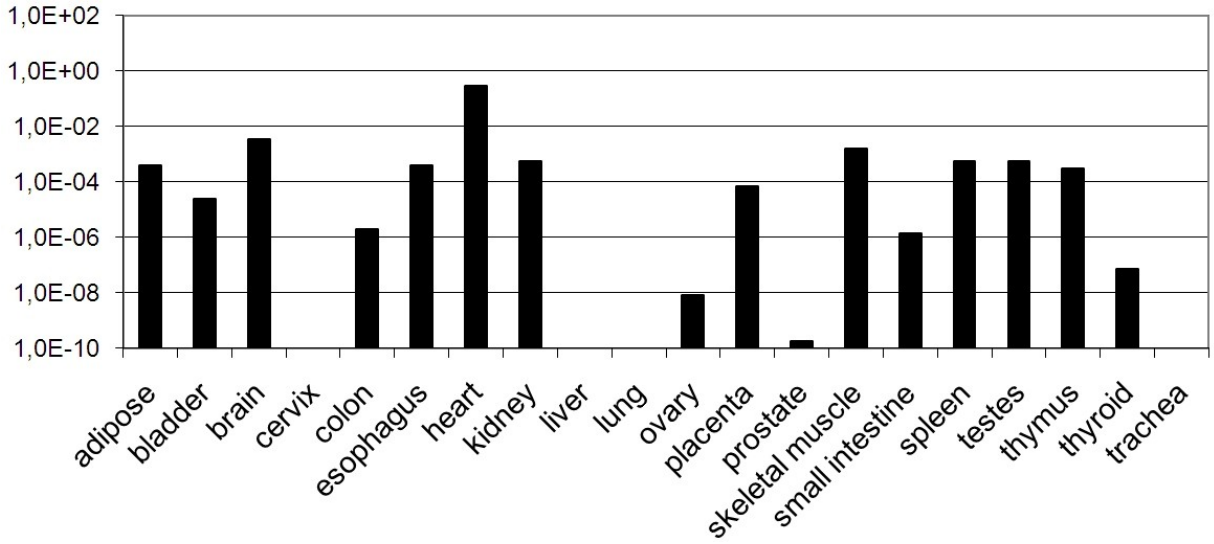

Figure 4.13: MiR-302b expression relative to RNU6B in adult human RNA samples (Ambion First Choice RNA). The highest expression is found in RNA derived from heart. Compared to GH testicular cancer cells (Figure 4.11), the expression is more than 10^2-fold lower.

The low expression in various adult tissues is compatible with the specific expression described by Landgraf et al. 2007 and indicates a possible upregulation in testicular cancer.

GH cells were subsequently transfected with the firefly luciferase constructs containing the wild type p63α 3' UTR or one of the two miR-302 binding site mutant UTRs described in section 4.2.2. For comparison, U2OS osteosarcoma cells were transfected similarly as they lack detectable miR-302 expression (Figure 4.12). Dual-luciferase-assays were performed 48h after transfection. While the four constructs yielded similar relative luciferase-activities in U2OS cells, the activities differed from each other in GH cells. The construct containing the wild type UTR showed the lowest RLA and the construct with the UTR lacking both miR-302 binding sites showed the highest (Figure 4.14). In fact, the results strongly resemble Figure 4.11 B. This implicates that endogenous miR-302 in GH can target the p63α 3' UTR and cause a measurable decrease in cellular protein-concentration.

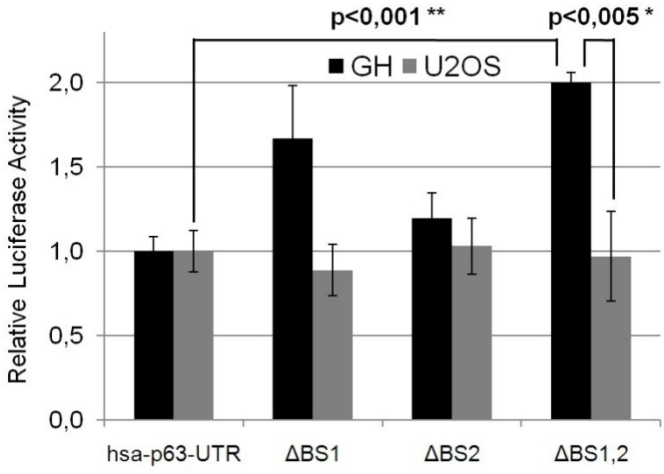

Figure 4.14: Expression of luciferase reporter in GH cells. Constructs of the p63α 3' UTR with or without miR-302 binding sites were transfected into miR-302 positive GH cells and miR-302 negative U2OS cells.
Transfection of 50ng firefly luciferase expression plasmid containing the indicated UTR insert, 50ng renilla luciferase expression plasmid, and 500ng empty vector (miR-Vec control). Luciferase-assays performed 48h after transfections, obtained RLAs normalized to the RLA of the wild type sequence. Independent biological triplicates, mean and standard deviation are indicated in each case. Student's T tests were performed to test significance.

4.3.2 Antagonization of miR-302 causes increased p63-expression

GH cells endogenously express p63. However, the base line levels are insufficient for detection on immunoblots. This issue can be resolved by inhibiting histone deacetylases (HDAC), as shown earlier in different cell species (Sayan et al. 2007). HDAC-inhibition by Trichostatin A (TSA) causes a profound increase in p63-expression in GH cells, particularly of TAp63α. Real-time PCR analysis of miR-302 indicated that expression of miR-302 is not affected by TSA-treatment.

To investigate if endogenous miR-302 contributes to suppression of endogenous p63, GH cells were transfected with 200nM of an antagonizing oligonucleotide (AO) to block endogenous miR-302. Subsequently, p63 expression was stimulated by 150nM TSA and the cells were analyzed by immunoblots.

Since the miR-302 cluster gives raise to four closely related, 23nt long miRNAs 302 a-d which only differ towards their 3' end, the AO was designed to bind only first 21nt with perfect complementarity to miR-302b and a single mismatch when binding each of the other three homologs (Figure 4.16), thus it binds all miR-302 family members. Of the many possible chemical modifications available for AOs (Meister et al. 2004, Lennox et al. 2006), three strategies were combined to yield a balance of efficiency and side effects: First, the oligo is a RNA-DNA gapmer consisting of 11 DNA-bases framed by 5 RNA-bases on each side. The formation of DNA-RNA duplexes with the targeted miRNAs is assumed to trigger RNA-H and cause degradation of the miRNA rather than just steric blockage (Lennox et al. 2006). Second, the RNA-bases are O-methylated at position 2 of the ribose to increase stability and third, the phosphoro-groups linking the DNA-nucleosides are substituted by phosphorothioat-groups which confer a certain resistance to hydrolysis by DNAses. As a control, a similarly modified oligo with reversed sequence was used which is neither complementary to miR-302 nor does it mimic its sequence.

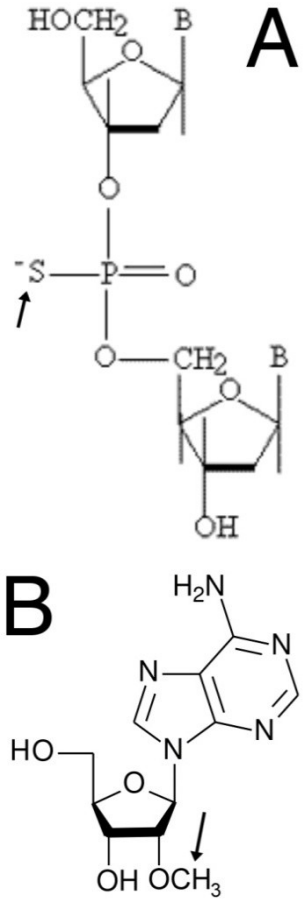

Figure 4.15: Chemical modifications employed in antagonization of miR-302 (arrows). **(A)** DNA-Nucleosides linked by a phosphorothioat diester-bridge, **(B)** 2'-O-methylated RNA-Base (Structures adapted from the Sigma-Aldrich Online Catalogue; St.Louis, MO, USA, http://www.sigmaaldrich.com).

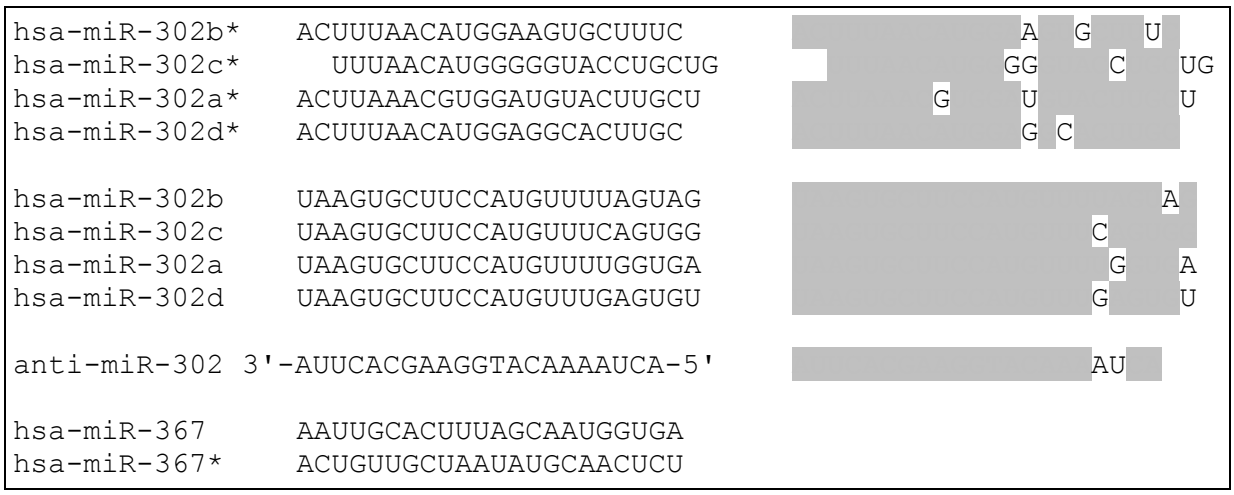

Figure 4.16: Mir-302 sequences. Mature miRNAs expressed from the miR-302 cluster (left), asterisks* indicate minor products. Right: Differences highlighted by displaying conserved nucleotides as grey blocks. 'Anti-miR-302' is a RNA/DNA-gapmer target against all miR-302 major products (left), here, complementary nucleotides are indicated as grey blocks. Sequences adapted from miR-Base miRNA database (Griffiths-Jones et al. 2006).

Immunoblot analysis revealed that TAp63 levels were indeed higher upon miR-302 blockage as compared to cells treated with the control oligo or the transfection-reagent alone (Figure 4.17). The identity of the detected band was confirmed by transfection of a siRNA against p63 exon 6 and by an untreated control, both of which showed the expected absence of a signal. This finding suggests that endogenous levels of miR-302 are capable of suppressing endogenous p63.

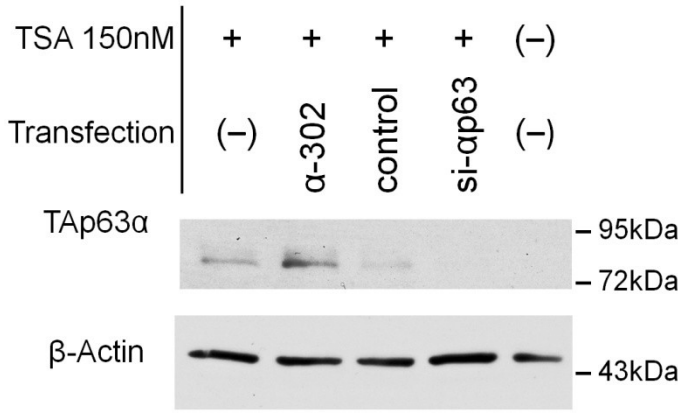

Figure 4.17: Antagonization of miR-302 in testicular cancer cells causes increased p63 protein levels. GH cells were transfected with the indicated oligonucleotides for 24h. α-302 is a 2'-O-MeOH-RNA/DNA antisense gapmer targeting miRNAs 302a-d, control is a similar oligonucleotide with reversed sequence. As a specificity control, a siRNA against p63 was used. TAp63 was subsequently induced by exposing the cells to 150nM Trichostatin A for 16h. p63 was then detected by SDS-PAGE and immunoblot analysis.

4.4 Characterization of the miR-485 p53 interaction

4.4.1 MiR-485 attenuates p53 in U2OS cells

The miR-485~668 cluster emerged as the most interesting candidate to regulate p53. Given that the p53 3' UTR features 3 putative miR-485 binding sites (TargetScan, Lewis et al. 2005), a possible regulation was verified by transfection synthetic premiR-485 (Ambion) into U2OS cells (Figure 4.18) which do not express miR-485 (Figure 4.19). For comparison, two control miRNAs with random sequence ('NC1', 'NC2') were used. Immunoblot analysis revealed that miR-485 transfection caused p53 protein levels to drop below detectable amounts in unstimulated cells. In U2OS cells stimulated with topoisomerase I inhibitor camptothecin, p53 is stabilized by activation of the DNA damage response; transfection of miR-485 prior to camptothecin treatment strongly reduced p53 induction.

Besides p53, its target p21 was also investigated. While not detectable in unstimulated U2OS cells, p21 is strongly induced by p53 activation upon camptothecin stimulation. Transfection of premiR-485 completely abolished p21 induction, no protein could be detected even with very long exposure times during chemoluminescence detection.

DNA damage was analyzed by staining γ-phosphorylated H2A.X histone proteins, a hallmark of DNA strand-breaks. MiR-485 transfection is sufficient to increase these γH2A.X to detectable amounts in unstimulated cells, while in camptothecin treated cells, increased amounts of γH2A.X were present (Figure 4.18). Apparently, miR-485 causes decreased p53 levels in 5637 and in U2OS cells and also strongly influences p53 functioning in U2OS cells as indicated by the complete absence of p21 induction.

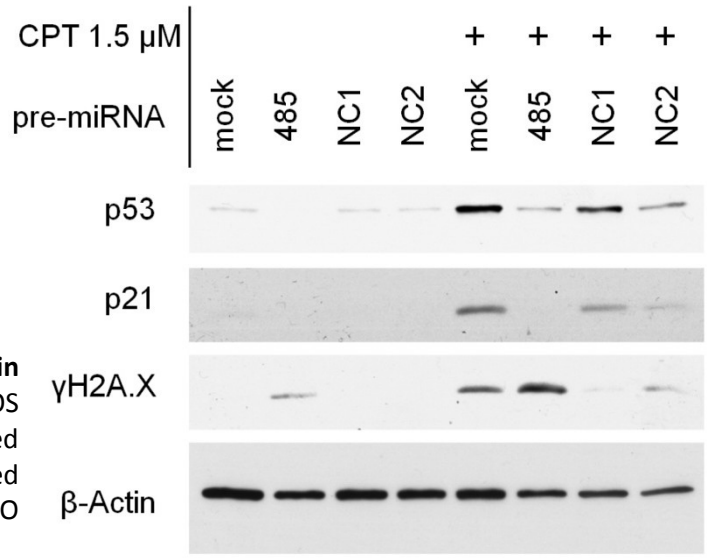

Figure 4.18: MiR-485 antagonizes p53 in U2OS cells. Wild type p53 expressing U2OS cells were transfected with the indicated synthetic miRNAs for 36h and treated either with camptothecin ('CPT') or DMSO for 12h. 'NC1', 'NC2': Non coding controls.

4.4.2 MiR-485 does not affect p53 in GH cells

GH cells were found to express high levels of endogenous miR-485 (Figure 4.19). Therefore, an antisense-oligonucleotide was designed by a similar strategy as in section 4.3.2 to antagonize miR-485. However, such an oligo neither had an effect on wild type p53 in unstimulated GH cells, nor in camptothecin stimulated GH cells (Figure 4.20). This was surprising, as the transfection conditions were precisely the same as in figure 4.17, where a strong effect of miR-302 on p63 was revealed.

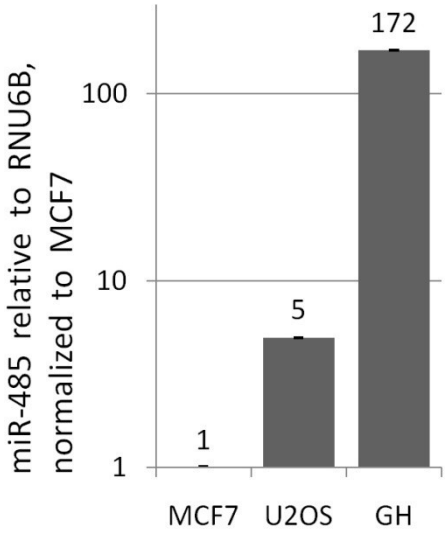

Figure 4.19: Relative miR-485 expression. Expression quantified with TaqMan assays relative to RNU6B. Data normalized to MCF7; average of technical triplicates.

Subsequently, synthetic premiR-485 was transfected into GH cells to verify that the interaction actually occurs in this cell line. It turned out that overexpression of miR-485 in GH cells does not cause p53 levels to decrease, nor does p21 induction upon camptothecin stimulation vanish, nor do any changes in γH2A.X pattern occur (Figure 4.21). Evidently, the effects observed in the 5637 and U2OS cells are not universal and depend on the cellular context

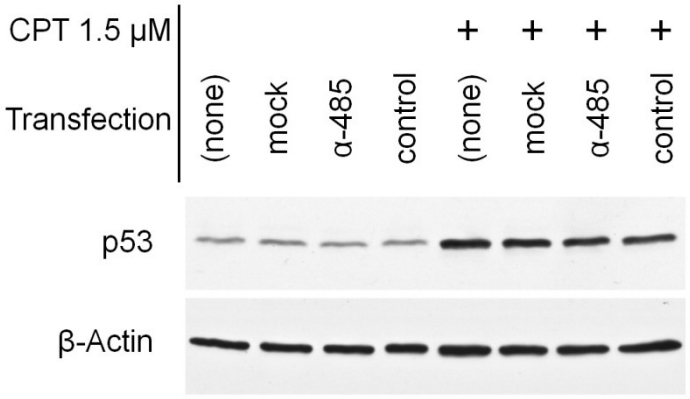

Figure 4.20: Endogenous miR-485 in GH cells does not regulate p53. GH cells were transfected for 24h with 'α-485', a 2'-O-MeOH-RNA/DNA antisense gapmer targeting miRNA 485, 'control', a similar oligonucleotide with reversed sequence or 'mock', transfection reagent alone and subsequently stimulated with camptothecin ('CPT') for 12h.

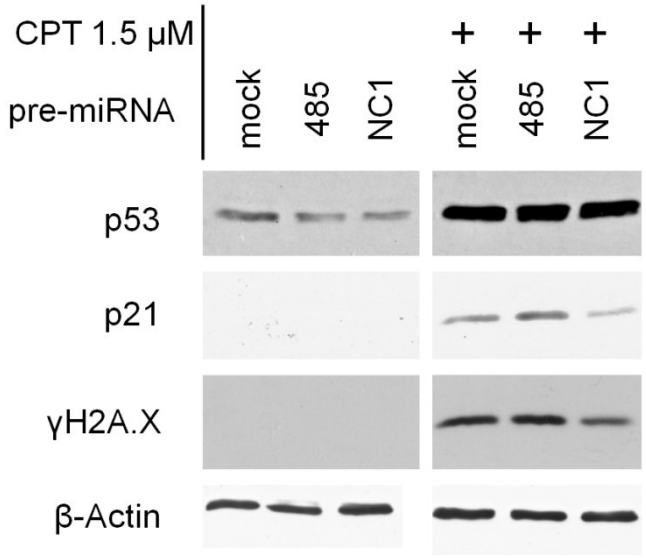

Figure 4.21: MiR-485 does not regulate p53 in GH cells. Wild type p53 expressing GH cells were transfected with the indicated synthetic miRNAs for 36h and treated either with camptothecin ('CPT') or DMSO for 12h. In contrast to U2OS cells, no downregulation of p53 is observed under either condition.

4.4.3 No direct interaction of miR-485 and the 3' untranslated region of p53

Given the findings in the GH cells (Figures 4.19-21) it was questionable whether miR-485 can actually directly bind p53 mRNA through the predicated binding sites. To investigate this putative interaction, the 1.1 kBp 3' UTR of p53 was cloned into a luciferase reporter plasmid ('pMIR-report' by Ambion). Coexpression of the reporter plasmid and plasmids expressing miR-485~668 or miR-22 showed no significant changes in luciferase activity compared to a control expression plasmid ('hTR', Figure 4.22). This finding makes a direct interaction unlikely. It might still be that such an interaction could depend on the exact structure of the p53 mRNA and does not happen with luciferase-p53 3' UTR mRNA. However, given the strong effects observed in figure 4.18, at least a small effect would have been expected. It rather seems that the effect of miR-485 on p53 is indirect and relies on some unknown mediator. The absence of an effect by miR-485 in GH cells might indicate that this putative mediator is not expressed in these cells, in contrast to U2OS and 5637 cells.

Figure 4.22: MiR-485 does not bind p53 3' UTR. The 1.1 kBp 3' UTR of p53 was cloned into a luciferase reporter plasmid and coexpressed with the indicated miRNAs or a control plasmid ('hTR'). Ratios of Firefly/Renilla luciferase normalized to 'hTR'. Columns represent means of biological triplicates, bars are the standard deviation.

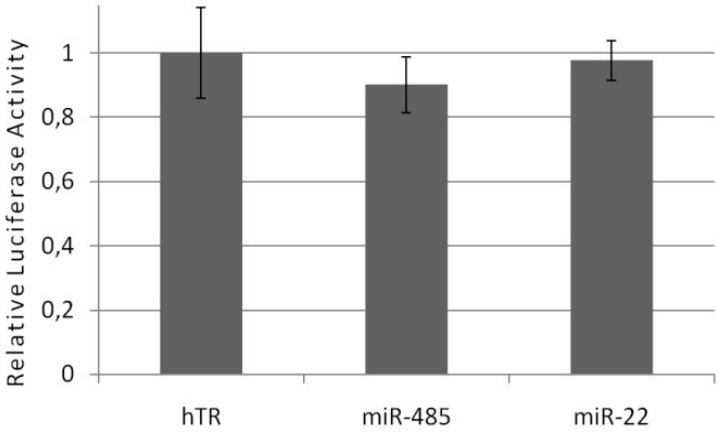

5 DISCUSSION

5.1 Overview

Overexpression screening of a large collection of miRNA encoding plasmids identified miR-302 as a novel family of p63-regulating miRNAs. Additionally, miR-485 was demonstrated as a possible indirect regulator of p53. The employed quantitative immunofluorescence technique seems adapt to identify novel regulators for any protein of interest.

At the beginning of this work, no miRNA-regulation of the p53-family had been demonstrated. Recently, miR-203 was found to regulate ΔNp63α during keratinocyte differentiation (Yi et al. 2008, Lena et al. 2008) and was thoroughly investigated in-vitro and in-vivo. Also, miR-21 (Papagiannakopoulos et al. 2008) and miR-92 (Manni et al. 2009) have been claimed to target p63. MiR-125b has been demonstrated as a direct regulator of p53 in the zebrafish and in human cell lines (Le et al. 2009).

MiR-302 downregulates p63 in malignant germ cell tumors and might play a physiological role during oocyte maturation, a context that is distinct from miRs-203/21/92. A broader picture of p63 regulation emerges in which each context of p63 expression also features a distinct p63-regulatory miRNA.

5.2 Immunofluorescence-based screening to identify regulatory microRNAs

In this project, comprehensive quantitative immunofluorescence analysis was established to identify regulatory miRNAs. This technique can be applied to identify regulators of any gene product that can be immunostained with sufficient sensitivity and specificity. When compared to the more commonly used coexpression of miRNAs with reporter constructs containing target 3' UTRs (Bartel 2004, le Sage et al. 2007), the immunostaining approach has several advantages: Endogenous proteins pose a more physiological read-out and are subject to both direct (e.g. miR-302) and indirect (e.g. miR-485) regulatory mechanisms. The absence of a reporter plasmid reduces the chance of unspecific effects e.g. via binding of miRNAs to the plasmid itself. The investigation of separately transfected miRNAs, as opposed to transfecting or transducing pools of different miRNAs and selecting for the most interesting candidate (Voorhoeve et al. 2006), yields unbiased results. Selection-steps are highly complex given the number of factors that influence selection-specificity which on the one hand might provoke the need for extensive full-up investigations of identified 'hits' and on the other hand might mask interesting findings that do not prevail the selection in the

respective setup. Finally, the immunofluorescence approach should be equally applicable to regulatory mechanisms other than RNA-interactions such as posttranslational modifications by kinases, phosphatases, ubiquitin-ligases and –hydrolyases, or acetyltransferases (Varjosalo et al. 2008). Automated transfection and staining procedures enable the parallel comparison of hundreds of putative regulators at a relatively high throughput and with little variation of experimental conditions between wells. This technique may thus prove generally useful in the identification of regulators for a given target in an unbiased and comprehensive analysis.

5.3 MiR-302 regulates p63

5.3.1 Importance of stage-specific p63 regulation in germ cell maturation

P63 has been identified in oocytes as well as in testicular cells; however, the most detailed analysis of its expression during different cell maturation stages was obtained in murine oocytes (Suh et al. 2006). Interestingly, detectable levels of TAp63α were observed in primordial and primary yet not in more advanced follicles; other p63 isoforms were not present. It has been shown that miR-302 is most highly expressed in the later stages of follicle maturation but is not present in ovulated oocytes (Tang et al. 2007). The temporal relation of these expression levels is summarized in figure 5.1. It is tempting to speculate that the pro-apoptotic function of TAp63α, although useful during meiotic arrest to avoid the accumulation of unnoticed DNA damage, may later be detrimental to mature oocytes. In any case, the disappearance of TAp63 in mature oocytes has not yet been explained mechanistically. Possibly, the increased expression of miR-302 in the stages immediately before ovulation at least contributes to this mechanism. Furthermore, even at earlier stages, miR-302 may reduce (although not eliminate) p63, avoiding excessive cell death and keeping a balance between DNA damage surveillance and cell survival. However, these concepts are

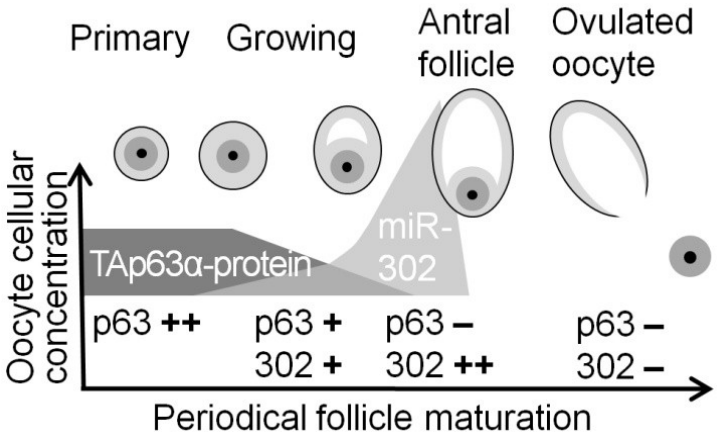

Figure 5.1: Putative regulation of TAp63α by miR-302 during oocyte maturation. This diagram summarized the TAp63α protein data by Suh et al. 2006 and the miR-302 expression data by Tang et al. 2007. Possibly, the disappearing of p63 happens simultaneously with a transient peak in miR-302 expression which might link the two events.

currently difficult to prove, given the obvious difficulties in obtaining sufficient amounts of oocytes for transfection with miR-302 antagonists and subsequent immunoblot analysis.

5.3.2 Putative roles of p63 in testes and testicular cancer

Testicular cancer cells such as GH and 833KE cells contain far less p63 mRNA and protein than normal testes, whereas they express high levels of miR-302 (U. Beyer, unpublished observations). MiR-302 was previously found as a characteristic of seminoma and embryonal carcinoma (Gillis et al. 2007). Although HDAC inhibition largely restores p63 levels in these cells, the amounts of p63 are further increased upon blockage of miR-302, suggesting that miR-302 at least contributes to the suppression of p63 in these tumor cells. Although it is tempting to speculate that the suppression of p63 represents a mechanism to avoid apoptosis and to increase resistance to genotoxic drugs, no major changes in cell death rates were observed in HDAC inhibitor-treated cells when p63 was removed by siRNA. Apparently, mechanisms other than p63 induction are at least sufficient to mediate death by HDAC inhibition. Yet, this does not preclude a pro-survival role of the miR-302-p63-antagonism at tumor stages where p63 transcription is not yet repressed.

Of note, the γ-isoform of p63 was detected in murine testes at unusually high levels (Petre-Lazar et al. 2006, 2007). This isoform is characterized by an alternative carboxyl terminus ending on exon 10' and has a 3' UTR that is distinct from the α- and β-isoforms. It is therefore conceivable that miR-302 targets the α and β but not γ isoforms of p63, thereby enhancing the relative fraction of gamma p63.

Furthermore, miR-302 can be expected to have additional targets on top of p63 and that this might also promote testicular cancer. For instance, cyclin D1 was recently found downregulated by miR-302, apparently leading to an enrichment of cells in the S phase of the cell cycle (Card et al. 2008). Similarly, the cyclin dependent kinase inhibitor p21 is subject to miR-302 regulation (Wang et al. 2008).

5.3.3 Regulation of miR-302

Given the fact that miR-302 can profoundly inhibit key genes in cell proliferation, the question arises how miR-302 levels are regulated. MiR-302 expression displays strong specificity for reproductive organ (Landgraf et al. 2007) and stem cells (Barroso-delJesus et al. 2008, Card et al. 2008). It was recently reported that this regulation is carried out by transcription factors expressed early during embryogenesis and in embryonic stem cells

(Card et al. 2008). Oct4 and Sox2 strongly induce miR-302 and the drop in Oct4/Sox2 levels during differentiation correlates with miR-302 reduction. Oct4 is also found strongly expressed in testicular cancer (Cheng et al. 2007) and in oocyte (Schöler et al. 1989). Interestingly Oct4 can itself be regulated by miRNAs, miR-134, miR-296, and miR-470 as part of cell differentiation (Tay et al. 2008). It suggests itself that miR-302 constitutes a key link that allows embryo-specific transcription factors, despite the limited set of their direct target promoters, to indirectly govern the expression of numerous genes to determine proliferation and differentiation.

5.3.4 MiR-203 regulates p63 in the epidermis

Additional miRNAs have been shown to regulate p63. By skin-specific conditional knockout of the essential miRNA processing enzyme Dicer, Yi et al. demonstrated the importance of miRNAs for proper development of epithelia and their appendage structures (Yi et al. 2008). This finding could be traced to miR-203 which directly represses p63. MiR-203 was detected in the suprabasel layers of the skin but not in the stem cell containing basal layer. MiR-203 expression was found to be rapidly induced between E13.5 and E15.5 and correlated with keratinocyte differentiation. Both in-vivo experiments using transgenic mice expressing miR-203 under control of the keratin 14 promoter as well as in-vitro overexpression caused accelerated depletion of p63-positive skin stem cells by reducing their proliferative potential. Conversely, specific antagonization of miR-203 with chemically modified antisense-oligonucleotides in-vivo and in-vitro as well as skin-specific inducible knockout of the essential miRNA processing enzyme Dicer increased epidermal proliferation and caused an atypical expansion of p63 expression. Immunoblots and luciferase-assays confirmed a direct interaction of miR-203 and p63-mRNA through two target sites which mainly cause translational inhibition. Lena et al. confirmed these findings but point out that though in-vitro overexpression of miR-203 enhances keratinocyte differentiation, it is not sufficient for full differentiation (Lena et al. 2008).

MiR-302 has not yet been described in the skin but in the light of the recent findings of Su et al. (2009) it seems worthy to have a second look: Given the new role of TAp63 in the regulation of adult stem cells located in specialized niches of the skin, it would be interesting to investigate if miR-302 might be involved in regulating p63 in those cells. Such a regulation might particularly occur when skin precursor cells are mobilized and start to proliferate, for example during wound healing.

5.3.5 MiR-21 and -92 as potential p63 regulators

MicroRNA-21 was among the first miRNAs found upregulated in human tumors (Landgraf et al. 2007). Most tumors overexpress miR-21 which seems to contribute to several hallmarks of malignancy, yet the responsible targets of this miRNA have not been elucidated satisfyingly (reviewed in Krichevsky and Gabriely 2008). Papagiannakopoulos et al. (2009) claim TAp63 to be among the major targets of miR-21 in glioblastoma. They use a computational approach to divide predicted miR-21 targets into functional groups and construct a network model. This model includes p63, but oddly the authors do not discriminate between different isoforms and their respective function. Real-time PCR of U251 glioblastoma cells is used to verify predicted targets. Given that most miRs regulate translation efficiency rather than mRNA stability (Bartel 2004, Carthew and Sontheimer 2009) this approach is uncommon. A direct interaction between miR-21 and p63 mRNA is claimed by showing that a 60bp fragment of p63 3' UTR causes ~20% downregulation when coexpressed with 50nmol pre-miR-21 (Ambion) in a luciferase reporter assay. 60bp are not representative of an UTR encompassing several thousand bps, 50nmol is a very high concentration for using synthetic miRNAs and a negative control of the experiment shows a high standard deviation, rendering the significance of this finding disputable. Also, no mutagenesis of the predicted binding site is performed. Next, the authors show by immunoblotting that antagonization of miR-21 causes elevated protein levels in U251 cells. However, no controls to verify the specificity of the employed antibody are present, such as overexpressed protein or a siRNA control (Papagiannakopoulos et al. 2009, Figure 4 A), even though an uncommon commercial polyclonal TAp63 antibody is used. In fact, additional bands can be seen on the immunoblot both above and below the claimed specific band which the authors do not comment about. Finally, HeLa cells are transfected with miR-21 and analyzed by immunoblotting using the same polyclonal TAp63 antibody and a decrease of endogenous TAp63 is claimed, again without specificity controls. The use of HeLa cells to study endogenous TAp63 is surprising as they are derived from cervical cancer, a squamous cell carcinoma of the cervix uteri which is known for its expression of ΔNp63α within the stratified squamous epithelium. Taken together, an effect of oncogenic miR-21 on p63 expression is possible and might influence cell survival, however, the data by Papagiannakopoulos et al. do not convincingly demonstrate such a regulation.

MiR-92 is part of the miR-17~92 cluster which has been demonstrated both as an oncogene and as an important developmental gene (Ventura et al. 2008). Manni et al. find miR-92 upregulated in murine 32D cells, a myeloid cell line. MiR-92 expression enhances proliferation of 32D cells which the authors attribute to downregulation of endogenous ΔNp63β. Using real-time PCR and immunoblotting, a translational repression of p63β mRNA is demonstrated. Overexpression of miR-92 reduces p63β in 32D cells and ΔNp63α in HaCaT cells, a human keratinocyte cell line. While the data obtained by overexpression of miR-92 show a clear decrease of p63α and β proteins, the effect of antagonization of endogenous miR-92 in 32D cells is not convincing: Judged by eye the protein levels of untreated and α-miR-92-LNA-treated 32D cells look comparable and the bands have not been quantified (Manni et al. 2009, Figure 4 A). MiR-92 expression does have an influence on proliferation of 32D cells as is reflected by the increase in proliferation upon overexpression and the decrease of proliferation upon antagonization and high levels of miR-92 do seem to antagonize p63α/β. However, the effect of endogenous miR-92 on endogenous p63 is not satisfyingly demonstrated. Also the use of the 4A4 antibody which is raised against human p63, on murine cells is arguable and should be safeguarded by siRNA controls. Still the finding is interesting, as p63 deregulation has been implicated in certain types of leukemia, e.g. both $p63^{+/-};p53^{+/-}$ and $p63^{+/-};p73^{+/-}$ double heterozygous knockout mice develop spontaneous myelogenous leukemia (Flores et al. 2005) and the miR-17~92 has also been implied in hemic diseases.

5.4 MiR-485 regulates p53

5.4.1 Possible mechanisms

MiR-485 first appeared to be a direct regulator of p53, as its overexpression causes decreased levels of both wild type p53 in U2OS cells and mutant R280T p53 in 5637 cells. Also, three putative binding sites within the p53 3' UTR were predicted by TargetScan. However, a luciferase reporter plasmid which produces a luciferase-p53 3' UTR mRNA is not at all regulated by coexpressed miR-485, making a direct interaction unlikely. On the one hand, a reporter assay does not rule out a direct interaction, as the precise conformation of the entire mRNA might be of importance, after all, inhibition of translation of the RISC is considered to involve formation of a loop between the 3' UTR and the 5' end of the respective mRNA (Figure 1.8, Carthew and Sontheimer 2009). On the other hand, the

absence of miR-485 effects on p53 in GH cells supports the assumption that the predicted binding sites are just physically present, not biologically functional: A RNA-RNA interaction should occur in any cellular system and GH are capable of producing functional mature miRNAs as is demonstrated by miR-302. Also, a possible expression of different p53 isoforms in GH cannot be suspected to be responsible for the absence of miR-485 regulation as all claimed p53 isoforms share the same 3' UTR (Murray-Zmijewski et al. 2006).

The current observations might be best explained by an indirect mechanism: MiR-485 might repress an activator of p53 or repress an inhibitor of a negative regulator. The $p19^{ARF}$-MDM2 loop would be of interest, if the miR-Vec screen had not been performed with mutant p53 which is presumably not degraded by MDM2 anymore. Another possibility might be that miR-485 negatively regulates ubiquitin specific peptidase HAUSP which has been demonstrated to deubiquitinate and stabilize p53 (Li et al. 2002). Mutant p53 protein does have an extended half-life yet will ultimately also be degraded by certain pathways which might involve ubiquitination. MiR-485 might also act upon factors which are required for the successful translation of p53 mRNA in some but not all tissues, or the regulation might be mediated by a longer, more complicated signaling pathway.

A strategy to identify a possible mediator of miR-485 regulation of p53 could take advantage of the context specificity of the effect. Comparative expression analysis of GH vs. U2OS and 5637 cells might identify differentially expressed proteins which might be involved. Depending on the length of the resulting list, it could be further narrowed down by checking which of the differentially expressed genes have predicated miR-485 binding-sites or if they are already implicated in p53 regulation.

Given the interesting fact that miR-485 does seem to be able to decrease both wild type and mutant p53 it appears worthy to further investigate this issue as it might yield the identification of a novel, universal p53 regulator.

5.4.2 Regulation of miR-485

In the human genome, mir-485 and 668 are part of a cluster of 38 miRNAs which spans ~ 45 kBp genomic sequence on chromosome 14q31 and is termed miR-379~410. It was demonstrated both by reporter assays and by ChIP that transcription factor Mef2 can activate transcription of miR-379~410 by directly binding its promoter. Experimental evidence suggests that the cluster is transcribed as one large polycistron. Interestingly, Mef2-dependent activation of the cluster has been found in neurons in response to

increased neuronal activity in-vitro and in-vivo (Fiore et al. 2009). Mef2 regulates dendrite-outgrowth of neurons and synapses-formation and some miRNAs of the miR-379~410 cluster are apparently required for successful dendrite-outgrowth. Given that neuronal activity is an important factor during development of the nervous system, it could be imagined that regulation of p53 by miR-485 might contribute to adjust apoptosis and survival according to neuronal activity.

MiR-125b has recently been described as a novel regulator of p53 (Le et al. 2009) and is also expressed in the nervous system. MiR-125b is assumed to regulate apoptosis during development and is repressed in response to genotoxic stress which contributes to p53 accumulation. MiR-125b is upregulated in certain neuronal tumors but was also found expressed in tumors of other origin such as pancreatic cancer.

It would be interesting to test in a neuronal model if Mef2-induced expression of miR-485 counteracts p53 and if such a suppression was also encountered in different contexts, similar to the activation of miR-125b in various contexts. Especially myogenesis could be of interest as both Mef2 and the p53-family have been demonstrated to essentially contribute to myogenic differentiation (Cam et al. 2006).

6 Summary

P63 is a homolog of tumor suppressor p53 and shares many of its structural and functional properties. However, its main functions are distinct and are essential during development and in maintenance of tissue stem cells as well as germ cells.

This work presents an immunofluorescence based screening approach which revealed microRNAs of the 302-cluster (miR-302) as novel regulators of p63 protein levels. Thorough investigation of the interaction between the p63α 3' UTR and miR-302 confirmed the direct mode of the regulation and demonstrated two responsible sequence elements. Isoforms with the γ carboxyl terminus have a distinct 3' UTR lacking miR-302 binding-sites. Transfection of miR-302 expression plasmid and of synthetic miR-302b successfully downregulated overexpressed and endogenous p63 in four different cell lines (5637, H1299, U2OS, GH). Both TAp63α and ΔNp63α are targeted by miR-302.

It could be shown that endogenous miR-302 is capable of regulating endogenous p63 levels in testicular cancer cells. As testicular cancers frequently lose p63 expression, this might be a mechanism contributing to the malignant phenotype. Known expression data for p63 and miR-302 suggest that this interaction might occur physiologically during oocyte maturation These results were recently published in a peer-reviewed journal (Scheel et al. 2009).

MicroRNA-485 (miR-485) was identified as a putative regulator of p53. In '5637' cells, miR-485 expression reduces levels of mutant p53, expression in 'U2OS' osteosarcoma cells reduces wild type p53, inhibits p21 induction upon genotoxic stress and causes elevated levels of γ-phosphorylated H2A.X histone proteins. This interaction seems to be indirect as miR-485 does not bind p53 mRNA in reporter assays. The observed effects did not occur in GH cells and are likely cell type specific. P53 attenuation by miR-485 might play a role in neurons during increased neuronal activity.

7 Literature

Barroso-delJesus A, Romero-López C, Lucena-Aguilar G, Melen GJ, Sanchez L, Ligero G, Berzal-Herranz A, Menendez P (2008): *Embryonic stem cell-specific miR302-367 cluster: human gene structure and functional characterization of its core promoter.* Mol Cell Biol 28(21), 6609-19

Bartel DP (2004): *MicroRNAs: genomics, biogenesis, mechanism, and function.* Cell 116(2), 281-97

Beaudenon S, Huibregtse JM (2008): *HPV E6, E6AP and cervical cancer.* BMC Biochem 21(9), Suppl 1:S4

Bonetta L (2009): *RNA-based therapeutics: ready for delivery?* Cell 136(4), 581-4

Bourdon JC (2007): *p53 and its isoforms in cancer.* Br J Cancer 97(3), 277-82

Braun CJ, Zhang X, Savelyeva I, Wolff S, Moll UM, Schepeler T, Ørntoft TF, Andersen CL, Dobbelstein M (2008): *p53-Responsive micrornas 192 and 215 are capable of inducing cell cycle arrest.* Cancer Res 68(24), 10094-104

Brummelkamp TR, Bernards R, Agami R (2002): *A system for stable expression of short interfering RNAs in mammalian cells.* Science 296(5567), 550-3

Cam H, Griesmann H, Beitzinger M, Hofmann L, Beinoraviciute-Kellner R, Sauer M, Hüttinger-Kirchhof N, Oswald C, Friedl P, Gattenlöhner S, Burek C, Rosenwald A, Stiewe T (2006): *p53 family members in myogenic differentiation and rhabdomyosarcoma development*. Cancer Cell 10(4), 281-93

Card DA, Hebbar PB, Li L, Trotter KW, Komatsu Y, Mishina Y, Archer TK (2008): *Oct4/Sox2-regulated miR-302 targets cyclin D1 in human embryonic stem cells*. Mol Cell Biol 28(20), 6426-38

Carthew RW, Sontheimer EJ (2009): *Origins and Mechanisms of miRNAs and siRNAs.* Cell 136(4), 642-55

Chambers JM, Cleveland WS, Kleiner B, Tukey PA: *Graphical Methods for Data Analysis.* The Wadsworth statistics/probability series, Duxbury Press, Pacific Groove CA, USA 1983

Cheng L, Sung MT, Cossu-Rocca P, Jones TD, MacLennan GT, De Jong J, Lopez-Beltran A, Montironi R, Looijenga LH (2007): *OCT4: biological functions and clinical applications as a marker of germ cell neoplasia.* J Pathol 211(1), 1-9

Cho Y, Gorina S, Jeffrey PD, Pavletich NP (1994): *Crystal structure of a p53 tumor suppressor-DNA complex: understanding tumorigenic mutations*. Science 265(5170), 346-55

Cooper TA, Wan L, Dreyfuss G (2009): *RNA and disease.* Cell 136(4), 777-93

Costinean S, Zanesi N, Pekarsky Y, Tili E, Volinia S, Heerema N, Croce CM (2006): *Pre-B cell proliferation and lymphoblastic leukemia/high-grade lymphoma in E(mu)-miR155 transgenic mice.* Proc Natl Acad Sci U S A 103(18), 7024-9

Davis LD, Zhang W, Merseburger A, Young D, Xu L, Rhim JS, Moul JW, Srivastava S, Sesterhenn IA (2002): *p63 expression profile in normal and malignant prostate epithelial cells.* Anticancer Res 22(6C), 3819-25

Davison TS, Vagner C, Kaghad M, Ayed A, Caput D, Arrowsmith CH (1999): *p73 and p63 are homotetramers capable of weak heterotypic interactions with each other but not with p53.* J Biol Chem 274(26), 18709-14

Deyoung MP, Ellisen LW (2007): *p63 and p73 in human cancer: defining the network.* Oncogene 26(36), 5169-83

Ding HF, McGill G, Rowan S, Schmaltz C, Shimamura A, Fisher DE (1998): *Oncogene-dependent regulation of caspase activation by p53 protein in a cell-free system.* J Biol Chem 273(43), 28378-83

Donehower LA, Harvey M, Slagle BL, McArthur MJ, Montgomery CA Jr, Butel JS, Bradley A (1992): *Mice deficient for p53 are developmentally normal but susceptible to spontaneous tumours.* Nature 356(6366), 215-21

Dyer BW, Ferrer FA, Klinedinst DK, Rodriguez R (2000): *A noncommercial dual luciferase enzyme assay system for reporter gene analysis.* Anal Biochem 282(1), 158-61

el-Deiry WS, Kern SE, Pietenpol JA, Kinzler KW, Vogelstein B (1992): *Definition of a consensus binding site for p53.* Nat Genet 1(1), 45-9

Elbashir SM, Harborth J, Lendeckel W, Yalcin A, Weber K, Tuschl T (2001): *Duplexes of 21-nucleotide RNAs mediate RNA interference in cultured mammalian cells.* Nature 411(6836), 494-8

Eliyahu D, Raz A, Gruss P, Givol D, Oren M (1984): *Participation of p53 cellular tumour antigen in transformation of normal embryonic cells.* Nature 312(5995), 646-9

Finlay CA, Hinds PW, Levine AJ (1989): *The p53 proto-oncogene can act as a suppressor of transformation.* Cell 57(7), 1083-93

Fiore R, Khudayberdiev S, Christensen M, Siegel G, Flavell SW, Kim TK, Greenberg ME, Schratt G (2009): *Mef2-mediated transcription of the miR379-410 cluster regulates activity-dependent dendritogenesis by fine-tuning Pumilio2 protein levels.* EMBO J 28(6), 697-710

Fire A, Xu S, Montgomery MK, Kostas SA, Driver SE, Mello CC (1998): *Potent and specific genetic interference by double-stranded RNA in Caenorhabditis elegans.* Nature 391(6669), 806-11

Flores ER, Sengupta S, Miller JB, Newman JJ, Bronson R, Crowley D, Yang A, McKeon F, Jacks T (2005): *Tumor predisposition in mice mutant for p63 and p73: evidence for broader tumor suppressor functions for the p53 family.* Cancer Cell 7(4), 363-73

Fogh J (1978): *Cultivation, characterization, and identification of human tumor cells with emphasis on kidney, testis, and bladder tumors*. Natl Cancer Inst Monogr 49, 5-9

Fomenkov A, Huang YP, Topaloglu O, Brechman A, Osada M, Fomenkova T, Yuriditsky E, Trink B, Sidransky D, Ratovitski E (2003): *P63 alpha mutations lead to aberrant splicing of keratinocyte growth factor receptor in the Hay-Wells syndrome.* J Biol Chem 278(26), 23906-14

Friedman PN, Chen X, Bargonetti J, Prives C (1993): *The p53 protein is an unusually shaped tetramer that binds directly to DNA.* Proc Natl Acad Sci U S A 90(8), 3319-23

Friedman RC, Farh KK, Burge CB, Bartel DP (2009): *Most mammalian mRNAs are conserved targets of microRNAs.* Genome Res 19(1), 92-105

Gaiddon C, Lokshin M, Ahn J, Zhang T, Prives C (2001): *A subset of tumor-derived mutant forms of p53 down-regulate p63 and p73 through a direct interaction with the p53 core domain.* Mol Cell Biol 21(5), 1874-87

García-Cao I, García-Cao M, Martín-Caballero J, Criado LM, Klatt P, Flores JM, Weill JC, Blasco MA, Serrano M (2002): *"Super p53" mice exhibit enhanced DNA damage response, are tumor resistant and age normally.* EMBO J 21(22), 6225-35

Gilbert W (1986): *The RNA world.* Nature 319(6055), 618

Gillis AJ, Stoop HJ, Hersmus R, Oosterhuis JW, Sun Y, Chen C, Guenther S, Sherlock J, Veltman I, Baeten J, van der Spek PJ, de Alarcon P, Looijenga LH (2007): *High-throughput microRNAome analysis in human germ cell tumours.* J Pathol 213(3), 319-28

Griffiths-Jones S, Grocock RJ, van Dongen S, Bateman A, Enright AJ (2006): *miRBase: microRNA sequences, targets and gene nomenclature*. Nucleic Acids Res 34(Database issue), D140-4

Hanahan D, Weinberg RA (2000): *The hallmarks of cancer.* Cell 100(1), 57-70

Hayflick L (1965): *The limited in vitro lifetime of human diploid cell strains.* Exp Cell Res 37, 614-36

Hermeking H (2007): *p53 enters the microRNA world.* Cancer Cell 12(5), 414-8

Hibi K, Trink B, Patturajan M, Westra WH, Caballero OL, Hill DE, Ratovitski EA, Jen J, Sidransky D (2000): *AIS is an oncogene amplified in squamous cell carcinoma.* Proc Natl Acad Sci U S A 97(10), 5462-7

Hicks GG, Egan SE, Greenberg AH, Mowat M (1991): *Mutant p53 tumor suppressor alleles release ras-induced cell cycle growth arrest.* Mol Cell Biol 11(3), 1344-52

Higashikawa K, Yoneda S, Tobiume K, Taki M, Shigeishi H, Kamata N (2007): *Snail-induced down-regulation of DeltaNp63alpha acquires invasive phenotype of human squamous cell carcinoma.* Cancer Res 67(19), 9207-13

Hoeijmakers JH (2009): *DNA damage, aging, and cancer.* N Engl J Med 361(15), 1475-85

Huang Q, Gumireddy K, Schrier M, le Sage C, Nagel R, Nair S, Egan DA, Li A, Huang G, Klein-Szanto AJ, Gimotty PA, Katsaros D, Coukos G, Zhang L, Puré E, Agami R (2008): *The microRNAs miR-373 and miR-520c promote tumour invasion and metastasis.* Nat Cell Biol 10(2), 202-10

Johnston WK, Unrau PJ, Lawrence MS, Glasner ME, Bartel DP (2001): *RNA-catalyzed RNA polymerization: accurate and general RNA-templated primer extension.* Science 292(5520), 1319-25

Jost CA, Marin MC, Kaelin WG Jr (1997): p73 *is a simian p53-related protein that can induce apoptosis*. Nature 389(6647), 191-4

Kaghad M, Bonnet H, Yang A, Creancier L, Biscan JC, Valent A, Minty A, Chalon P, Lelias JM, Dumont X, Ferrara P, McKeon F, Caput D (1997): *Monoallelically expressed gene related to p53 at 1p36, a region frequently deleted in neuroblastoma and other human cancers.* Cell 90(4), 809-19

Keyes WM, Wu Y, Vogel H, Guo X, Lowe SW, Mills AA (2005): *p63 deficiency activates a program of cellular senescence and leads to accelerated aging.* Genes Dev 19(17), 1986-99

Keyes WM, Vogel H, Koster MI, Guo X, Qi Y, Petherbridge KM, Roop DR, Bradley A, Mills AA (2006): *p63 heterozygous mutant mice are not prone to spontaneous or chemically induced tumors.* Proc Natl Acad Sci U S A 103(22), 8435-40

Koster MI, Kim S, Mills AA, DeMayo FJ, Roop DR (2004): *p63 is the molecular switch for initiation of an epithelial stratification program.* Genes Dev 18(2), 126-31

Koster MI, Lu SL, White LD, Wang XJ, Roop DR (2006): *Reactivation of developmentally expressed p63 isoforms predisposes to tumor development and progression.* Cancer Res 66(8), 3981-6

Krichevsky AM, Gabriely G (2008): *miR-21: a small multi-faceted RNA.* J Cell Mol Med 13(1), 39-53

Kumar MS, Lu J, Mercer KL, Golub TR, Jacks T (2007): *Impaired microRNA processing enhances cellular transformation and tumorigenesis.* Nat Genet 39(5), 673-7

Lahav G, Rosenfeld N, Sigal A, Geva-Zatorsky N, Levine AJ, Elowitz MB, Alon U (2004): *Dynamics of the p53-Mdm2 feedback loop in individual cells.* Nat Genet 36(2), 147-50

Landgraf P, Rusu M, Sheridan R, Sewer A, Iovino N, Aravin A, Pfeffer S, Rice A, Kamphorst AO, Landthaler M, Lin C, Socci ND, Hermida L, Fulci V, Chiaretti S, Foà R, Schliwka J, Fuchs U, Novosel A, Müller RU, Schermer B, Bissels U, Inman J, Phan Q, Chien M, Weir DB, Choksi R, De Vita G, Frezzetti D, Trompeter HI, Hornung V, Teng G, Hartmann G, Palkovits M, Di Lauro R, Wernet P, Macino G, Rogler CE, Nagle JW, Ju J, Papavasiliou FN, Benzing T, Lichter P, Tam W, Brownstein MJ, Bosio A, Borkhardt A, Russo JJ, Sander C, Zavolan M, Tuschl T (2007): *A mammalian microRNA expression atlas based on small RNA library sequencing*. Cell 129(7), 1401-14

Lane DP, Crawford LV (1979): *T antigen is bound to a host protein in SV40-transformed cells.* Nature 278(5701), 261-3

Le MT, Teh C, Shyh-Chang N, Xie H, Zhou B, Korzh V, Lodish HF, Lim B (2009): *MicroRNA-125b is a novel negative regulator of p53.* Genes Dev 23(7), 862-76

Lee HO, Lee JH, Choi E, Seol JY, Yun Y, Lee H (2006): *A dominant negative form of p63 inhibits apoptosis in a p53-independent manner*. Biochem Biophys Res Commun 344(1), 166-72

Lee RC, Feinbaum RL, Ambros V (1993): *The C. elegans heterochronic gene lin-4 encodes small RNAs with antisense complementarity to lin-14.* Cell 75(5), 843-54

Lena AM, Shalom-Feuerstein R, Rivetti di Val Cervo P, Aberdam D, Knight RA, Melino G, Candi E (2008): *miR-203 represses 'stemness' by repressing DeltaNp63.* Cell Death Differ 15(7), 1187-95

Lennox KA, Sabel JL, Johnson MJ, Moreira BG, Fletcher CA, Rose SD, Behlke MA, Laikhter AL, Walder JA, Dagle JM (2006): *Characterization of modified antisense oligonucleotides in Xenopus laevis embryos.* Oligonucleotides 16(1), 26-42

Levine AJ (2009): *The common mechanisms of transformation by the small DNA tumor viruses: The inactivation of tumor suppressor gene products: p53.* Virology 384(2), 285-93

Levine AJ, Hu W, Feng Z (2006): *The P53 pathway: what questions remain to be explored?* Cell Death Differ 13(6), 1027-36

Lewis BP, Burge CB, Bartel DP (2005): *Conserved seed pairing, often flanked by adenosines, indicates that thousands of human genes are microRNA targets.* Cell 120(1), 15-20

Li M, Chen D, Shiloh A, Luo J, Nikolaev AY, Qin J, Gu W (2002): *Deubiquitination of p53 by HAUSP is an important pathway for p53 stabilization.* Nature 416(6881), 648-53

Linzer DI, Levine AJ (1979): *Characterization of a 54K dalton cellular SV40 tumor antigen present in SV40-transformed cells and uninfected embryonal carcinoma cells.* Cell 17(1), 43-52

Livera G, Petre-Lazar B, Guerquin MJ, Trautmann E, Coffigny H, Habert R (2008): *p63 null mutation protects mouse oocytes from radio-induced apoptosis.* Reproduction 135(1), 3-12

Ma L, Teruya-Feldstein J, Weinberg RA (2007): *Tumour invasion and metastasis initiated by microRNA-10b in breast cancer.* Nature 449(7163), 682-8

Manni I, Artuso S, Careccia S, Rizzo MG, Baserga R, Piaggio G, Sacchi A (2009): *The microRNA miR-92 increases proliferation of myeloid cells and by targeting p63 modulates the abundance of its isoforms.* FASEB J 23(11), 3957-66

Marchenko ND, Zaika A, Moll UM (2000): *Death signal-induced localization of p53 protein to mitochondria. A potential role in apoptotic signaling.* J Biol Chem 275(21), 16202-12

Meister G, Tuschl T (2004): *Mechanisms of gene silencing by double-stranded RNA.* Nature 431(7006), 343-9

Meister G, Landthaler M, Dorsett Y, Tuschl T (2004): *Sequence-specific inhibition of microRNA- and siRNA-induced RNA silencing.* RNA 10(3), 544-50

Melino G, Lu X, Gasco M, Crook T, Knight RA (2003): *Functional regulation of p73 and p63: development and cancer.* Trends Biochem Sci 28(12), 663-70

Mills AA, Zheng B, Wang XJ, Vogel H, Roop DR, Bradley A (1999): *p63 is a p53 homologue required for limb and epidermal morphogenesis*. Nature 398(6729), 708-13

Moffat J, Grueneberg DA, Yang X, Kim SY, Kloepfer AM, Hinkle G, Piqani B, Eisenhaure TM, Luo B, Grenier JK, Carpenter AE, Foo SY, Stewart SA, Stockwell BR, Hacohen N, Hahn WC, Lander ES, Sabatini DM, Root DE (2006): *A lentiviral RNAi library for human and mouse genes applied to an arrayed viral high-content screen.* Cell 124(6), 1283-98

Moll UM, Slade N (2004): *p63 and p73: roles in development and tumor formation.* Mol Cancer Res 2(7), 371-86

Murray-Zmijewski F, Lane DP, Bourdon JC (2006): *p53/p63/p73 isoforms: an orchestra of isoforms to harmonise cell differentiation and response to stress.* Cell Death Differ 13(6), 962-72

Oliner JD, Pietenpol JA, Thiagalingam S, Gyuris J, Kinzler KW, Vogelstein B (1993): *Oncoprotein MDM2 conceals the activation domain of tumour suppressor p53.* Nature 362(6423), 857-60

Osada M, Ohba M, Kawahara C, Ishioka C, Kanamaru R, Katoh I, Ikawa Y, Nimura Y, Nakagawara A, Obinata M, Ikawa S (1998): *Cloning and functional analysis of human p51, which structurally and functionally resembles p53.* Nat Med 4(7), 839-43

Papagiannakopoulos T, Shapiro A, Kosik KS (2008): *MicroRNA-21 targets a network of key tumor-suppressive pathways in glioblastoma cells.* Cancer Res 68(19), 8164-72

Petre-Lazar B, Moreno SG, Livera G, Duquenne C, Habert R, Coffigny H (2006): *p63 expression pattern in foetal and neonatal gonocytes after irradiation and role in the resulting apoptosis by using p63 knockout mice*. Int J Radiat Biol 82(11), 771-80

Petre-Lazar B, Livera G, Moreno SG, Trautmann E, Duquenne C, Hanoux V, Habert R, Coffigny H (2007): *The role of p63 in germ cell apoptosis in the developing testis.* J Cell Physiol 210(1), 87-98

Radoja N, Guerrini L, Lo Iacono N, Merlo GR, Costanzo A, Weinberg WC, La Mantia G, Calabrò V, Morasso MI (2007): *Homeobox gene Dlx3 is regulated by p63 during ectoderm development: relevance in the pathogenesis of ectodermal dysplasias.* Development 134(1), 13-8

R Development Core Team (2007). *R: A language and environment for statistical computing.* R Foundation for Statistical Computing, Vienna, Austria. ISBN 3-900051-07-0, URL http://www.R-project.org

Rossi M, Aqeilan RI, Neale M, Candi E, Salomoni P, Knight RA, Croce CM, Melino G (2006): *The E3 ubiquitin ligase Itch controls the protein stability of p63*. Proc Natl Acad Sci U S A 103(34), 12753-8

Roth J, Dobbelstein M (2003): *Interaction of p53 with the adenovirus E1B-55 kDa protein.* Methods Mol Biol 234, 135-49

le Sage C, Nagel R, Egan DA, Schrier M, Mesman E, Mangiola A, Anile C, Maira G, Mercatelli N, Ciafrè SA, Farace MG, Agami R (2007): *Regulation of the p27(Kip1) tumor suppressor by miR-221 and miR-222 promotes cancer cell proliferation.* EMBO J 26(15), 3699-708

Sah VP, Attardi LD, Mulligan GJ, Williams BO, Bronson RT, Jacks T (1995): *A subset of p53-deficient embryos exhibit exencephaly.* Nat Genet 10(2), 175-80

Sayan BS, Sayan AE, Yang AL, Aqeilan RI, Candi E, Cohen GM, Knight RA, Croce CM, Melino G (2007): *Cleavage of the transactivation-inhibitory domain of p63 by caspases enhances apoptosis.* Proc Natl Acad Sci U S A 104(26), 10871-6

Scheel AH, Beyer U, Agami R, Dobbelstein M (2009): *Immunofluorescence-based screening identifies germ cell associated microRNA 302 as an antagonist to p63 expression.* Cell Cycle 8(9), 1426-32

Scheel C, Onder T, Karnoub A, Weinberg RA (2007): *Adaptation versus selection: the origins of metastatic behavior.* Cancer Res 67(24), 11476-9

Schöler HR, Hatzopoulos AK, Balling R, Suzuki N, Gruss P (1989): *A family of octamer-specific proteins present during mouse embryogenesis: evidence for germline-specific expression of an Oct factor.* EMBO J 8(9), 2543-50

Serber Z, Lai HC, Yang A, Ou HD, Sigal MS, Kelly AE, Darimont BD, Duijf PH, Van Bokhoven H, McKeon F, Dötsch V (2002): *A C-terminal inhibitory domain controls the activity of p63 by an intramolecular mechanism.* Mol Cell Biol 22(24), 8601-11

Su X, Cho MS, Gi YJ, Ayanga BA, Sherr CJ, Flores ER (2009a): *Rescue of key features of the p63-null epithelial phenotype by inactivation of Ink4a and Arf.* EMBO J 28(13), 1904-15

Su X, Paris M, Gi YJ, Tsai KY, Cho MS, Lin YL, Biernaskie JA, Sinha S, Prives C, Pevny LH, Miller FD, Flores ER (2009b): *TAp63 prevents premature aging by promoting adult stem cell maintenance.* Cell Stem Cell 5(1), 64-75

Suh EK, Yang A, Kettenbach A, Bamberger C, Michaelis AH, Zhu Z, Elvin JA, Bronson RT, Crum CP, McKeon F (2006): *p63 protects the female germ line during meiotic arrest.* Nature 444(7119), 624-8

Tang F, Kaneda M, O'Carroll D, Hajkova P, Barton SC, Sun YA, Lee C, Tarakhovsky A, Lao K, Surani MA (2007): Maternal microRNAs are essential for mouse zygotic development. Genes Dev 21(6), 644-8

Tay Y, Zhang J, Thomson AM, Lim B, Rigoutsos I (2008): *MicroRNAs to Nanog, Oct4 and Sox2 coding regions modulate embryonic stem cell differentiation*. Nature 455(7216), 1124-8

Trink B, Okami K, Wu L, Sriuranpong V, Jen J, Sidransky D (1998): *A new human p53 homologue*. Nat Med 4(7), 747-8

Tuschl T, Thomson JB, Eckstein F (1995): *RNA cleavage by small catalytic RNAs.* Curr Opin Struct Biol 5(3), 296-302

Tyner SD, Venkatachalam S, Choi J, Jones S, Ghebranious N, Igelmann H, Lu X, Soron G, Cooper B, Brayton C, Hee Park S, Thompson T, Karsenty G, Bradley A, Donehower LA (2002): *p53 mutant mice that display early ageing-associated phenotypes*. Nature 415(6867), 45-53

Varjosalo M, Björklund M, Cheng F, Syvänen H, Kivioja T, Kilpinen S, Sun Z, Kallioniemi O, Stunnenberg HG, He WW, Ojala P, Taipale J (2008): *Application of active and kinase-deficient kinome collection for identification of kinases regulating hedgehog signaling.* Cell 133(3), 537-48

Vassilev LT, Vu BT, Graves B, Carvajal D, Podlaski F, Filipovic Z, Kong N, Kammlott U, Lukacs C, Klein C, Fotouhi N, Liu EA (2004): *In vivo activation of the p53 pathway by small-molecule antagonists of MDM2.* Science 303(5659), 844-8

Ventura A, Jacks T (2009): *MicroRNAs and cancer: short RNAs go a long way.* Cell 136(4), 586-91

Ventura A, Young AG, Winslow MM, Lintault L, Meissner A, Erkeland SJ, Newman J, Bronson RT, Crowley D, Stone JR, Jaenisch R, Sharp PA, Jacks T (2008): *Targeted deletion reveals essential and overlapping functions of the miR-17 through 92 family of miRNA clusters.* Cell 132(5), 875-86

Vogelstein B, Lane D, Levine AJ (2000): *Surfing the p53 network*. Nature 408(6810), 307-10

Voorhoeve PM, le Sage C, Schrier M, Gillis AJ, Stoop H, Nagel R, Liu YP, van Duijse J, Drost J, Griekspoor A, Zlotorynski E, Yabuta N, De Vita G, Nojima H, Looijenga LH, Agami R (2006): *A genetic screen implicates miRNA-372 and miRNA-373 as oncogenes in testicular germ cell tumors*. Cell 124(6), 1169-81

Wahl MC, Will CL, Lührmann R (2009): *The spliceosome: design principles of a dynamic RNP machine.* Cell 2009 136(4), 701-18

Waltermann A, Kartasheva NN, Dobbelstein M (2003): *Differential regulation of p63 and p73 expression.* Oncogene 22(36), 5686-93

Wang Y, Baskerville S, Shenoy A, Babiarz JE, Baehner L, Blelloch R (2008): *Embryonic stem cell-specific microRNAs regulate the G1-S transition and promote rapid proliferation.* Nat Genet 40(12), 1478-83

Weinberg RA: *The Biology of Cancer*. Garland Science, Taylor & Fracis Group, New York, USA, 2007

Westfall MD, Mays DJ, Sniezek JC, Pietenpol JA (2003): *The Delta Np63 alpha phosphoprotein binds the p21 and 14-3-3 sigma promoters in vivo and has transcriptional repressor activity that is reduced by Hay-Wells syndrome-derived mutations*. Mol Cell Biol 23(7), 2264-76

Winberg G, Matskova L, Chen F, Plant P, Rotin D, Gish G, Ingham R, Ernberg I, Pawson T (2000): *Latent membrane protein 2A of Epstein-Barr virus binds WW domain E3 protein-ubiquitin ligases that ubiquitinate B-cell tyrosine kinases.* Mol Cell Biol 20(22), 8526-35

Wolff S, Talos F, Palacios G, Beyer U, Dobbelstein M, Moll UM (2009): *The alpha/beta carboxy-terminal domains of p63 are required for skin and limb development. New insights from the Brdm2 mouse which is not a complete p63 knockout but expresses p63 gamma-like proteins*. Cell Death Differ 16(8), 1108-17

Yang A, Kaghad M, Wang Y, Gillett E, Fleming MD, Dötsch V, Andrews NC, Caput D, McKeon F (1998): *p63, a p53 homolog at 3q27-29, encodes multiple products with transactivating, death-inducing, and dominant-negative activities.* Mol Cell 2(3), 305-16

Yang A, Schweitzer R, Sun D, Kaghad M, Walker N, Bronson RT, Tabin C, Sharpe A, Caput D, Crum C, McKeon F (1999): *p63 is essential for regenerative proliferation in limb, craniofacial and epithelial development.* Nature 398(6729), 714-8

Yi R, Poy MN, Stoffel M, Fuchs E (2008): *A skin microRNA promotes differentiation by repressing 'stemness'.* Nature 452(7184), 225-9

Zangen R, Ratovitski E, Sidransky D (2005): *DeltaNp63alpha levels correlate with clinical tumor response to cisplatin.* Cell Cycle 4(10), 1313-5

Zhang Y, Xiong Y, Yarbrough WG (1998): *ARF promotes MDM2 degradation and stabilizes p53: ARF-INK4a locus deletion impairs both the Rb and p53 tumor suppression pathways.* Cell 92(6), 725-34

8 Appendix

8.1 Supplemental Table 1: Screen results for p63

Plate 1 of 4, p63-fluorescence of GFP-positive cells

	Lower Whisker	Lower Hinge	Median	Upper Hinge	Upper Whisker	**Trimmed Mean**	**z-score**
sh-p63 (2)	424	495	521	553	636	521	-4,1
sh-p63 (1)	413	499	524	561	646	525	-4,0
ITCH (2)	440	522	579	693	944	617	-2,3
ITCH (1)	479	536	586	712	925	629	-2,0
miR-302a:d	445	564	624	695	890	633	-2,0
miR-199a-1	411	592	680	762	1007	681	-1,1
miR-10b	442	596	671	764	1016	685	-1,0
miR-148a	423	608	685	765	1000	687	-0,9
miR-128b	442	593	677	768	1030	689	-0,9
miR-21	438	595	679	772	1038	691	-0,9
miR-197	429	598	685	771	1031	691	-0,9
miR-184	446	607	682	771	1014	693	-0,8
miR-191	435	614	692	773	1010	695	-0,8
miR-151	433	598	685	781	1051	696	-0,8
miR-108	439	613	691	777	1024	698	-0,7
miR-101	398	605	694	789	1060	699	-0,7
miR-106	428	614	699	778	1024	699	-0,7
miR-372,371	426	611	694	784	1042	701	-0,7
miR-148b	423	613	692	786	1043	701	-0,7
miR-200c, 141	452	614	692	780	1025	701	-0,7
miR-219	418	610	694	793	1064	704	-0,6
miR-199a-2	464	636	710	779	992	708	-0,6
miR-27b	459	616	697	795	1059	712	-0,5
miR-192,194-2	446	623	707	799	1063	716	-0,4
BHRF1-1	428	625	710	802	1067	716	-0,4
miR-123	417	626	711	805	1071	716	-0,4
miR-339	438	645	717	796	1022	717	-0,4
miR-25	446	629	716	799	1052	718	-0,4
Vector Ctrl (2)	472	619	695	804	1080	718	-0,4
miR-145	446	632	717	804	1061	721	-0,3
miR-346	455	645	726	802	1029	724	-0,3
miR-34	426	641	722	810	1064	724	-0,2
miR-152	408	640	723	817	1082	726	-0,2
miR-30c	435	634	724	813	1080	727	-0,2
miR-337	484	654	721	802	1019	727	-0,2
miR-374	445	649	721	812	1054	728	-0,2
miR-136	448	641	724	818	1080	732	-0,1
miR-368	568	665	729	786	966	732	-0,1
Let-7a1	450	665	729	813	1033	732	-0,1
miR-223	447	638	728	818	1087	733	-0,1
Let-7e	490	658	730	814	1029	735	0,0
miR-30	430	658	737	824	1071	737	0,0
miR-15a	466	660	732	818	1054	737	0,0
miR-23	469	643	729	824	1094	739	0,0
miR-187	449	663	737	825	1063	740	0,0
miR-204	438	656	740	831	1094	743	0,1
miR-323	490	667	734	822	1052	743	0,1
miR-130a	474	677	746	819	1030	743	0,1

miR-97	457	668	751	827	1064	746	0,2
miR-217	424	658	746	838	1108	747	0,2
miR-32	447	650	740	839	1121	748	0,2
miR-16/15a	418	658	744	843	1120	748	0,2
sh-p53	458	666	744	836	1085	749	0,2
miR-135b	451	671	747	835	1079	749	0,2
miR-320	484	666	746	830	1075	750	0,2
miR-9	417	662	754	846	1122	753	0,3
Vector Ctrl (1)	494	665	743	834	1088	753	0,3
miR-34c	438	652	750	846	1132	753	0,3
miR-100	468	675	751	838	1072	753	0,3
BHRF1-2	452	653	741	848	1135	753	0,3
miR-23b	496	688	755	830	1041	755	0,3
miR-370	525	662	746	832	1081	755	0,3
miR-125a	479	678	752	841	1086	758	0,4
miR-182	458	675	750	850	1106	759	0,4
miR-196b	420	660	752	861	1161	760	0,4
miR-206	475	669	751	848	1117	761	0,4
miR-128	486	667	753	851	1124	764	0,5
miR-194	497	680	764	848	1080	765	0,5
miR-29c	528	683	762	857	1036	766	0,5
miR-330	487	689	760	856	1103	770	0,6
miR-221	490	683	761	856	1113	770	0,6
Let-7C	452	691	769	860	1112	770	0,6
miR-19a	483	685	764	864	1133	775	0,7
miR-296	467	680	768	871	1157	777	0,7
miR-139	438	681	774	877	1169	778	0,8
miR-33	406	686	775	884	1177	779	0,8
BART-2	505	705	786	855	1076	779	0,8
miR-24/189	433	688	777	880	1168	781	0,8
miR-99b	508	686	772	870	1128	781	0,8
miR-154	500	709	783	864	1092	782	0,8
miR-126	444	696	787	892	1185	792	1,0
Let-7g	467	701	786	887	1165	792	1,0
miR-30b	481	715	792	884	1128	793	1,0
miR-18	499	725	790	887	1131	799	1,2
miR-213	451	711	802	897	1168	799	1,2
miR-376a	471	689	787	902	1220	800	1,2
miR-134	448	688	792	909	1237	802	1,2
miR-99	503	722	795	892	1142	802	1,2
miR-137	450	694	805	924	1265	814	1,4
miR-208	430	724	824	941	1266	828	1,7
miR-181b	514	729	816	929	1228	830	1,7
miR-142	451	744	833	940	1233	834	1,8
ITCH C830A	537	721	828	932	1242	837	1,9
Untrfx.	NA	NA	NA	NA	NA	NA	NA
					Mean	738	
					SD	53	

Plate 2 of 4, p63-fluorescence of GFP-positive cells

	Lower Whisker	Lower Hinge	Median	Upper Hinge	Upper Whisker	**Trimmed Mean**	**z-score**
sh-p63 (1)	444	508	537	574	669	540	-4,2
sh-p63 (2)	466	521	543	579	650	546	-4,1
ITCH	481	551	610	698	915	635	-2,2
miR-X49	399	580	649	713	897	643	-2,0
miR-X110	431	580	651	733	958	660	-1,7
cand-216	376	515	651	762	1091	661	-1,7
miR-X112	455	600	665	725	909	663	-1,6
miR-X118	459	601	663	729	913	665	-1,6
miR-X143	498	583	649	731	952	667	-1,5
miR-X269	469	629	691	759	938	691	-1,0
miR-X39	407	597	702	787	1016	694	-0,9
cand-279	477	637	697	764	951	698	-0,9
miR-490	485	634	693	768	955	699	-0,9
miR-X167	470	631	702	769	975	701	-0,8
miR-517c	445	635	702	775	983	702	-0,8
cand-219	467	644	704	777	970	706	-0,7
miR-X215	507	646	704	769	948	707	-0,7
miR-X254	499	648	709	779	950	710	-0,6
miR-X189	520	634	707	780	976	712	-0,6
miR-X194	492	651	713	778	967	713	-0,6
cand-347	503	667	724	780	938	718	-0,5
miR-X147	493	655	722	787	981	720	-0,4
miR-450	492	644	719	793	1017	722	-0,4
miR-X87	509	674	733	785	945	725	-0,3
miR-X252	471	653	723	799	1018	725	-0,3
miR-X145	456	662	728	803	1009	726	-0,3
cand-420	474	662	732	797	997	726	-0,3
miR-X197	513	670	727	790	970	727	-0,3
miR-519e	503	652	725	797	1010	727	-0,2
miR-X238	471	639	726	808	1045	728	-0,2
miR-X170	513	678	728	794	969	730	-0,2
miR-X100	473	673	737	811	1007	735	-0,1
miR-X15	485	659	733	813	1029	735	-0,1
miR-519c	567	663	718	807	989	736	-0,1
miR-511	471	655	737	815	1050	737	0,0
miR-487	546	685	739	798	955	738	0,0
miR-X226	461	667	741	818	1038	739	0,0
cand-707	509	683	743	805	983	739	0,0
miR-X129	466	670	745	817	1032	740	0,0
miR-432	498	685	748	812	1002	744	0,1
miR-X177	509	687	748	812	999	745	0,1
miR-X91	508	685	748	813	1005	745	0,1
miR-X120	520	690	740	814	998	745	0,1
miR-X260	505	673	745	817	1033	746	0,1
miR-X223	470	677	751	823	1037	746	0,1
miR-X172	511	685	738	820	1015	746	0,2
miR-X151	518	690	745	814	998	746	0,2
miR-X245	470	681	755	824	1036	748	0,2
miR-X126	485	685	750	823	1026	748	0,2
miR-X156	490	687	752	822	1023	749	0,2

miR-X264	500	657	743	829	1081	750	0,2
miR-X205	516	690	752	822	1002	750	0,2
miR-527	559	682	744	817	1012	752	0,3
miR-X184	510	690	751	827	1033	755	0,3
miR-X233	496	693	762	830	1029	757	0,4
miR-518a	485	689	758	836	1054	758	0,4
miR-X262	520	671	748	849	1052	758	0,4
miR-X271	488	680	758	840	1070	759	0,4
miR-485	500	693	760	833	1042	759	0,4
miR-X203	538	704	760	825	1005	760	0,4
cand-502	517	702	761	830	1018	760	0,4
miR-X163	495	692	758	837	1055	760	0,5
miR-X154	530	697	763	828	1021	760	0,5
miR-X219	583	681	759	838	1002	762	0,5
miR-X65	568	698	749	829	1024	763	0,5
miR-X133	523	699	761	839	1049	766	0,6
miR-X267	490	700	769	848	1060	768	0,6
miR-X228	514	700	764	849	1052	769	0,6
sh-p53	492	693	767	852	1080	769	0,6
miR-X187	470	699	771	853	1085	770	0,7
miR-498	520	707	772	842	1042	770	0,7
miR-X240	548	713	772	836	1019	771	0,7
miR-X159	491	698	766	854	1086	771	0,7
miR-X181	552	712	771	839	1028	773	0,7
miR-516	507	711	775	848	1054	773	0,7
miR-X212	494	697	770	856	1093	774	0,7
miR-X107	517	714	778	848	1042	774	0,8
miR-X210	556	719	774	840	1019	775	0,8
miR-X201	521	710	774	850	1055	775	0,8
miR-X248	569	719	787	837	1006	777	0,8
miR-X103	495	709	778	857	1079	777	0,8
miR-505	552	703	778	856	1064	781	0,9
miR-524	510	701	776	865	1102	781	0,9
ITCH C830A	541	713	781	862	1061	784	1,0
miR-520d	498	712	788	864	1090	784	1,0
miR-X175	554	731	787	850	1026	784	1,0
miR-453	542	712	782	867	1097	789	1,1
miR-X140	495	714	797	883	1106	793	1,2
miR-513	533	736	799	872	1045	793	1,2
miR-X250	535	737	795	878	1086	799	1,3
miR-X231	552	729	803	879	1102	804	1,4
miR-X236	545	733	815	893	1119	812	1,6
miR-X257	471	727	810	911	1184	813	1,6
Untrfx.	NA	NA	NA	NA	NA	NA	NA
					Mean	739	
					SD	47	

Plate 3 of 4, p63-fluorescence of GFP-positive cells

	Lower Whisker	Lower Hinge	Median	Upper Hinge	Upper Whisker	**Trimmed Mean**	**z-score**
sh-p63 (1)	423	499	526	564	661	529	-3,7
sh-p63 (2)	432	510	537	571	662	537	-3,5
miR-216	420	565	629	700	903	634	-1,6
ITCH	443	547	601	718	960	637	-1,6
miR-190	412	568	637	715	934	644	-1,4
miR-129	429	575	639	720	935	649	-1,3
miR-195	434	578	643	720	934	652	-1,3
miR-342	436	584	645	724	933	655	-1,2
miR-103	419	588	651	741	969	664	-1,1
miR-140	435	595	657	734	943	664	-1,1
miR-505	408	585	654	745	982	665	-1,0
miR-372,371	440	582	651	741	979	666	-1,0
miR-373	443	587	652	744	979	669	-1,0
miR-328	425	581	656	750	999	670	-0,9
miR-331	433	583	655	750	998	671	-0,9
miR-196	433	605	669	749	962	675	-0,8
miR-153	423	602	672	755	984	678	-0,8
miR-107	420	608	673	756	976	679	-0,8
miR-335	463	589	653	760	1016	680	-0,7
BART-1	427	591	667	765	1024	682	-0,7
miR-30e	422	597	671	764	1016	683	-0,7
miR-214	437	599	671	762	1007	684	-0,7
miR-220	413	607	679	767	1007	686	-0,6
miR-102	437	603	678	767	1013	688	-0,6
miR-193	423	601	677	771	1027	689	-0,6
miR-125b	433	613	680	768	1000	689	-0,6
miR-147	435	615	683	766	992	689	-0,6
miR-10a	451	606	678	770	1016	692	-0,5
Let-7b	431	606	680	775	1027	693	-0,5
miR-381	437	616	681	774	1008	693	-0,5
miR-133b	417	613	685	777	1023	694	-0,5
miR-198	430	617	689	775	1011	695	-0,4
miR-186	424	612	685	779	1028	696	-0,4
miR-130b	438	607	678	781	1041	696	-0,4
Let-7i	440	608	681	780	1036	697	-0,4
Let-7f	418	607	686	785	1050	698	-0,4
miR-105	418	611	687	787	1049	700	-0,4
miR-30a	413	610	690	788	1054	700	-0,3
miR-324	435	616	690	784	1028	700	-0,3
miR-199b	434	622	698	790	1042	707	-0,2
Let-7d	418	590	690	801	1117	707	-0,2
miR-367	437	643	707	789	1008	710	-0,1
miR-98	425	614	701	806	1092	715	-0,1
miR-361	450	626	696	801	1065	715	-0,1
miR-203	440	628	703	804	1067	717	0,0
miR-146	469	640	703	799	1032	718	0,0
miR-31	440	615	703	810	1101	719	0,0
miR-30d	417	638	717	809	1065	721	0,1
miR-29	424	627	711	814	1091	722	0,1
miR-211	471	648	713	803	1032	724	0,1

BHRF1-3	456	637	716	812	1074	727	0,2
miR-141	440	617	710	821	1127	728	0,2
miR-19b	422	627	716	822	1113	728	0,2
miR-106b	452	635	714	817	1086	729	0,2
miR-1	434	640	718	819	1087	729	0,2
miR-124a	429	626	722	825	1124	732	0,3
miR-22	438	634	719	830	1122	735	0,3
miR-222	450	655	728	821	1068	736	0,3
miR-93	477	649	722	822	1081	738	0,4
miR-155	449	651	726	827	1091	738	0,4
sh-p53 (1)	488	640	719	827	1090	738	0,4
miR-122a	429	642	725	837	1128	740	0,4
miR-7	442	643	728	833	1118	741	0,4
miR-150	448	647	729	832	1107	741	0,4
miR-29b	406	657	735	838	1109	742	0,5
miR-218	477	664	733	824	1063	742	0,5
miR-95	477	645	735	831	1103	745	0,5
miR-91	444	644	730	840	1132	745	0,5
miR-26	434	646	736	842	1133	747	0,6
miR-20	454	658	750	838	1095	750	0,6
miR-181a	464	661	741	842	1112	753	0,7
miR-24	447	644	738	851	1159	754	0,7
miR-144	441	666	750	850	1124	757	0,8
miR-135	461	665	747	847	1119	757	0,8
miR-138	426	661	752	859	1154	760	0,8
miR-183	475	674	751	852	1118	763	0,9
miR-127	455	658	753	862	1166	765	0,9
miR-208	439	649	749	871	1203	767	1,0
miR-321	461	668	764	870	1171	774	1,1
miR-224	454	676	768	878	1179	779	1,2
miR-96	439	682	769	881	1179	780	1,2
miR-299	437	685	774	880	1172	780	1,2
sh-p53 (2)	466	688	776	873	1147	780	1,2
miR-99a	476	689	775	872	1142	781	1,2
ITCH C830A	516	676	766	868	1156	781	1,2
miR-26b	448	672	765	884	1202	781	1,2
miR-133	495	686	766	879	1165	785	1,3
miR-377	445	688	781	889	1191	788	1,4
miR-17	461	689	782	896	1205	794	1,5
miR-131	450	679	781	900	1231	794	1,5
miR-143	460	708	799	900	1182	801	1,6
miR-181c	425	695	792	912	1236	802	1,6
miR-301	456	714	805	919	1225	814	1,9
miR-205	459	708	808	922	1241	816	1,9
Untrfx.	NA	NA	NA	NA	NA	NA	NA
					Mean	718	
					SD	51	

Plate 4 of 4, p63-fluorescence of GFP-positive cells

	Lower Whisker	Lower Hinge	Median	Upper Hinge	Upper Whisker	**Trimmed Mean**	**z-score**
sh-p63 (2)	437	514	544	583	686	547	-4,4
sh-p63 (1)	439	514	545	602	721	556	-4,2
ITCH	450	556	622	729	981	651	-2,1
miR-X246	433	595	666	764	1014	682	-1,4
miR-448	446	603	675	765	1004	687	-1,3
miR-X179	424	608	676	769	1010	688	-1,3
miR-X199	440	608	681	774	1022	694	-1,2
miR-514	442	597	674	780	1055	695	-1,1
miR-X249	421	603	680	789	1068	699	-1,0
miR-X204	432	612	687	785	1045	701	-1,0
miR-X150	428	621	692	785	1030	702	-1,0
miR-X266	447	607	684	789	1061	703	-0,9
miR-X155	431	606	686	792	1070	704	-0,9
miR-X196	459	601	674	793	1075	704	-0,9
miR-517a	445	604	686	792	1073	705	-0,9
miR-X114	474	613	686	785	1041	705	-0,9
miR-492	441	614	690	793	1062	707	-0,9
miR-X253	430	619	696	795	1058	708	-0,8
miR-X119	446	615	692	796	1066	710	-0,8
miR-X227	422	622	701	805	1079	715	-0,7
miR-X263	423	598	681	818	1143	715	-0,7
miR-501	462	635	707	797	1038	717	-0,6
miR-X202	445	622	699	807	1086	718	-0,6
miR-X176	439	623	704	808	1083	719	-0,6
miR-X127	443	620	702	808	1090	719	-0,6
miR-X152	447	626	700	808	1080	719	-0,6
miR-452	410	618	702	818	1116	720	-0,6
miR-512	476	640	712	797	1030	720	-0,6
miR-X235	436	631	710	811	1081	722	-0,5
miR-X56	431	622	701	819	1112	723	-0,5
miR-X225	438	644	717	808	1055	724	-0,5
miR-491	462	636	711	808	1060	724	-0,5
miR-X171	454	624	706	819	1110	727	-0,4
miR-X158	445	631	716	823	1110	732	-0,3
miR-X182	442	646	724	820	1080	733	-0,3
miR-X173	432	632	719	829	1124	734	-0,3
miR-X146	433	636	724	827	1112	735	-0,2
miR-X130	446	634	719	827	1115	735	-0,2
miR-X268	439	611	709	837	1174	736	-0,2
miR-X232	449	651	728	822	1077	736	-0,2
miR-X208	418	647	729	830	1103	736	-0,2
miR-X241	483	633	711	825	1113	736	-0,2
miR-X256	452	648	729	823	1084	737	-0,2
Vector Ctrl.	468	649	728	820	1076	737	-0,2
miR-520c	434	632	720	834	1134	737	-0,2
miR-X101	452	641	723	829	1106	738	-0,2
miR-X89	447	625	722	834	1146	739	-0,1
miR-518e	459	623	715	835	1151	739	-0,1
miR-X111	440	634	719	837	1139	740	-0,1
miR-X136	430	636	726	836	1133	740	-0,1

miR-X86	447	648	731	828	1098	740	-0,1
miR-X98	421	630	721	841	1157	740	-0,1
miR-X217	442	650	730	834	1111	742	-0,1
miR-523	461	657	733	829	1088	743	-0,1
cand-217	431	621	718	848	1184	743	0,0
miR-X144	455	654	734	832	1097	744	0,0
ITCH C830A	494	652	741	827	1084	747	0,0
miR-X123	441	652	733	844	1131	748	0,1
miR-X104	432	649	741	848	1148	752	0,1
miR-506/507	474	657	739	845	1124	755	0,2
miR-X230	438	633	719	868	1219	757	0,2
miR-519d	450	667	746	854	1133	759	0,3
cand-262	421	645	744	865	1195	760	0,3
sh-p53 (1)	453	670	754	852	1126	761	0,3
miR-X43	428	656	746	865	1178	762	0,4
cand-343	436	658	748	864	1172	763	0,4
miR-X270	449	660	748	867	1178	767	0,5
miR-X239	473	653	737	868	1189	767	0,5
cand-523	440	671	754	867	1161	768	0,5
miR-X169	480	639	729	876	1219	768	0,5
miR-X185	452	666	756	866	1165	769	0,5
miR-X261	450	674	759	867	1157	770	0,6
cand-350	438	671	764	872	1173	773	0,6
cand-428	455	670	755	874	1180	774	0,6
sh-p53 (2)	468	682	764	869	1149	775	0,7
miR-X211	449	667	762	877	1190	776	0,7
miR-488	473	682	761	874	1159	778	0,7
miR-X161	461	668	765	881	1198	780	0,8
miR-X222	481	657	754	886	1226	782	0,8
miR-X142	438	694	785	894	1195	792	1,0
miR-X26	435	692	787	904	1222	797	1,2
miR-X165	443	686	787	907	1236	799	1,2
miR-X258	448	695	789	911	1230	803	1,3
miR-X108	424	699	803	922	1255	810	1,4
miR-486	492	691	791	919	1259	813	1,5
miR-X192	465	697	794	926	1268	815	1,6
miR-X237	428	713	809	930	1255	818	1,6
miR-489	478	723	811	918	1207	818	1,6
cand-853	448	703	807	930	1269	819	1,6
miR-X188	470	706	805	932	1267	822	1,7
miR-X214	437	728	825	945	1271	832	1,9
miR-449	477	730	828	938	1250	834	2,0
miR-526a	480	711	824	956	1318	841	2,1
miR-520e	483	744	843	968	1299	855	2,5
Untrfx.	NA	NA	NA	NA	NA	NA	NA
					Mean	745	
					SD	45	

8.2 Supplemental figures of screen results for p63

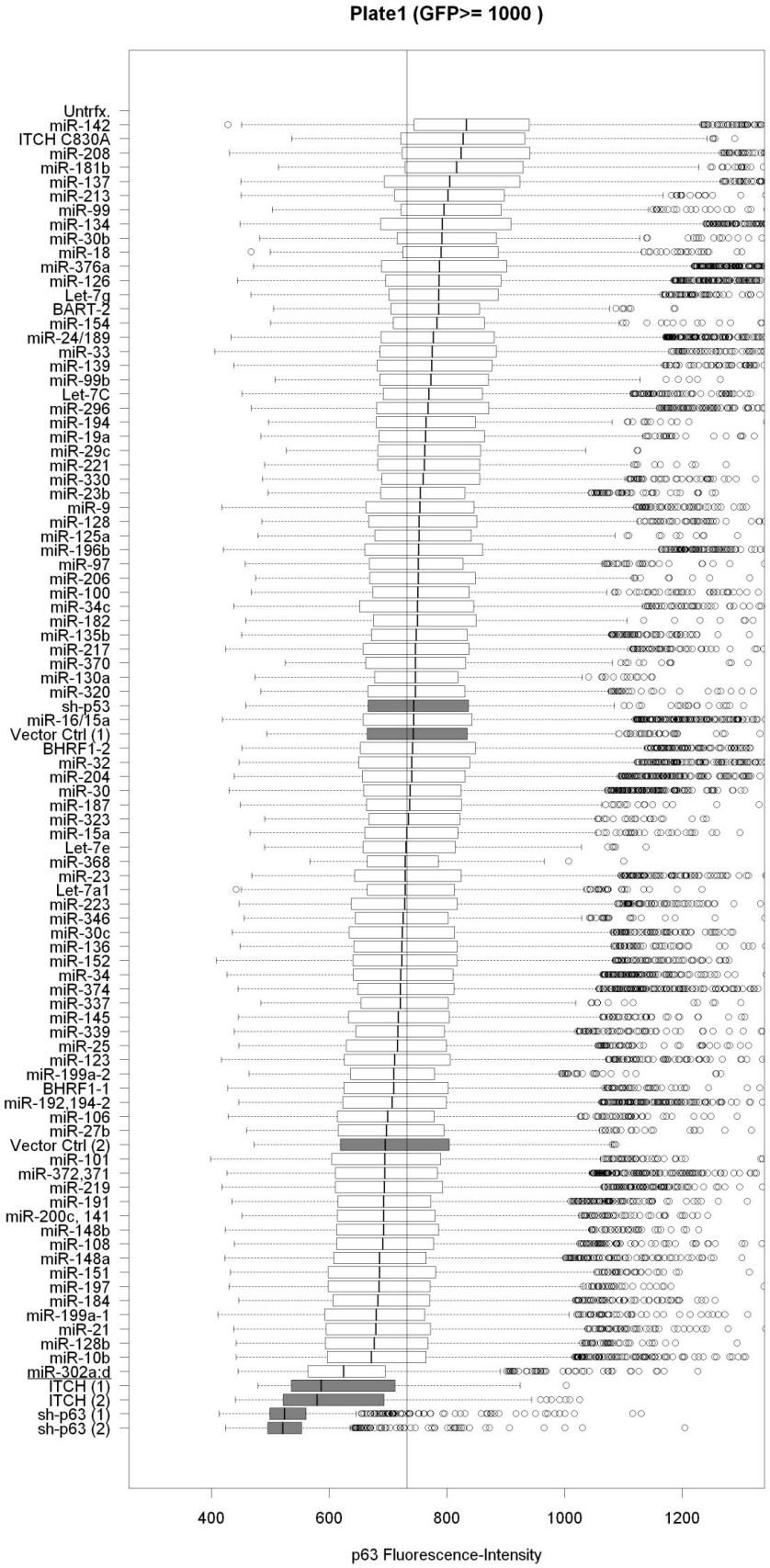

Figure 8.1a: Results of plate 1. Boxplots summerizing the fluorescence from p63-bound antibodies in GFP positive cells (GFP >= 1000). Combined data of two independent experiments. Control samples are highlighted by grey boxes. Samples are ordered according to their median p63-derived fluorescence. The vertical grey line is the median value of all samples. X-axis: Intensity as quantified by the 12bit CCD-camera (0= black, 4095 = white)

Figures 8.1b,c,d are similar for the other 3 plates of the screen.

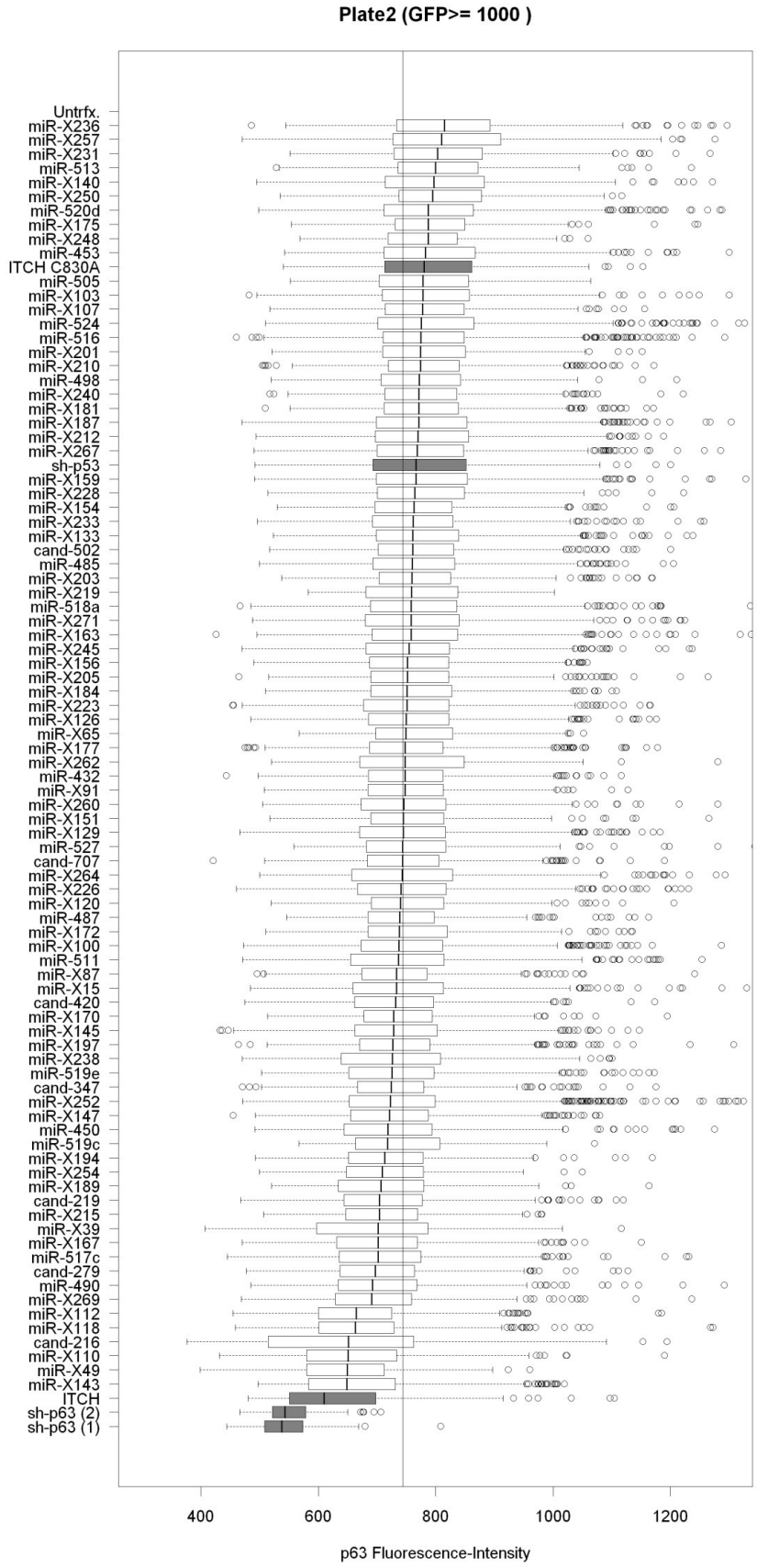

Figure 8.1b: Results of plate 2.

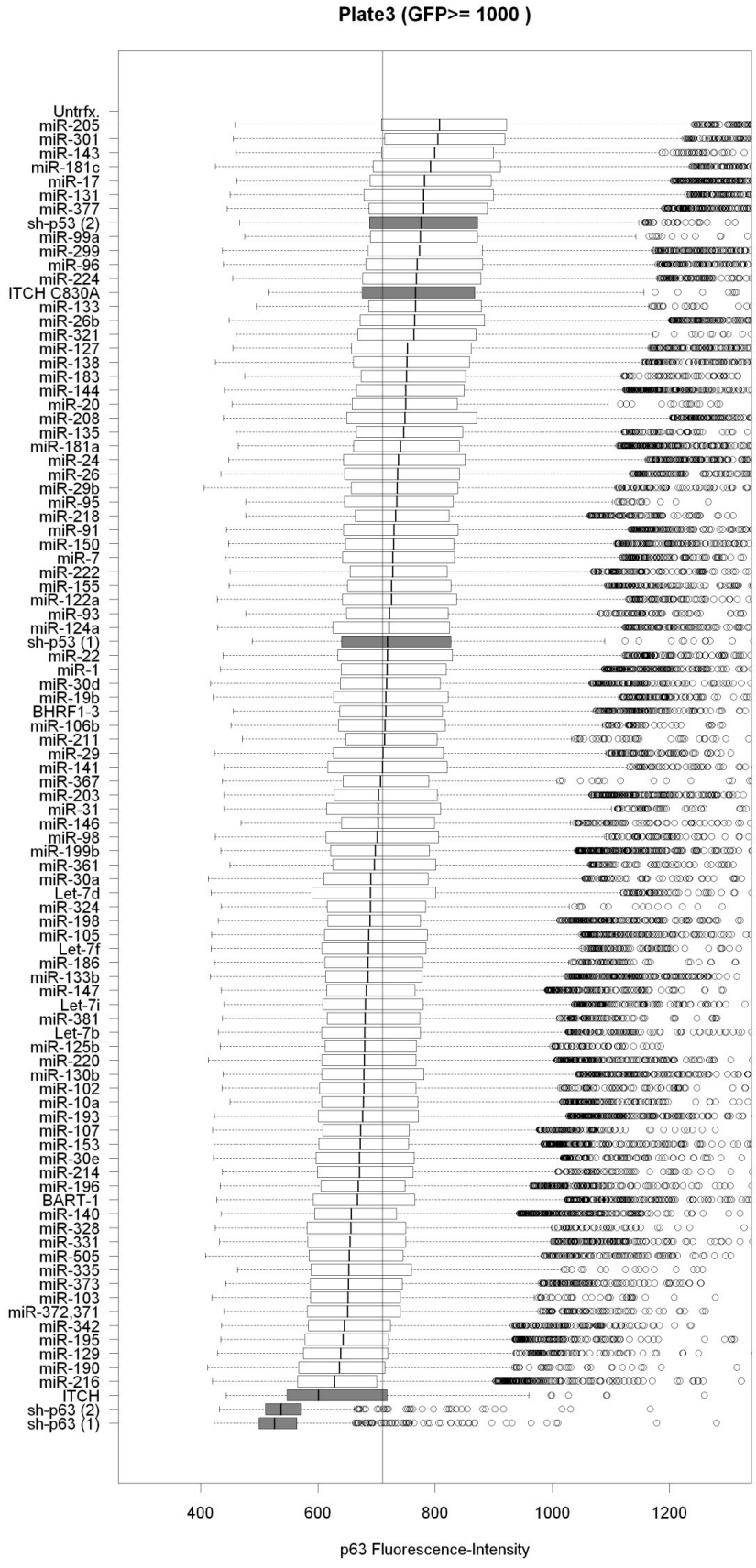

Figure 8.1c: Results of plate 3.

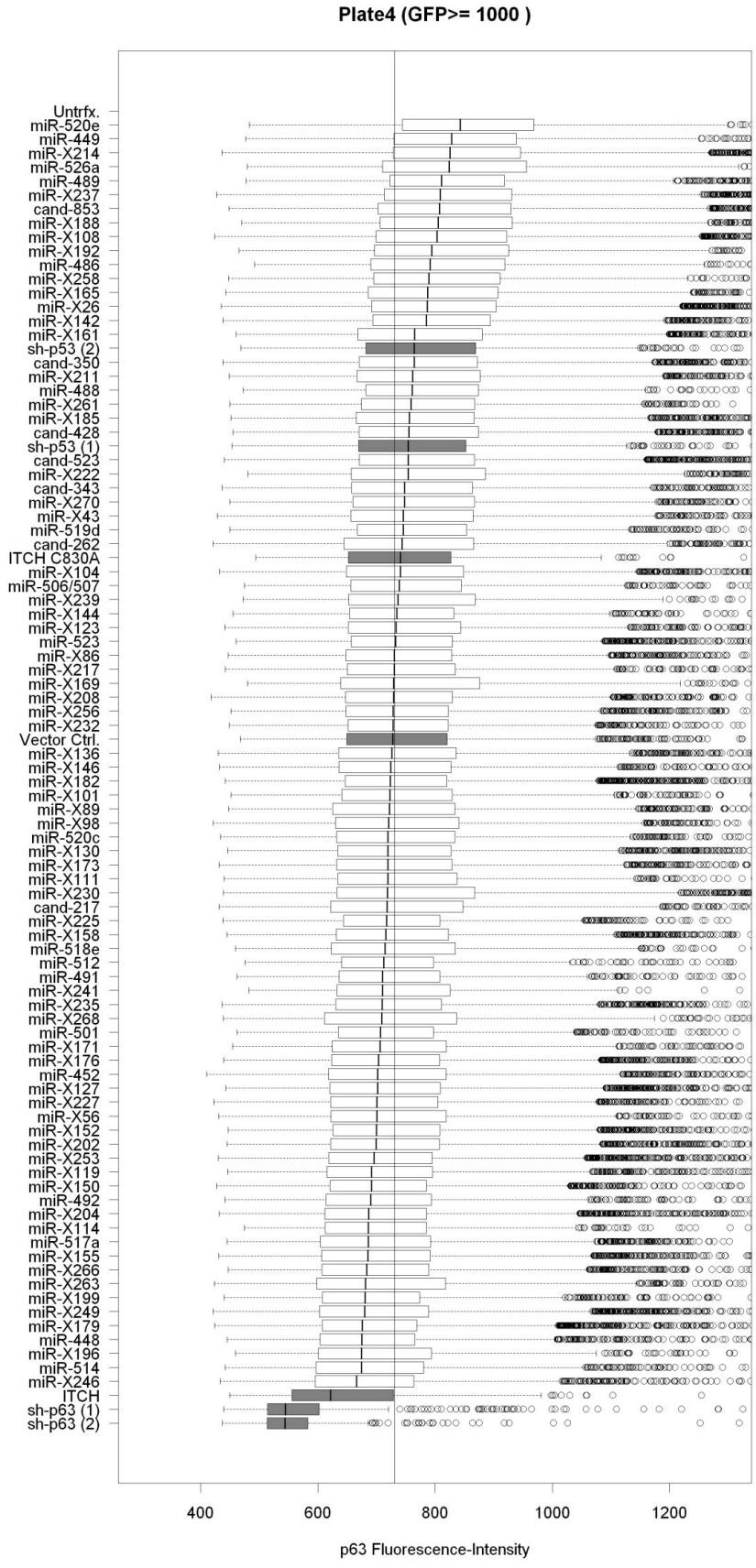

Figure 8.1d: Results of plate 4.

Acknowledgements

It has been a long way from my first laboratory experiences to this project. Many people have supported and guided me on this way, whom I am very thankful for their help. Here, I would like to highlight some who especially help me in the conducting of this work:

In particular, I would like to thank Matthias Dobbelstein for adopting me into his group and for providing me with the topic of this work as well as all necessary tools and guidance to successfully conduct my first 'big' scientific project. It is invaluable to have a mentor who is always interested in new data, regardless how controversial they might be, who keeps the door of his office open not only during regular working hours and with whom one can discuss even the craziest ideas that occupy one's mind … thank you!

I would like to thank the 'MolOnkol' team which became like a family to me. This work would not have been possible without the positive atmosphere in the lab, the friendly people patiently introducing me into new molecular techniques, the sharing of tasks and the support of each other's projects, the vivid discussions about desired and strange observations and all the other details necessary to make oneself give everything for the project. Especially I would like to thank Ulrike Beyer for introducing me to p63, Xin Zhang, Christian Braun and Muriel Lizé for helping me mastering microRNAs and the miR-Vec library, Antje Dickmanns and Cathrin Hippel for excellent technical support and laboratory organization, Patricia Räke-Kügler for keeping the administration in check for us and for the organization of so many things big and small that essentially contribute to the team spirit and Sonja Holzmann and Monika Bug for answering so many of my technical questions.

For the kind gift of a replicate of the miR-Vec library, I am much obliged to Reuven Agami. This generous present and the great work behind its creation was a strong source of motivation. I would also like to thank Tony Pawson, Casimir Bamberger and Caterina Missero for kindly providing us with plasmids.

Finally, I would like to thank Christina Scheel who always lends me an ear for my scientific issues as well as my parents for supporting me throughout my medical studies.